A New Thin Layered Structural Coating on a Metal Substrate for Enhanced hydrogen Production from Steam Methane Reforming

Thesis

Master of Science (Chemical Engineering)

at

The City College of New York

of the

City University of New York

Submitted by:

Michael Alexander Lugo Pimentel
25th of May, 2017

Approved:

_____

Dr. Marco J. Castaldi, Thesis Advisor

_____

Dr. Ilona Kretzschmar, Chair
Department of Chemical Engineering

Table of Contents

Abstract

In the past decade the use of hydrogen has become more ubiquitous. Its applications range from the upgrading of fossil fuels, to the production of ammonia, to the hydrogenation of fats, to the production of muriatic acid and methanol, all without including the efforts being taken to move towards a hydrogen economy. Its widespread use and its increasing demand lays pressure to find more efficient techniques of hydrogen production. Because the overwhelming majority of hydrogen produced nowadays comes from the steam reforming of natural gas (SMR), it appears that the most adept way to improve yields is by improving the SMR process. This thesis compiles the efforts taken to characterize the performance and kinetics of a new type of catalyst coating technique, which promises enhanced hydrogen production from SMR. To achieve this, a total of 49 experiments were performed at different temperature, pressure and space-time conditions for different inlet distributions.

Resumen

En la última década el uso de hidrógeno se ha vuelto más y más ubicuo. Sus aplicaciones van desde la mejora de calidad de combustibles fósiles, a la producción de amoníaco, a la hidrogenación de grasas, a la producción de ácido muriático y metanol, todo sin contar los esfuerzos actuales en curso a la economía de hidrógeno. Dado que la gran mayoría del hidrógeno producido hoy en día proviene el proceso de reformado de gas natural con vapor de agua (SMR, por sus siglas en inglés), la forma más adepta de mejorar la producción es mejorando el proceso de SMR. Esta tesis compila los esfuerzos realizados para caracterizar el rendimiento y parámetros cinéticos de un nuevo tipo de técnica de revestimiento de catalizadores, la cual promete una producción de hidrógeno mejorada a partir del proceso de SMR. Para lograr esto, un total de 49 experimentos fueron realizados bajo condiciones diferentes de temperatura, presión y factores de tiempo para diferentes distribuciones de especies de entrada.

Dedicación

Esta gota en el océano del conocimiento va dedicada a muchas personas. A mis padres, María y Alexandro, quienes inculcaron con ejemplo el hábito de trabajo arduo y riguroso. A mi recua de hermanos, Marín, Eric, Masi, Jesi, Gregorio y Joelo, quienes me proveen la inspiración de ser un buen ejemplo.

Y sobre todo a dos personas muy especiales para mi: a una de las personas que más tiempo llevo conociendo, Mamá Ana; y a una personita que no llevo tanto tiempo conociendo, el Capitán Bebo.

Acknowledgements

I would like to express my sincere gratitude to my lab mates, especially to Jeff LeBlanc, Swanand Tuphsakhare and Tim Sharobem whose critiques were always very accurate.

I would also like to thank Alloy Surfaces for their collaboration, especially to Rajinder Gill for his timely advice.

I would like to thank and acknowledge Prof. Juray DeWilde for his input and support. His guidance remains well appreciated.

Finally, but definitely not ‘leastly’, I would like to thank my advisor Dr. Marco Castaldi, and my coadvisors Dr. Nicholas Tiliakos and Dr. Dean Modroukas. My most sincere gratitude for their continuous support, patience and thoughtful guidance. Not frequently one finds mentors willing to help you out of το σπήλαιο and show you the true forms that make the shadows’ σχήματα.

List of Figures

List of Tables

Chapter 1: Introduction

The current population of the world is estimated to be 7.5 billion people and it is expected to rise to 9.5 billion by the year 2050 [1]. Given the limited resources of the planet, these new population milestones come with very difficult challenges that must be addressed at record speeds. The most urgent of such challenges is perhaps the UN-identified food, energy and water (F.E.W.) nexus [2], which combines three of the most essential and interconnected human necessities that will be put under severe strain in coming years due to population growth. In addition to the three main components of FEW, there are many appurtenant issues that must be faced as well. For example, the expected increase in world population is projected to include a larger middle class than ever before seen [3], which is also expected to incur consumption patterns similar to that of the developed world.

Hydrogen is at the forefront of the FEW and its efficient production will provide key support in our efforts to address the nexus. Hydrogen is a fundamental component in the production of ammonia, with ammonia being the primary method of nitrogen fixation in the soil both by direct use and/or by its conversion into urea, turning hydrogen essential for food production. Hydrogen (in syngas) also plays an important role in energy generation. The syngas can be used directly either by combustion or through fuel cells, or it can be used in the generation of liquid fuels from gas or through the coal-to-liquids and biomass-to-liquids processes. Finally, hydrogen is also used in the production of hydrogen peroxide which, due to its antimicrobial and fungicidal properties as well as its biological degradability, is used in waste water treatment, drinking water preparation and food processing.

About 95% of the total hydrogen produced in the United States comes from the steam-methane reforming (SMR) process [4]. According to the United States Energy Information Administration the price per million BTU of natural gas has remained relatively constant at USD$4.43 from 1998 to the present date as reported from Henry's Hub [5]. Given that about 38% of the US supply of natural gas comes from shale gas and also given the constantly increasing rate of shale gas production, it is only a matter of time before the prices of shale gas and natural gas fall and subsequently the prices of all the derivative products produced from these raw materials should also. Although the current reserves of natural gas are vast and the price of natural gas is foreseen to fall, it is still a worthwhile endeavor to develop the technologies and deploy the systems that would take the most advantage out of our resources given that natural gas is nonrenewable. Therefore, the role of catalysis is crucial in developing catalysts that are more selective, less susceptible to deactivation and poisoning, and can handle larger throughputs.

The purpose of this work is to characterize the performance of a new nickel catalyst. Among the advantages of this catalyst is its application process, which is coated on a metal substrate producing a very strong bond between the substrate and the catalyst. The formulation and application process are the intellectual property of Alloy Surfaces (ASC), which is a subsidiary of the Chemring Group.

Due to the presence of sulfur, which poisons reforming catalysts [6], the SMR process begins with a desulfurization step. Methane, in the form of natural gas, is delivered through a zinc oxide bed at temperatures between 300 – 400°C [7]. The sweet gas (i.e., sulfur-less natural gas) is then carried through the reformer. The actual reaction occurs in reformer tubes, which are catalyst-filled tubes that go in and out of a firebox. The firebox is a refractory brick housing that insulates the heat provided from the surroundings to drive the reaction. The heat is supplied through burners located at various locations. Depending on the location of the burners, reformers are classified as top fired, wall fired or terraced wall fired as shown below in Figure 1.

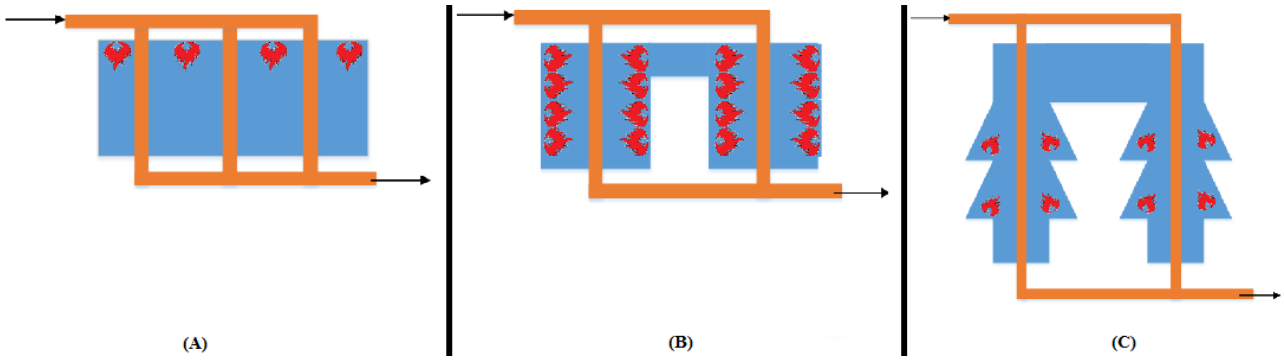

Figure 1 Main reformer configurations: (A) top fired; (B) wall fired; (C) terraced wall fired.

The effluent of the reformer is then delivered through a high temperature shift (HTS) reactor. HTS reactors typically use iron/chromium/copper oxides catalysts to generate more hydrogen at relatively high temperatures. The HTS effluent is subsequently cooled and delivered through a low temperature shift (LTS) reactor. LTS reactors use a copper oxide catalyst to further the hydrogen generation. These reactors are used to achieve higher plant efficiency due to the fact that the water-gas shift reaction achieves higher equilibrium at lower temperatures [8][9].

The complete reaction mechanism to produce hydrogen from methane is thought to be very complex including gas−gas, and gas−solid reactions. However, due to ample amounts of empirical confirmation the product distribution can be modeled by the following reactions:

$$CH_4 + H_2O = CO + 3H_2;\ \Delta H = +206\ kJ/mol \quad \text{(eq. 1)}$$

$$CH_4 + 2H_2O = CO_2 + 4H_2;\ \Delta H = +165\ kJ/mol \quad \text{(eq. 2)}$$

and the water gas shift

$$CO + H_2O = CO_2 + H_2;\ \Delta H = -41\ kJ/mol \quad \text{(eq. 3)}$$

For this work, a cylindrical reactor has been used. The temperatures ranged between 400 − 900 °C and the pressure was normally maintained at 1.5 bar, although some tests were conducted at higher pressures. This project was divided in three phases. The major difference among phases is the morphology of the catalyst.

Phases 1 and 2 used 2.54 cm diameter perforated, corrugated metal plates on to which the catalyst was deposited. These plates were stacked on top of each other to construct a fixed bed reactor configuration. Phases 3a, 3b and 3c used 3 mm diameter punch outs as a catalyst substrate, dispersed through an inert α-alumina packed bed. This work is presented with the following structure:

Chapter 2 provides a literature review where the incremental developments that led to the kinetic model used in this thesis is explored. Chapter 3 provides details on the execution of SMR tests as well as the iterations performed in order to achieve the final experimental design. Chapter 4 harbors the experimental results. The first four subchapters describe the criteria used to assess the data collected, while the last four subchapters describe the analysis performed on the data as well as the discussion of the findings. Finally, Chapter 5 presents the conclusion of this study along with recommendations for future work.

Chapter 2: Literature review

As early as 1943, Hougen and Watson published one of the earliest articles on solid catalysis [10]. This article applied activation theory and general rate equations to derive a general description of surface catalytic reactions. This paper resulted in the suggested rate equation,

$$r = \frac{s}{2L}(kc_A c_B - k' c_R c_i)$$

(eq. 4)

where r is the reaction rate; s is the number of equidistant sites adjacent to each active center; k is the forward reaction velocity constant; c_A, c_B and c_R are the concentrations of species A, B and R; k' is the reverse reaction velocity constant; c_i is the concentration of vacant adsorption sites; s is the number of equidistant sites adjacent to each active center; and L is the total molal adsorption sites per unit mass of catalyst.

In 1950 Hougen continued the work on solid catalysis, but [11] was focused on reactions in the gas phase. This article furthered the concepts of rate-controlling mechanism and adsorption term, which includes adsorption equilibrium constants. After this development the rate equation modeling catalyzed gaseous reactions began to take a form closer to the models we use nowadays.

Later in 1975 Allen et al. [12] made some of the first attempts to characterize the rate of reaction of SMR. Up to that date, the previous work on steam reforming had been primarily dedicated to olefins. The work of Allen et al. [12] takes two approaches to data analysis. On the more simplistic approach, a polynomial regression was suggested, which correlated the conversion of methane to the space-time, where a regression was done for each operating pressure.

On the more sophisticated approach, they modelled the data piecewise. Between temperatures of 400 – 600 ^oC they followed from Brodov et al. [13],

$$r = k' \frac{P_{CH4}}{P_{H2}}$$

(eq. 5)

while above 700^oC they found the data could be correlated by

$$r = \frac{k\, P_{CH4}}{1 + a\frac{P_{CH4}}{P_{H2}} + bP_{CO}}$$

(eq. 6)

However, by applying the ideas of Hougen and Watson [10] they were able to suggest a rate of CO formation equation and an equation for the rate of CO_2 formation.

In 1989 Xu and Froment [14] suggested one of an SMR intrinsic kinetics model. Their model took into account not only SMR but also methanation and water – gas shift, all at different operating pressures. Froment's model suggests that oxygen is the limiting reagent given that carbon reacting with adsorbed oxygen are the limiting step. Their work resulted in one of the best SMR models to date, and two possible reaction mechanisms. The present work borrows from Froment's work because the model has proven to work well whether it is applied to fluidized beds [15], to reactions carried on anodes [16][17], or to large pore catalysts [18].

Recently, efforts have been undertaken by Mastri et al [19] to put forth a microkinetic model of SMR. The aim of their work is to determine the fundamental steps that the reactions follow in order to finalize the long controversy of the mechanism SMR tracks on to. Their reduced model encompasses 28 reactions from which they have been able to make some important observations. Among the most important is the determination of the limiting step, which they concluded was the activation of methane since it first has to pyrolyze before it is oxidized by an OH.

Chapter 3: Experimental Section

3.1: Introduction

A facility was designed and assembled to carry out all the testing required. The whole facility was sized such that the nominal total flow rate downstream of the reactor was 4.2 L/min. This constraint was the minimum flow rate requirement from one of the chemical species analyzers used. The facility was also sized for the maximum temperature and pressure conditions expected to be encountered during test. The facility was subdivided into four major groups: delivery panel, mixing panel, hot zone, and analyzer panel. Each section was designed with pertinent redundant safety measures.

The delivery panel was designed to accept reactants, in the form of pressurized k-bottles, and regulate them down to test pressures and flow rates. The delivery panel was subdivided into four legs namely hydrogen leg, diluent (nitrogen) leg, methane leg, and deionized water leg. All legs used electronic mass flow controllers except for the water leg, which used a metering valve coupled with a rotameter. The delivery panel was set vertically on an aluminum plate 122 cm high by 91.6 cm wide and 4 mm thick.

Copper tubing (6.35 mm in diameter, 1.2 mm wall thickness) was used for all connections in the delivery panel. The hydrogen, diluent and methane legs were equipped with 7 micron filters and relief valves, along with shutoff valves, check valves, and pressure gauges. All three legs were also equipped with electronic MFCs.

The hydrogen leg used a Tylan FC-280S MFC with a range of $0 - 50$ standard cubic centimeters per minute (sccm) for phases 1 and 2. For phase 3 this MFC was changed to a Tylan FC-280S with a $0 - 3$ standard liters per minute (SLPM) range.

The diluent leg was bifurcated as to serve the dual purpose of independent furnace purging and system dilution. For the furnace purge, nitrogen gas was fed into the furnace to maintain the concentration of any flammable gases below their flammability thresholds had there been a leak in the system. The purge flow rate was controlled with a 0.4066 mm orifice. For the system dilution, during phases 1 and 2 an MFC Aalborg GFC37 with a $0 - 10$ L/min range was used. For phase 3 this MFC was replaced by a Tylan FC-280S range $0 - 50$ sccm.

The methane leg was arranged with a Tylan FC-280S MFC with a $0 - 2$ SLPM range. All MFCs were calibrated with their pertinent gases, i.e., H_2 MFC was calibrated with H_2 and so on. Calibration curves are shown in appendix A.

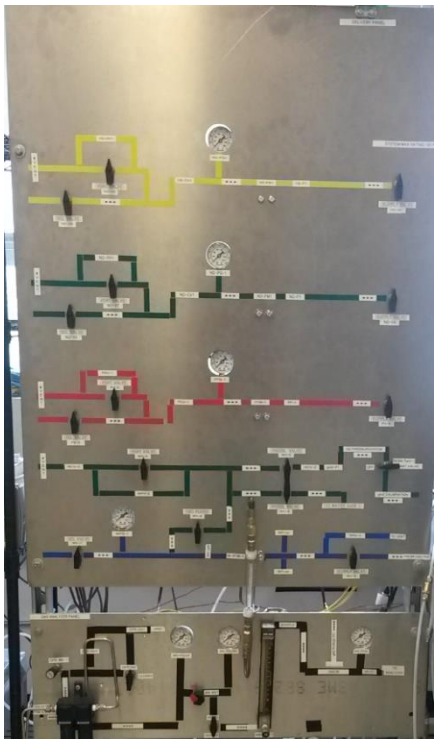

Figure 2: Delivery panel (top) and analyzer panel (bottom)

Part of the water delivery leg was designed to deliver liquid water to a vaporizer. The liquid water was loaded in a reservoir and pressurized with a nitrogen head, which delivered it through a flow controller. The liquid water flowed through a 10 μm filter, a Swagelok SS-4MG metering valve, and a Gilmont instruments GF-2060 compact shielded flowmeter with a range 0 − 40 sccm of liquid water. The pressurized water was delivered through the vaporizer coil, but before vaporization occurred the steam/water mixture was diverted towards an overboard pail to get visual confirmation of vaporization. Once vaporization was confirmed, the stream was redirected towards the mixing chamber. Figure 2 shows a photograph of the delivery panel described above.

The delivery panel was interfaced with the mixing panel. All the copper lines were connected to smooth bore seamless stainless steel tubing (6.35 mm in diameter, 1.2446 mm wall thickness) via Swagelok stainless steel couplings. The hydrogen and the methane legs connect directly into the mixing panel, while the diluent and the water legs first go through the hot zone for preheat and vaporizing.

The mixing panel, thus, accepts hydrogen, warm nitrogen at a nominal temperature of 300ºC, room temperature methane and superheated steam into a manifold built from stainless steel tees, couplings and check valves with 6.35 mm connections. The pressure of all reactants was initially atmospheric and once temperature conditions were achieved then the pressure was increased to the pressure condition, this is described in the test procedure below. This manifold was, in turn, connected into a mixing chamber. The mixing chamber was built from Inconel-625 25.6 mm in diameter and an L/D = 10, which ensured good mixing at the Reynolds numbers used during these tests. All the piping in the mixing panel was wrapped in heat tape and insulation. A k-type thermocouple was used to monitor the surface temperature of the mixing chamber. An overboard pail was placed in the steam line to ensure full water vaporization. Figure 3 shows a schematic of the mixing panel.

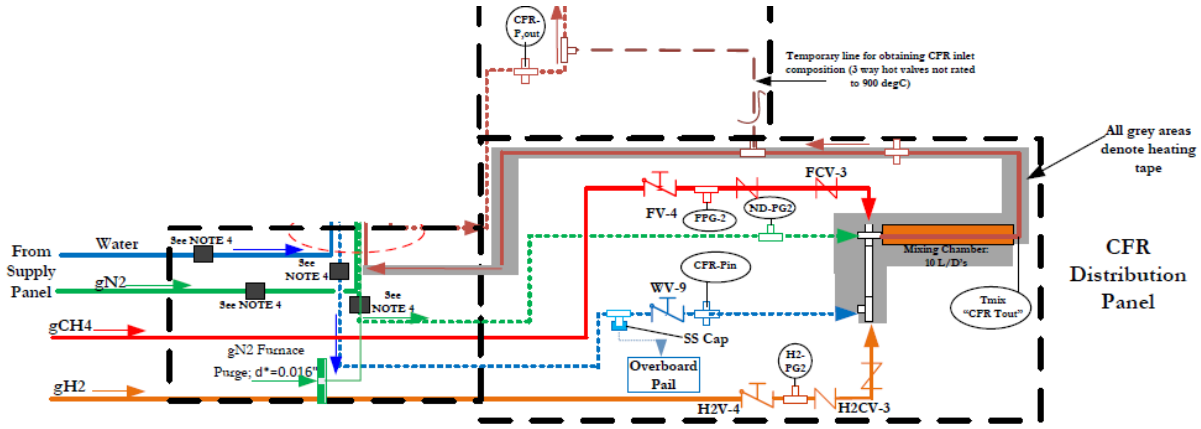

Figure 3: schematic of the mixing panel. Solid lines represent cold streams. Dotted lines represent preheated streams.

The hot zone was located inside an electric furnace. The furnace was a Mellen split vulcan heating element, SV series with 5 heating zones. It had 168.2 cm in length and 11.5 cm in diameter. The furnace's supply voltage was 208 volts while the current varied with the zone as follows: zones 1 and 3: 7.2 amps, zone 2: 6 amps, and zones 4 and 5: 24 amps.

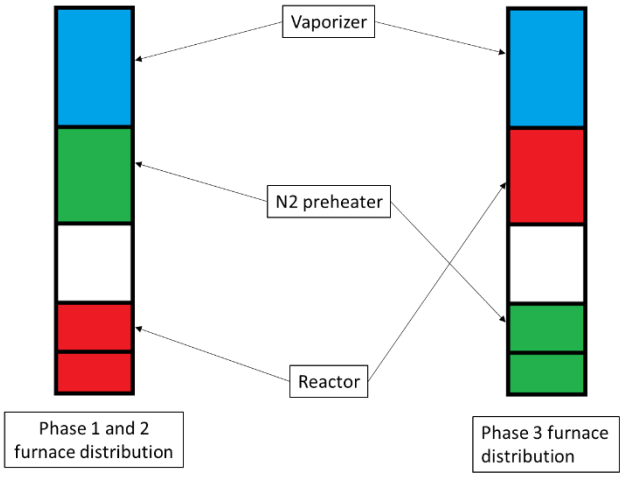

Figure 4: distribution of furnace use through test phases.

The hot zone was subdivided into reactive and nonreactive. During phases 1 and 2 the reactive subdivision was located in the furnace's heating zones 4 and 5 and was in essence the reactor. The non-reactive subdivision was located in zone 1, where the vaporizer coil was located, and zone 2, where the diluent pre-heater was located. During phase 3 the reactor was moved to the furnace's heating zone 2 and the diluent pre-heater was moved to zones 4 and 5, as seen on Figure 4.

The vaporizer coil and the pre-heater were made from smooth-bore seamless stainless steel tubing 6.35 mm in diameter. Both coils had 8.5 cm in outer diameter. There were significant changes in the reactor from phase to phase and those will be discussed in more detail in the coming phase-specific sections.

The reactor effluent was delivered to the analytical equipment through a stainless steel coil an iced water bath, the water condensed into a knockout tank, and the dry effluent was subsequently delivered through a water trap. For phase 1 the condenser coil was placed horizontally in the iced water bath and the knockout tank was a stainless steel 300 cm^3 bottle. During phase 2 the condenser was placed vertically in the iced water bath and the knockout tank was replaced by a 20 L steel tank. By phase 3 the knockout tank was phased out and instead a dehydrator downstream of the water trap was put in place. Through all changes the stream temperature was measured with a k-type thermocouple.

Once the reactor effluent was sufficiently dehydrated the stream was delivered through the analyzer panel. The initial function of the analyzer panel was to measure the total flow rate of the effluent and bifurcate it. One of the stream branches were destined to online gas analyzers: Fuji Electronics CO2/CO monitor ZRF26FF2-2B5YY-KK0YYFY; Fuji Electronics CO monitor ZRH1BLY2-6BAYY; and Rosemount Analytical flame ionization detector 194106. The other stream was being directed towards an Agilent 4 column microGC 3000.

Unfortunately, due to human error and instrument malfunction, the online analyzers branch of the analyzer panel had to be repurposed. For all phases the online analyzer branch was redirected towards the vent. A metering valve was added to control back pressure, and a rotameter was added to have visual confirmation of flow. The micro GC (μGC) branch had a metering valve as well to aid with the back pressure control. During phase 1 the μGC was connected via a tee on the exhaust and a reduction from 6.35 mm to 1.6 mm. For phases 2 and 3 a factory made inlet manifold was added to the μGC, which added over pressurization safety and a visual confirmation of flow.

An orifice was located upstream of the analyzer panel. The orifice offered two advantages: it maintained a minimum back pressure through the system, and it enabled the calculation of the total dry flow rate at the effluent. To achieve this, a series of orifices were used throughout the test efforts, using different orifice diameters depending on the required test conditions (i.e., pressure, temperature and volumetric outflow). The required diameter for the orifices was calculated as to maintain the system backpressure as close to the test condition required reactor inlet pressure for a given total inlet flow rate, as shown below,

$$\dot{m} = \frac{AP_t}{\rho\sqrt{T_t}}\sqrt{\frac{\gamma}{R}}M\left(1+\frac{\gamma-1}{2}M^2\right)^{-\frac{\gamma+1}{2(\gamma-1)}}$$

(eq. 8)

Where, $\dot{m}$ is the mass flow rate, A is the effective area, P_t is the total pressure, T_t is the total temperature, γ is the specific heat ratio, R is the universal gas constant, ρ is the density of the mixture, and M is the Mach number. In this calculation M was set to 1 in order to ensure choked flow. The flow rate and temperature would remain constant and the effective area would be changed to get the desired operating pressure.

The orifice featured an upstream and a downstream pressure transducers. Both pressure transducers were acquired from Omega Engineering, and both had a $0 - 34$ bara range. The fact that the orifices were not ASME standard coupled with the wide range of measurements of the pressure transducers rendered this method of calculating the total effluent useless after phase 1. For phases 2 and 3 a known amount of inert

tracer was used, which coupled with the μGC allowed us to calculate the total effluent volume with high accuracy.

3.2: Phase 1

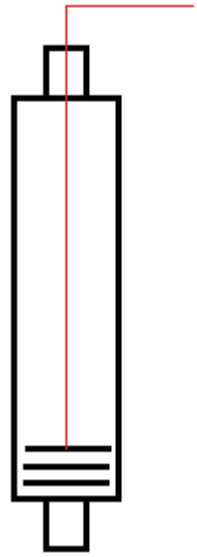

Figure 5: reactor arrangement during phase 1.

The reactor in phase 1 was built out of Inconel-625 with 25.4 mm inner diameter and 148 mm in height. The inlet and the outlet of the reactor were connected to 6.25 mm smooth-bore seamless stainless steel tubing via Swagelok reduction couplings. The inlet of the reactor, at the top, featured a tee, one end of which was used to feed the reactants, while the other end was used to introduce a k-type thermocouple through the reactor vessel until it touched the surface of the catalyst (see Fig. 5).

The catalyst was made from corrugated metal sheets on which the catalyst was bonded via methods proprietary to ASC. The catalyst sheets were circular in shape with 2.54 cm in diameter. Eight of these disks were stacked in 90^{o} rotations as per the direction of the corrugations achieving about 1.1 cm in height, and each disk had eight perforations roughly 3 mm in diameter each. The purpose of the 90^{o} rotations was to add tortuosity to the reactor, which helped renewing the boundary layer on the catalyst, while maintaining a low pressure drop. The catalyst, from hereby referred to as the monolith, was wrapped around quartz wool and descended into the reactor's bottom. Figure 6 shows the 8 catalyst disks used in phases 1, the same type of disk was used in phase 2. As shown in Figure 6, each disk has 8 randomly dispersed perforations. Images of catalyst used in phase 3 are in Appendix B.

A total of fifteen test conditions were conducted using this reactor setup. The total number of tests is summarized in Table 1, where test condition 1 was repeated 3 times and test condition 9 was not tested. Test condition 1 was chosen as the reference condition. Test condition 9 was unattainable at the current test rig pressure specifications. Later modifications were done in order to ensure higher pressure capabilities.

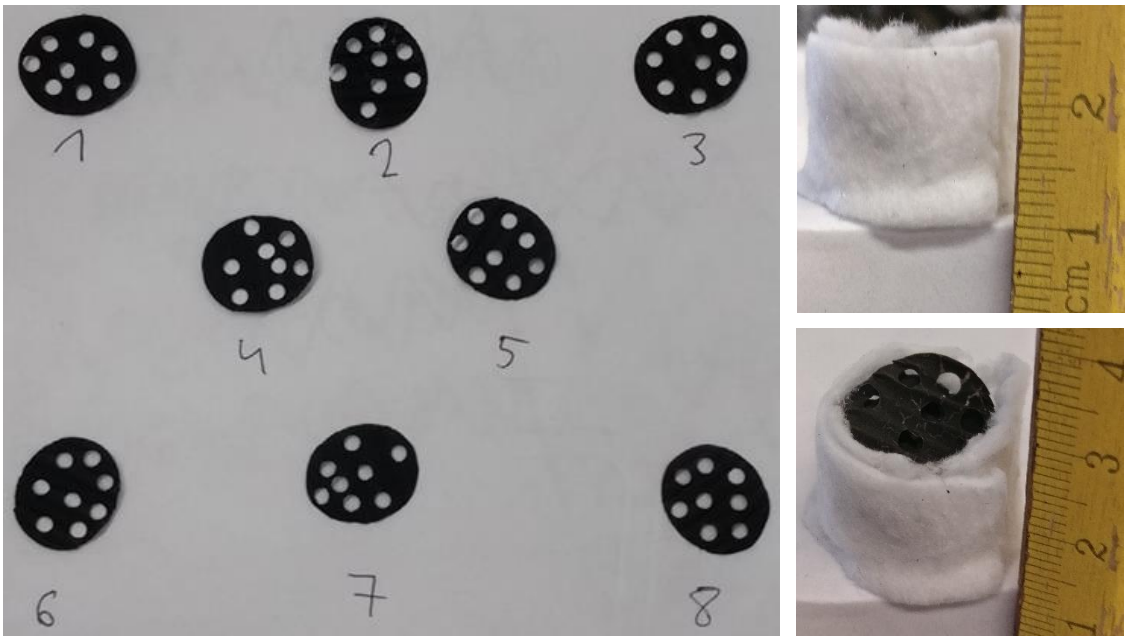

Figure 6: Left shows catalyst disks used in phase 1 reactor. Upper right shows the assembled reactor in quartz wool at its length of 1.1 cm. Lower right shows a top view of the reactor.

Test condition	Partial pressure		Flow rate	System pressure [atm]	Temperature [C]	S/C
	CH4	H2O				
1	0.383	1.130	1	1.56	700	3
2	0.383	1.130	2	1.50	700	3
3	0.383	1.130	3	1.50	700	3
4	0.383	1.130	4	1.50	700	3
5	0.250	1.245	1	1.50	700	5
6	0.250	1.245	2	1.50	700	5
7	0.250	1.245	3	1.50	700	5
8	0.250	1.245	4	1.50	700	5
9	1.600	4.800	1	6.40	700	3
10	0.383	1.130	1	1.56	400	3
11	0.383	1.130	1	1.56	500	3
12	0.383	1.130	1	1.56	600	3
13	0.383	1.130	1	1.56	800	3
14	0.383	1.130	1	1.50	900	3

Table 1: test matrix for phase 1.

The overall startup procedure followed during this phase can be described as follows:

1. Preheat the system;
2. Bring reactive species;
3. Bring system up to condition;
4. Sample effluent;
5. Shut system down.

The monolith was reduced before its first use and again on the sixth and ninth test days. These days were chosen at random as monolith reduction was not part of the day–to–day testing. During the reduction, 17%(v|v) hydrogen in nitrogen were introduced into the room temperature system for a total flow rate of 231 sccm. The temperature was then incremented at 20°C/min until 600°C were reached. The monolith was then reduced until there were no more changes in the hydrogen concentration as measured by the μGC (typically 1.5 hours). The system would be brought down in temperature and the regular testing procedure would follow.

Preheat the system

On a room temperature system, nitrogen was circulated for 30 minutes to displace any oxygen present in the system. The concentration of oxygen would be monitored on the μGC until it was undetecTable (~10 ppm). At this point the furnace would be set to 150°C.

Bring reactive species

Once the furnace reached its set point all components were brought into the monolith except for water. Water was circulated through the vaporizing coil and the overboard pail. According to suggestions from the monolith manufacturer, no liquid water should reach the catalyst. Thus, the team would visually inspect the steam line until no more liquid water exited. After confirmation, the steam was redirected towards the monolith via a stainless steel 3-way valve.

Bring the system up to condition

With the reactants flowing through the monolith, at the appropriate targeted volumetric flow rates, the reactor temperature was increased up to condition. In every test, the temperature setting was achieved first and then the back pressure was regulated until the desired reactor inlet temperature value was achieved. Nominally, the temperature program followed was to increase the reactor temperature in 100°C increments at 20°C/min until the desired reactor inlet temperature was reached. The backpressure was regulated by controlling the two metering valves located in the analyzer panel.

Sample effluent

The system was allowed to reach steady state and the effluent was sampled using the μGC. Between 3 — 5 samples were taken per test condition. The μGC was constantly sampling the effluent, however only the samples at conditions that were used for calculations. Thus, when "sampled" or "sampling" is mentioned, it is referring to data collected at condition.

Shut system down

Once the tests were completed all reacting species were shut off and nitrogen was circulated through the reactor system. For conditions where the required temperature was greater than 500°C the furnace, as per the furnace manufacturer's indications, was allowed to cool down to 500°C and then turned off. The system was then set in safe mode, i.e., no flow, all valves closed, atmospheric pressure, and furnace off.

The catalyst manufacturer chose to define steady state as the third consecutive μGC sample in which the hydrogen concentration had no change or a change of no more than ±5%. To achieve this, steady state flow rates, pressures and temperatures were maintained as close as possible to the test conditions supplied by ASC. Once these, so called, facility conditions had been met, then the effluent was sampled. This definition of steady state remained invariant for all phases.

The quality of the data taken at steady state rests upon the quality of the instrumentation calibration as well as the accuracy of the instrumentation and our ability to attain the desired target test conditions. Thus, to ensure the best quality possible with the instrumentation used for these tests, calibrations were performed before commencing testing. End-to-ends were also performed by conducting mock tests to observe if the response of the test rig was appropriate and where known standards were measured with the calibrated instrumentations and the yielded quantities were compared to determine the veracity of the data collected. Calibration checks were also performed periodically, albeit randomly. All calibrations can be seen in appendix A.

The data obtained in this phase will be presented and discussed in subsequent sections of this thesis, however, it is worthwhile to point out some of the shortcomings observed during this phase of testing. A single thermocouple was located at the center of the surface of the top disk of the monolith (see Fig. 5). From the caloric requirements of the reactions carried out, it was realized that the thermocouple was not providing an average temperature of the entire monolith but rather the temperature at a specific spot, i.e., a local temperature. Calculations confirming this hypothesis are provided in upcoming sections.

Another shortcoming of phase 1 is the lack of standardization of catalyst reduction schedules. During this phase the monolith was seldom reduced and those times when it was reduced, it was done aleatory. Due

to this, it is very hard, if not impossible, to draw any final conclusions from the data collected in phase 1. Although, good information was extracted from these data and the new knowledge applied to how the testing was conducted in phase 2.

3.3: Phase 2

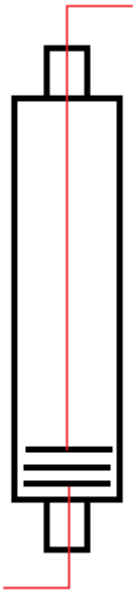

Figure 7: reactor arrangement during phase 2.

Much like phase 1, the reactor in phase 2 was built from Inconel-625 with 25.4 mm inner diameter and 148 mm in height. The inlet and the outlet were connected to 6.25 smooth-bore stainless steel tubing via Swagelok reduction couplings. As in phase 1, this reactor featured a tee at the inlet that allowed reactant flow and temperature measurement at the top of the monolith via a k-type thermocouple. This reactor also featured a tee at the outlet where another k-type thermocouple was introduced until it touched the bottom of the monolith, as shown in Figure 7.

The monolith was made much like phase 1, where perforated, corrugated disks were stacked on top of each other. Each disk was circular in shape with 2.54 cm in diameter and 8 perforations 3 mm in diameter each. The disks were stacked with 90 degrees rotations as per the direction of the ruffles up to a height of roughly 1.1 cm. The monolith was carefully wrapped in quartz wool and dropped to the bottom of the reactor. For reference, see Figures 6 and 7.

A total of 15 tests were conducted using this reactor. The total number of tests is summarized in Table 2, where test condition 9 was conducted twice.

Test Condition	Partial pressures [atm]			Flow rate	System pressure [atm]	Temperature [C]	S/C
	CH4	H2O	N2				
1	0.383	1.130	0.036	1	1.56	700	3
2	0.383	1.130	0.000	2	1.50	700	3
3	0.383	1.130	0.014	3	1.50	700	3
4	0.383	1.130	0.009	4	1.50	700	3
5	0.250	1.245	0.036	1	1.50	700	5
6	0.250	1.245	0.018	2	1.50	700	5
7	0.250	1.245	0.017	3	1.50	700	5
8	0.250	1.245	0.010	4	1.50	700	5
9	1.600	4.800	0.037	1	6.40	700	3
10	0.383	1.130	0.024	1	1.56	400	3
11	0.383	1.130	0.030	1	1.56	500	3
12	0.383	1.130	0.032	1	1.56	600	3
13	0.383	1.130	0.035	1	1.56	800	3
14	0.383	1.130	0.046	1	1.50	900	3

Table 2: test matrix for phase 2.

Although the reactor system was not perfect, the information learned during phase 1 helped improve the testing done in phase 2. The overall test procedure for phase 2 was very similar to the test procedure for phase 1. The only step where there was a major change was during the shutdown. Following recommendations from the manufacturer, the monolith was cooled down to 150°C under a nitrogen atmosphere after every test.

The reduction procedure remained exactly the same. 17 (v|v)% hydrogen in nitrogen was circulated through the monolith. During the reduction, the monolith began at room temperature and the temperature was increased at a rate of 20°C/min until 600°C were reached. During this phase the monolith was reduced every third test day.

Although the data collected during phase 2 was much more uniform, there were still some shortcomings. Although a second thermocouple was added to monitor the outlet temperature, the problem of measuring the temperature of a single spot rather than an overall average persisted. However, with the information obtained from these two thermocouple readings we were able to design a better reactor, which was used during phase 3.

Although a regular reduction schedule was implemented and the shutdown procedure was revised, there was still too much variability on the data. At the same time, the data showed catalyst underperformance when compared to phase 1. This issue was addressed on phase 3.

3.4: Phase 3

Phase 3 was divided in phase 3a, phase 3b, and phase 3c. The main difference between the 3 rounds of testing was the thickness of the catalyst on the substrate. Other than that, phases 3a and 3b were conducted using the same reactor morphology, test matrix, and test procedures, while phase 3c followed a slightly different test matrix.

Figure 8: reactor arrangement during phase 3.

Unlike previous phases, the reactor in phase 3 was manufactured from Inconel-625 with 10 mm inner diameter and 280 mm in height. The reactor inlet and outlet were connected to 6.25 mm diameter smooth-bore seamless stainless steel tubing via Swagelok reducing couplings. For this reactor both inlet and outlet tees were removed and instead 5, k-type, 1.6 mm diameter, thermocouples were located equidistantly along the height of the reactor. The thermocouples were connected via Swagelok nut and ferrules and the appropriate Swagelok bodies, which were modified and welded on the reactor. Figure 8 shows a reactor arrangement schematic.

The contents of the reactor during this phase was also significantly different from that of previous phases. Rather than using corrugated disks, this phase used 3 mm diameter

disks referred to as punch outs. These punch outs were mixed with 300 μm diameter inert α-alumina particles to approximate a packed bed. The reactor was subdivided in three zones: top inert zone, reactive zone, and bottom inert zone.

The top and bottom inert zones consisted entirely of α-alumina. From the specifications of the reactor both zones had to be 40 mm in height, which was equivalent to 6 g. The reactive zone made up the middle 200 mm along the height of the reactor, which was equivalent to 30 g. There was no special packing done anywhere on the packed bed. All zones were poured in the reactor, and then sealed. At the bottom of the reactor a quartz frit was placed on the bottom coupling and a thin layer of quartz wool was placed on the frit, thus preventing any runoff of the reactor contents. A quartz frit was also placed below the top coupling.

For the reactive zone, the punch outs were mixed with the α-alumina. The total amount of punch outs was calculated to be 5(w|w)% of the reactive zone. The reactive zone was equivalent to 30 g, out of which 28.5 g were α-alumina and 1.5 g were punch outs. The contents of the reactive zone were divided into 10 more or less equal weight portions and poured into the reactor to prevent agglomeration of punch outs.

For phase 3a, a total of 9 test conditions were performed (Table 3). Phase 3b had a total of 7 test conditions (Table 4). Phase 3c had a total of 4 test conditions (Table 5). A few test conditions, namely test condition 9 on phase 3A and test condition 4 on phase 3B, were determined during the active testing sequence based on data obtained during the campaign. That is, those were conditions that had not been previously planned and were thought of at the time to observe variations on the catalyst.

Test Condition	Partial Pressure [atm]				Flow rate L/min]	System pressure [atm]	Temperature [C]	S/C	H2/CH4
	CH4	H2O	N2	H2					
1	0.451	1.010	0.039	0.000	1.5	1.5	550	3	0
2	0.451	1.010	0.039	0.000	3.0	1.5	550	3	0
3	0.451	1.010	0.039	0.000	6.1	1.5	550	3	0
4	0.451	1.010	0.039	0.000	6.1	1.5	550	3	0
5	0.454	1.016	0.018	0.012	3.6	1.5	500	3	0.027
6	0.428	1.073	0.017	0.011	3.6	1.5	500	3	0.027
7	0.585	2.376	0.024	0.016	3.6	3.0	500	6	0.027
8	0.903	2.067	0.018	0.012	3.6	3.0	500	3	0.013
9	0.895	2.060	0.027	0.018	3.6	3.0	500	3	0.020

Table 3: test matrix for phase 3A.

Test Condition	Partial Pressure [atm]				Flow rate L/min]	System pressure [atm]	Temperature [C]	S/C	H2/CH4
	CH4	H2O	N2	H2					
1	0.239	0.717	0.025	0.403	3.6	1.38	500	3	1.69
2	0.185	1.110	0.025	0.403	3.6	1.72	500	6	2.18
3	0.345	1.034	0.025	0.806	3.6	2.21	500	3	2.34
4	0.320	0.961	0.025	1.251	4.4	2.56	500	3	3.91
5	0.241	0.723	0.027	0.403	3.6	1.39	550	3	1.67
6	0.185	1.109	0.027	0.403	3.6	1.72	550	6	2.18
7	0.345	1.034	0.027	0.806	3.6	2.21	550	3	2.34

Table 4: test matrix for phase 3B.

Test Condition	Partial Pressure [atm]				Flow rate L/min]	System pressure [atm]	Temperature [C]	S/C	H2/CH4
	CH4	H2O	N2	H2					
1	0.281	0.843	0.025	0.351	4.2	1.50	500	3	1.25
2	0.281	0.843	0.025	0.351	4.2	1.50	600	3	1.25
3	0.281	0.843	0.025	0.351	4.2	1.50	700	3	1.25
4	0.283	0.850	0.012	0.354	8.4	1.50	500	3	1.25

Table 5: test matrix for phase 3C.

The testing procedure for phase 3 was derived from the lessons learned during phases 1 and 2. Overall, the test procedure followed the following protocol:

1. bring reducing species;
2. reduce catalyst;
3. bring temperature down;
4. bring reacting species;
5. bring system up to condition;
6. sample effluent;
7. shut system down.

Bring reducing species

In a cold system 17(v|v)% hydrogen in nitrogen was circulated through the system. The cold, effluent species distribution was monitored with the μGC until no other species were detected other than hydrogen and nitrogen. The detectability limit of the μGC according to the manufacturer is ~10 ppm.

Catalyst reduction

Once the system was saturated with hydrogen and nitrogen the temperature was brought up to 600°C at a rate of 20°C/min. The system was reduced for a total of 1.5 hours at 600°C.

Bring temperature down

Upon completing the catalyst reduction the temperature was brought down to 125°C. The system was cooled down while circulating the same distribution of hydrogen and nitrogen.

Bring reacting species

Once the system was cooled down under a hydrogen/nitrogen atmosphere, the inlet species distribution was set according to the test matrix. Condition flow rates and pressures were set at this point and watched closely as the system was heat up.

Bring system up to condition

The system was brought up to condition in terms of temperature and pressure. During temperature ramp up the backpressure understandably drifted up, and therefore it was necessary to adjust it accordingly.

Sample effluent

The system's effluent was sampled during temperature ramp up and once at condition. 3 – 5 samples were taken at each test condition steady state.

Shut system down

During the shutdown procedure the flow of all reactive species, i.e., methane, steam, and hydrogen, was stopped while the system was flooded with inert. The flow of inert was kept on until the temperature along the reactor was below 125°C.

The main challenge during phase 3 was keeping the reactor temperature as uniform as possible. In order to achieve this, on the spot modifications had to be done on the temperature of the furnace's rector zone and the zones immediately above and below this. The inlet species distribution also had to be modified by increasing the proportion of hydrogen when needed. Hydrogen being a reaction inhibitor.

Chapter 4: Results and Discussion

4.1: Mass balances

The mass balances were measured via the addition of an inert nitrogen tracer during tests. For phase 1 an attempt to close the mass balances with an orifice rather than a tracer was made, however, the orifice proved to be inefficient timewise due to several factors among which were the fact that the orifices were not compliant with ASME standards, thus requiring constant and time consuming recalibrations. The strategy employed with the orifice was to measure the total dry volumetric flow rate of the system and calculate the effluent species distributions from the mole fractions.

The strategy employed to close the mass balance without the orifice was to divide the balances between a carbon balance and a water balance. For the carbon balance, the μGC was used to sample the dry effluent gas distribution. The total number of moles were calculated with the aid of the inert tracer. The total number of carbon moles measured at the effluent were then compared to the total number of moles introduced into the system. The equations used to calculate the carbon balance were the following:

$$Carbon\ balance = \frac{n_{CH4}^{in} - n_{C}^{out}}{n_{CH4}^{in}}$$

(eq. 9)

Where n_{CH4}^{in} is the molar flow rate of methane at the inlet of the reactor in [mol/min], and n_{C}^{out} is the molar flow rate of carbon in the form of gaseous chemical species at the outlet of the reactor in [mol/min].

The methane molar flow rate in was calculated from,

$$n_{CH4}^{in} = \frac{q_{CH4}^{in}\,\rho_{CH4}}{MW_{CH4}}$$

(eq. 10)

Where q_{CH4}^{in} is the volumetric flow rate of methane at the inlet as measured by the flow controllers in [sccm], ρ_{CH4} is the density of methane at the inlet conditions in [g/cm^3], and MW_{CH4} is the molecular weight of methane in [g/mol].

The carbon in the effluent was calculated by,

$$n_{CH4}^{out} = y_{C}^{dry,out}.\frac{q_{tot}^{dry,out}\,\rho_i}{\sum_i MW_i}$$

(eq. 11)

Where i represents CH_4, CO_2, or CO, $q_{tot}^{dry,out}$ is the dry total volumetric flow rate in [sccm], $y_C^{dry,out}$ is the mole fraction of carbon species in the dry effluent, ρ_i is the density of species i at effluent conditions in [g/cm^3], MW_i is the molecular weight of species i in [g/mol].

The water balance had to be measured indirectly due to the limitations of the setup. For the water balance the total number of oxygen containing species and hydrogen containing species were tracked enabling an atom balance to be used for calculation. Again with the aid of the inert tracer, the total number of equivalent oxygen moles were calculated for the dry effluent. In parallel, the total number of equivalent hydrogen moles were also calculated. With the assumption that the carbon balance closed, the water balance was calculated by comparing the number of moles obtained via oxygen measurements and the number of moles obtained via hydrogen measurements. The equations used to calculate the water balance were the following:

$$water\ balance = \frac{n_{H2O}^{O} - n_{H2O}^{H}}{n_{H2O}^{O}}$$

(eq. 12)

Where n_{H2O}^{O} is the average amount of oxygen at the effluent in [mol/min], and n_{H2O}^{H} is the average amount of hydrogen at the effluent in [mol/min].

$$n_{H2O}^{O} = n_{O}^{in} - (y_{CO}^{dry,out} + 2y_{CO2}^{dry,out})n_{tot}^{dry,out}$$

(eq. 13)

$$n_{H2O}^{H} = \frac{n_{H}^{in} - (2y_{H2}^{dry,out} + 4y_{CH4}^{dry,out})n_{tot}^{dry,out}}{2}$$

(eq. 14)

Table 6 shows the results of these calculations as fractional balances. These values represent an accounting of all the moles of carbon through the system and all the moles of water through the system. Ideally all these values should equal zero, however, due to systematic and random errors a degree of tolerance is employed during the interpretation of such calculations.

Test Condition	Phase 1		Phase 2		Phase 3A		Phase 3B		Phase 3C	
	Carbon Balnce	Water Balnce	Carbon Balnce	Water Balnce	Carbon Balnce	Water Balnce	Carbon Balnce	Water Balnce	Carbon Balnce	Water Balnce
1	0.014	0.552	0.232	0.079	0.044	0.048	0.044	0.048	0.060	-0.056
2	0.061	0.310	0.059	0.081	0.017	0.033	0.017	0.033	0.017	-0.090
3	-0.003	0.310	0.001	0.075	0.084	0.063	0.084	0.063	0.079	-0.100
4	0.006	0.310	0.011	0.115	0.026	0.025	0.026	0.025	0.060	-0.056
5	0.340	0.494	0.233	0.048	0.036	0.026	0.036	0.026	0.017	-0.032
6	0.460	0.494	0.004	0.037	0.032	0.010	0.032	0.010		
7	0.259	0.476	0.118	0.075	0.026	0.017	0.026	0.017		
8	0.264	0.476	0.179	0.074						
9	-	-	0.051	0.002						
9*			0.039	0.000						
10	0.270	0.494	0.044	0.000						
11	0.800	0.494	-0.015	0.000						
12	0.530	0.552	0.069	0.017						
13	0.180	0.552	0.041	0.116						
14	0.310	0.552	0.008	0.164						
15	0.014	0.476								
16	0.018	0.310								

Table 6: Fractional carbon balance and fractional water balance for phases 1 through 3. Carbon balance was measured experimentally while water balance was calculated from data (n = 49).

4.2: Product distribution

The product distributions for all tests was measured using the μGC. All these measurements were taken using the dry effluent leaving the condenser. The water distribution was calculated as described in the water balance.

The methane conversion was calculated from the product. This was possible because there was a single carbon source. In principle, such calculation could be done by comparing the input moles of methane to the output moles of methane, however after careful analysis of our data the former method was found to be more accurate than the latter. This is because small conversions of methane during the testing necessitated a calculation of a small change from a large number. However, when using the product gases, that calculation used a value (i.e., concentration of CO) compared to a zero initial value.

Figure 9 shows the product distribution for each test condition of phase 3A. The rest of the product distribution Figures are shown in Appendix C. Figure 9 is a good start for familiarizing oneself with the data, that said, due to the convolution of all the pertinent parameters (i.e., temperature, pressure, GHSV, reactant distribution, etc.), Figures 10 and on provide better insight on the behavior of the catalyst.

4.3: Temperature hysteresis

A hysteresis in temperature was observed. It was particularly prevalent in phase 2. It was observed that the catalyst was fully active after reaching 725℃. Once the catalyst was activated, it was possible to go up and down in temperature as desired.

During phase 1 the test condition temperature was selected from the beginning of the test. From phase 2 on the catalyst was activated prior to testing. The procedure has been outlined in the experimental section. This activation protocol was obviated for test conditions requiring temperatures above 725℃, because this was found to be the activation temperature of the catalyst.

4.4: Definition of accepTable data

For the purpose of these experiments the term “good quality” data was defined as a data point that has a mass balance within a +/- 5% range. In addition to closing its mass balance, every data point was also observed for trend continuity. A data point was labeled continuous if it followed an observed trend for any changing parameter. For example, when measuring conversion as a function of changing temperature, the observed trend is that of increasing conversion with increasing temperature. If at any given moment the calculated conversion would be an outlier in the opposite direction of that which was being observed, then the data point was deemed of “not good quality” and revisited. Oftentimes, when a data point was regarded as not good quality, it would be due to some other parameter that was not been inspected closely at a particular moment in which it would fall outside of the range it was expected to be. The handling procedure was to discard all data at the given condition and collect new, sufficient data before changing conditions.

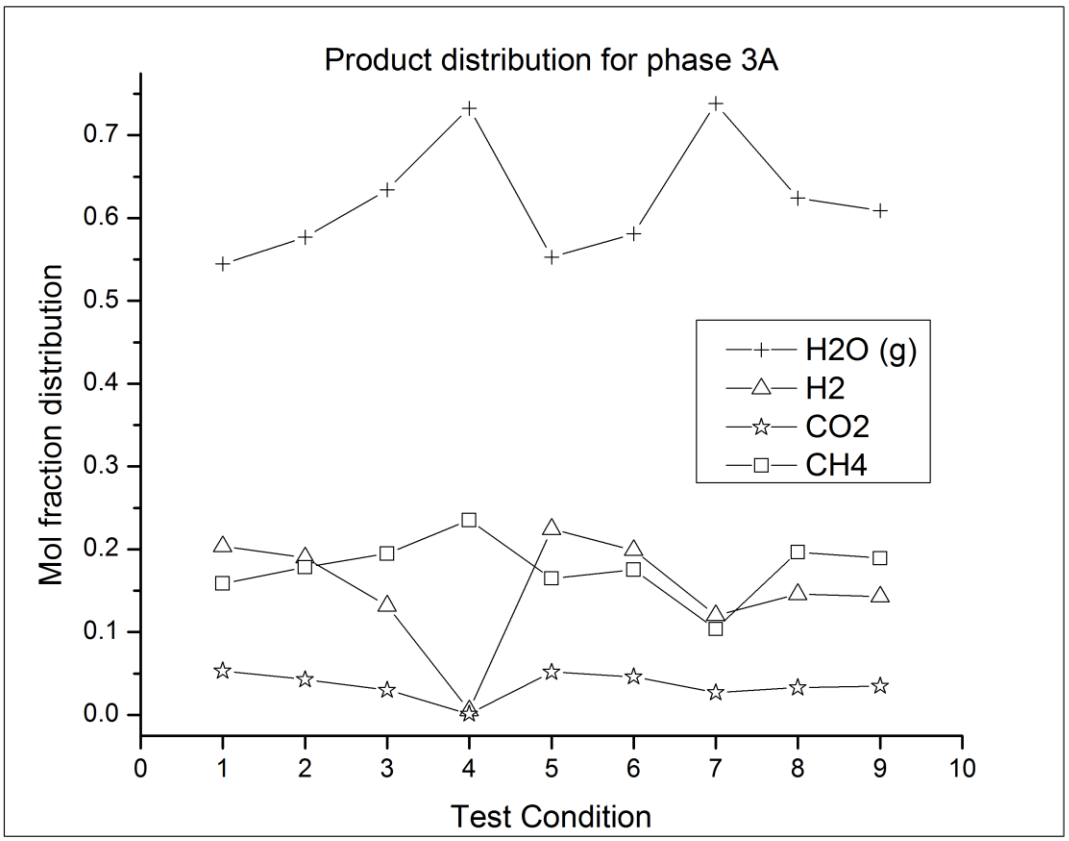

Test conditions	H2O (g)	H2	CO2	CH4
1	0.545	0.204	0.053	0.159
2	0.577	0.190	0.043	0.179
3	0.634	0.132	0.030	0.195
4	0.733	0.005	0.001	0.235
5	0.553	0.224	0.052	0.165
6	0.581	0.199	0.046	0.176
7	0.738	0.120	0.027	0.104
8	0.624	0.146	0.033	0.197
9	0.609	0.143	0.035	0.189

Figure 9: product distribution for phase 3A (above) along with ancillary Table (below). Figure shows steady state distribution for phase 3A as measured with μGC. No additional information on condition parameters (i.e., T and P) provided. Full data Table provided on Appendix C.

4.5: Catalyst performance

The performance of the catalyst used in this work was evaluated in terms of its methane conversion and its hydrogen selectivity. The methane conversion was calculated from the number of moles of methane before and after reaction. The conversion was calculated as follows:

$$X_{CH_4} = {\dot{n}_C^{out}}\Big/{\dot{n}_{CH_4}^{in}}$$

(eq. 15)

where X_{CH4} is the methane conversion, $\dot{n}_C^{out}$ is the converted carbon effluent molar flow rate, and $\dot{n}_{CH4}^{in}$ is the methane unreacted molar flow rate.

The hydrogen selectivity was calculated from the net reaction products. All these measurements were taken at the effluent. The hydrogen selectivity was calculated as follows:

$$S_{H_2} = \frac{\dot{n}_{H_2}^{out,net}}{\dot{n}_{H_2}^{out,net} + \dot{n}_{CO}^{out} + \dot{n}_{CO_2}^{out}}$$

(eq. 16)

where S_{H2} is the hydrogen selectivity, $\dot{n}_{H2}^{out,net} = \dot{n}_{H2}^{out} - \dot{n}_{H2}^{in}$ is the net moles of hydrogen produced, $\dot{n}_{CO}^{out}$ is the moles of carbon monoxide produced, and $\dot{n}_{CO2}^{out}$ is the moles of carbon dioxide produced.

During phase 1 there were no special precautions about the test sequence. However, after confirming the catalyst activation requirement, a protocol was implemented where the catalyst was activated before carrying the experiments. This protocol was used starting with phase 2. The experiments were carried out in a sweeping fashion, where the tests would start at the lower test temperature achieving steady state for each test condition. After data was collected, and it was determined that the data collected was of "good quality", the reactor's temperature was incremented to the next higher-temperature test condition.

The performance of the catalyst studied in this work was compared to that of Xu's work [14] whenever possible. This work was chosen because in it Xu outlines the most widely used catalytic intrinsic kinetics model for steam-methane reforming. From now on, the catalyst used in this work will be referred to as ASC's catalyst in its distinctive phases and the catalyst used in Xu's work will be referred to as Xu's catalyst.

4.6: Catalyst behavior as a function of temperature

When analyzing the behavior of ASC's catalyst, it was immediately apparent that there was variability from phase to phase. The clearest variability appeared to be that between the fixed phases and the dispersed phases. During phases 1 and 2 the morphology of the reactor was considered "fixed" because the perforated coin size corrugated disks were used. Conversely, during phases 3A,B,C the morphology of the reactor was considered "dispersed" because 3 mm punch outs were dispersed through a packed bed mixed with inert α-alumina. Both of these morphologies had been described in the experimental section.

A conversion vs temperature comparison was done between Xu's catalyst and ASC's catalyst through all phases. As expected there was a clear positive correlation between conversion and temperature. As shown in Figure 10 the data show a pronounced difference in conversion between Xu's catalyst and most ASC catalyst phases. With the exception of phase 3C, ASC phases show greater conversion than Xu's catalyst for temperatures within a similar range. It is important to remark that these are not direct comparisons as the conditions were not replicated exactly. The exception to this statement is ASC phase 3A where Xu's conditions were replicated.

From Figure 10 the rates of reaction were calculated and their natural logarithms and displayed on Figure 11. Figure 11 shows the natural logarithm of the reaction rate vs the inverse temperature for all ASC test phases in comparison to Xu. Figure 11 shows an approximate order of reaction of one, as observed by the nearly linear relation between the range and the domain.

Nonetheless, phase 3C shows a very mild dependence on temperature. A plausible explanation for this phenomenon might be the change in coating thickness that occurred in phase 3. For phase 3A the punch outs had a thickness of 50.8 μm, while phases 3B and 3C had a thickness of 101.6 μm. The total mass of active material, however, remained constant at 122.2475 mg.

In this work the turnover frequency (TOF) was calculated from

$$TOF = \frac{-r_A MW_{Ni}}{f_{act,site}} \qquad \text{(eq. 17)}$$

where $-r_A$ is the rate of reaction of methane, MW_{Ni} is the molecular weight of nickel, and $f_{act,site}$ is the fraction of active sites per mole of catalyst as supplied by ASC. Figure 12 shows a comparison of TOF vs temperature for Xu and ASC phase 3. As a reminder, all experiments in phase 3 were performed following Xu's guidelines. Figure 12 clearly shows much greater activity in phases 3A and 3B than Xu, and the data show a slightly higher activity profile of ASC phase 3C than Xu. Moreover, Figure 12 also shows that ASC's catalyst is very sensitive to temperature as shown by the slopes of the data.

Hydrogen selectivity could not be calculated from Xu's report due to lack of data. Therefore the hydrogen selectivity for all ASC phases is shown in Figure 13. As it can be observed, the lowest hydrogen selectivity obtained was 60% at a temperature of 680K during phase 1. It can also be observed the overall preeminence towards more hydrogen selection in the dispersed phases vs the fixed phases.

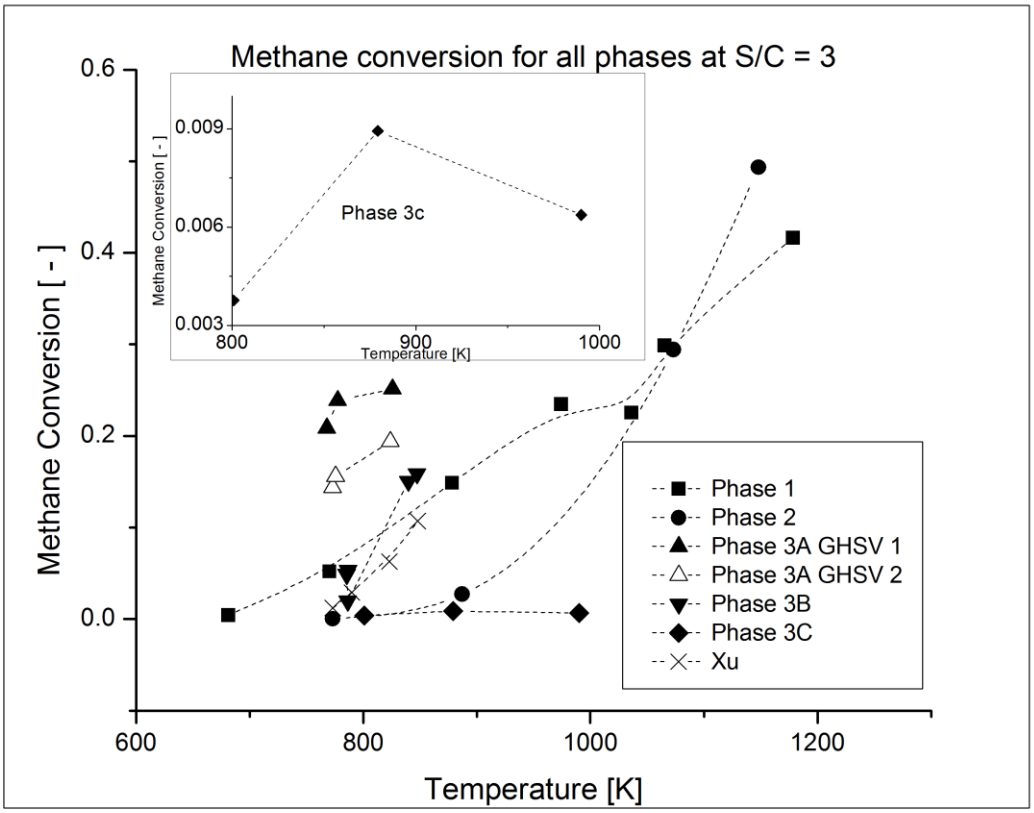

Temperature [K]	Methane Conversion [-]	Comment	Temperature [K]	Methane Conversion [-]	Comment
681	0.004	Phase 1	826	0.251	Phase 3A GHSV 1
768	0.209	Phase 3A GHSV 1	840	0.150	Phase 3B
770	0.052	Phase 1	847	0.158	Phase 3B
773	0.012	Xu	848	0.107	Xu
773	0.144	Phase 3A GHSV 2	878	0.149	Phase 1
773	0.000	Phase 2	879	0.009	Phase 3C
776	0.156	Phase 3A GHSV 2	887	0.027	Phase 2
778	0.239	Phase 3A GHSV 1	974	0.235	Phase 1
785	0.049	Phase 3B	990	0.006	Phase 3C
786	0.019	Phase 3B	1036	0.225	Phase 1
786	0.053	Phase 3B	1065	0.299	Phase 1
790	0.029	Xu	1073	0.294	Phase 2
801	0.004	Phase 3C	1148	0.494	Phase 2
823	0.063	Xu	1178	0.417	Phase 1
824	0.194	Phase 3A GHSV 2			

Figure 10: Methane conversion vs temperature at steam-to-carbon ratio of 3 for all phases (above) and ancillary Table (below). Figure shows steady state methane conversion at operating temperature in comparison to results obtained by Xu (n=25). Full data Table provided on Appendix C.

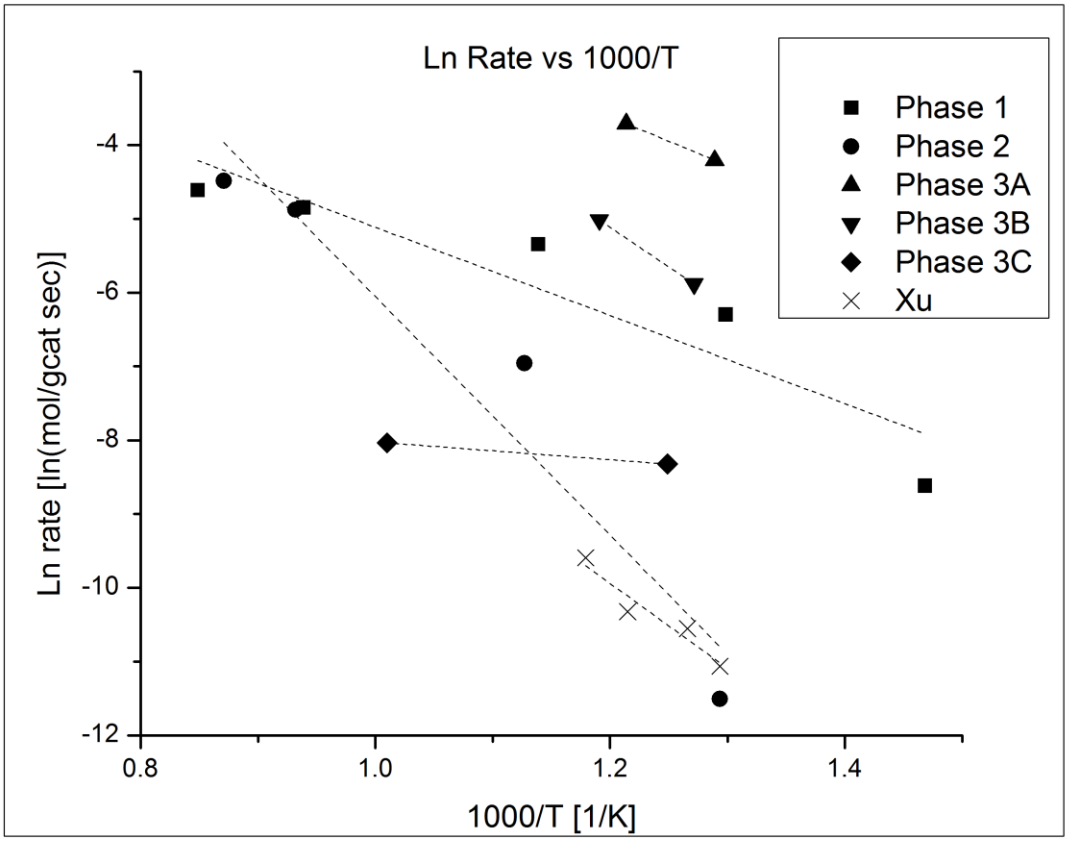

1000/T [1/K]	Ln Rate [ln(mol/gcat sec)]	Comment	1000/T [1/K]	Ln Rate [ln(mol/gcat sec)]	Comment
0.85	-4.61	Phase 1	1.22	-10.32	Xu
0.87	-4.48	Phase 2	1.25	-8.32	Phase 3C
0.93	-4.87	Phase 2	1.27	-10.55	Xu
0.94	-4.84	Phase 1	1.27	-5.88	Phase 3B
1.01	-8.03	Phase 3C	1.29	-4.21	Phase 3A
1.13	-6.96	Phase 2	1.29	-11.51	Phase 2
1.14	-5.34	Phase 1	1.29	-11.06	Xu
1.18	-9.59	Xu	1.30	-6.29	Phase 1
1.19	-5.01	Phase 3B	1.47	-8.62	Phase 1
1.21	-3.71	Phase 3A			

Figure 11: natural logarithm of reaction rate vs inverse temperature for all phases (above) and ancillary Table (below). Figure shows nearly linear range-to-domain relation (n=15). Full data Table provided on Appendix C.

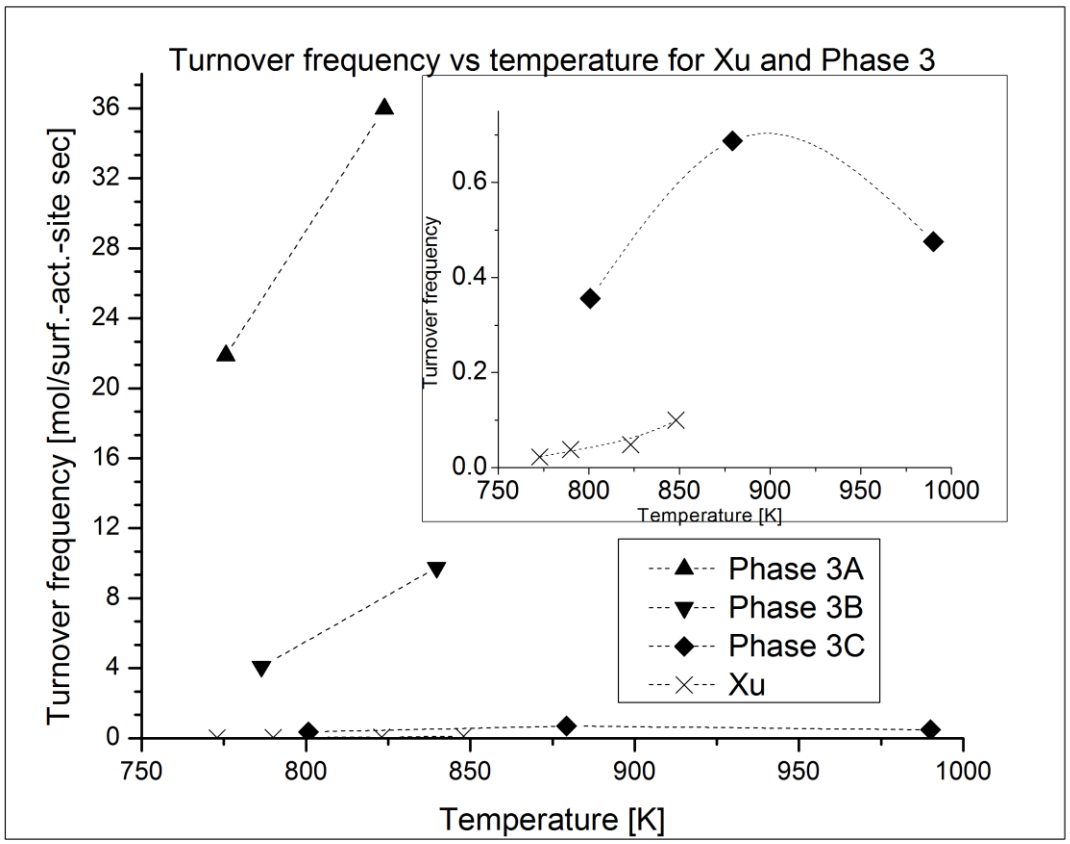

Temperature [K]	TOF [mol / surf.-act.-site sec]	Comment
773	0.023	Xu
776	21.888	Phase 3A
786	4.097	Phase 3B
790	0.038	Xu
801	0.356	Phase 3C
823	0.048	Xu
824	35.982	Phase 3A
840	9.750	Phase 3B
848	0.100	Xu
879	0.688	Phase 3C
990	0.476	Phase 3C

Figure 12: turnover frequency vs temperature for Xu's catalyst and ASC phases 3A, 3B and 3C (above), and ancillary Table (below). Figure shows TOF of ASC being much larger than Xu by 3 orders of magnitude (phase 3A), 2 orders of magnitude (phase 3B), and 17x (phase 3C) (n=7). Full data Table provided on Appendix C.

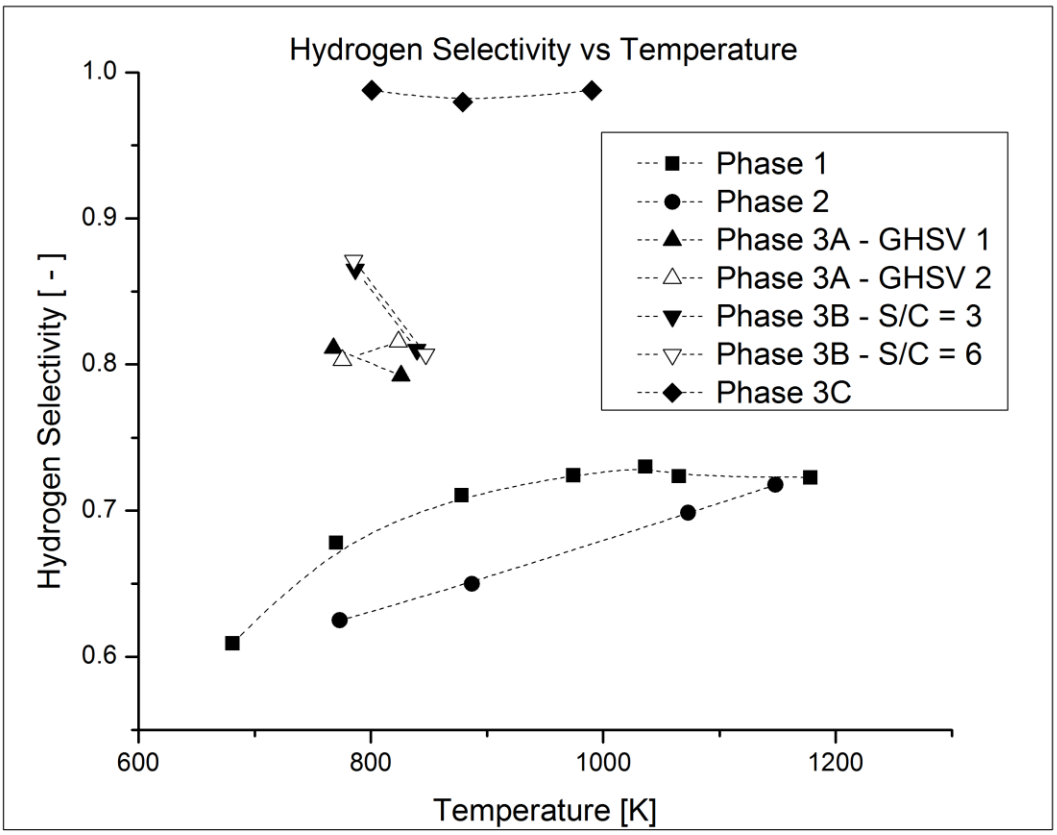

Temperature [K]	Hydrogen Selectivity [-]	Comment	Temperature [K]	Hydrogen Selectivity [-]	Comment
681	0.609	Phase 1	847	0.807	Phase 3B - S/C = 6
768	0.811	Phase 3A - GHSV 1	878	0.711	Phase 1
770	0.678	Phase 1	879	0.980	Phase 3C
773	0.625	Phase 2	887	0.650	Phase 2
776	0.803	Phase 3A - GHSV 2	974	0.724	Phase 1
785	0.871	Phase 3B - S/C = 6	990	0.988	Phase 3C
786	0.865	Phase 3B - S/C = 3	1036	0.730	Phase 1
801	0.988	Phase 3C	1065	0.724	Phase 1
824	0.816	Phase 3A - GHSV 2	1073	0.698	Phase 2
826	0.793	Phase 3A - GHSV 1	1148	0.718	Phase 2
840	0.810	Phase 3B - S/C = 3	1178	0.723	Phase 1

Figure 13: hydrogen selectivity vs temperature for all phases (above) and ancillary Table (below). Figure shows an overall superiority towards hydrogen selection of the dispersed phases above the fixed phases (n=22). Full data Table provided on Appendix C.

4.7: Catalyst behavior as a function of space-time

In addition to temperature variations, space-time variations were done for this work. The space-time is the time taken by the reactants to go through the reactor volume once for a fixed set of conditions. It was calculated from,

$$\frac{W}{F_o} = \frac{W_{act}}{\dot{n}_{CH_4}^{in}}$$

(eq. 18)

where W_{act} is the weight of active catalyst in [g], $\dot{n}_{CH_4}^{in}$ is the incoming mole flow rate of methane in [mol/hr]. There were several differences between the fixed and the dispersed phases on how these experiments were performed. During the fixed phases there was no hydrogen added, and the temperature was kept close to 973 K. All the space-time variations were done for a steam-to-carbon ratio of 3 and 5. In these experiments, the space-time was adjusted discretely from a baseline of 0.039 g-cat hr/mole CH_4 down 0.020, 0.009, and 0.005 g-cat hr/mole CH_4, that is the GHSV was doubled, tripled and quadrupled.

In contrast, during the dispersed phases hydrogen was added for all tests at a mole ratio of 1.25 hydrogen-to-methane. All these experiments were done at a steam-to-carbon ratio of 3, with exception of phase 3C where the steam-to-carbon ratio used was 5. Space-time observations were performed at different temperatures for phases 3A and 3B, where the temperature was maintained between 773 K and 823 K.

For this analysis the data were partitioned by phase, as in the previous subsection, and also by whether or not hydrogen was added during the experiment due to the inhibiting effect of hydrogen [20]. This effectively divides the data between fixed phases and dispersed phases. Although the data obtained from Xu will be used as an overall reference, they do not compare to the fixed phase data because of the hydrogen present on the inlet stream.

Figure 14 shows a comparison of methane conversion to space-time for the fixed phases. The methane conversion for ASC is on average 23% above the conversion obtained by Xu. However, phases 1 and 2 did not feature the addition of hydrogen to the reactant stream. Similarly, Figure 15 shows a plot of methane conversion to space-time for the dispersed phases. As with the fixed phases, the dispersed phases show an increased conversion with increasing space-time.

Figure 16 shows a plot of turnover frequency vs space-time for all the data. The data presented in Figure 16 follow the same partitioning as in Figure 14 and 15. From this Figure it can be appreciated that there is a clear demarcation between the fixed and the dispersed phases. From the fixed phases we can infer that the steam-to-carbon ratio had no major effect on the TOF. Similarly, from the dispersed phase it can be inferred that the temperature did not have a major effect either. This was expected due to the addition of hydrogen on the dispersed phases, hydrogen being an inhibitor.

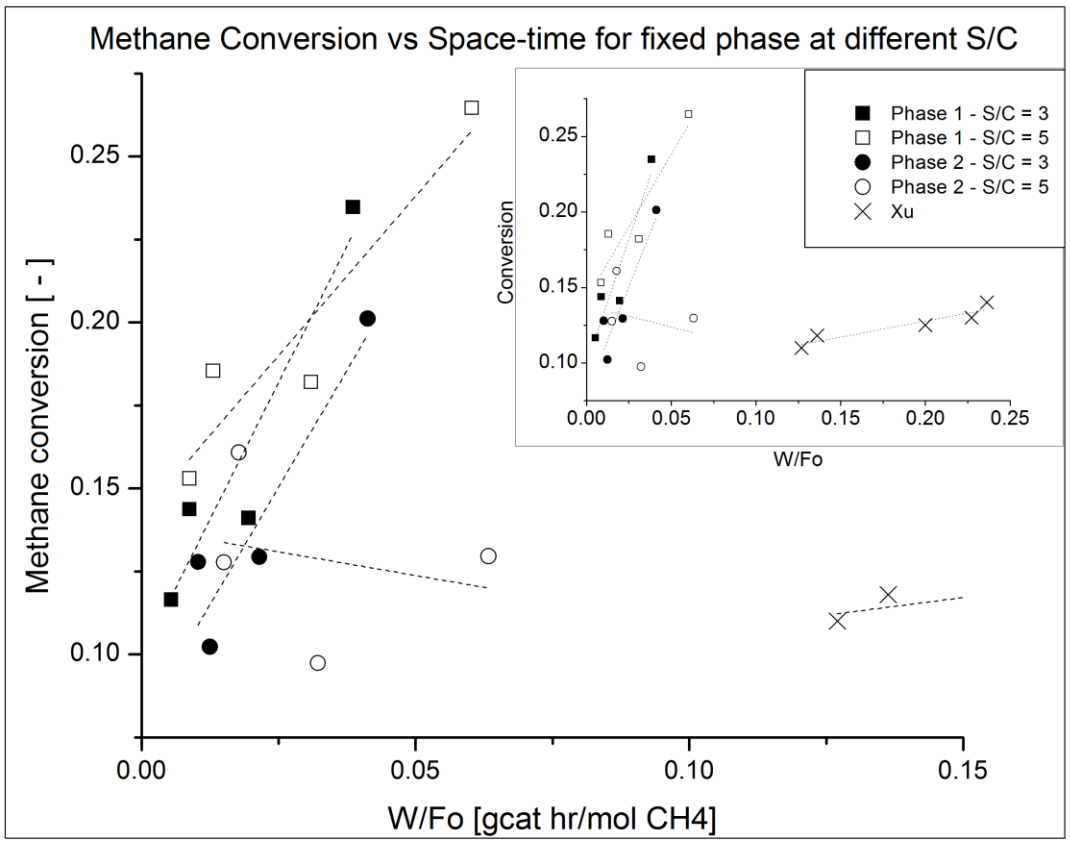

W/Fo [gcat hr/mol CH4]	Methane conversion	Comment	W/Fo [gcat hr/mol CH4]	Methane conversion	Comment
0.005	0.117	Phase 1 - S/C = 3	0.032	0.097	Phase 2 - S/C = 5
0.009	0.153	Phase 1 - S/C = 5	0.039	0.235	Phase 1 - S/C = 3
0.009	0.144	Phase 1 - S/C = 3	0.041	0.201	Phase 2 - S/C = 3
0.010	0.128	Phase 2 - S/C = 3	0.060	0.265	Phase 1 - S/C = 5
0.012	0.102	Phase 2 - S/C = 3	0.063	0.130	Phase 2 - S/C = 5
0.013	0.185	Phase 1 - S/C = 5	0.127	0.110	Xu
0.015	0.128	Phase 2 - S/C = 5	0.136	0.118	Xu
0.018	0.161	Phase 2 - S/C = 5	0.200	0.125	Xu
0.020	0.141	Phase 1 - S/C = 3	0.227	0.130	Xu
0.022	0.129	Phase 2 - S/C = 3	0.236	0.140	Xu
0.031	0.182	Phase 1 - S/C = 5			

Figure 14: Methane conversion vs space-time for the fixed phase (above) and ancillary Table (below). Figure shows a trend of increasing conversion with space-time (n=16). Full data Table provided on Appendix C.

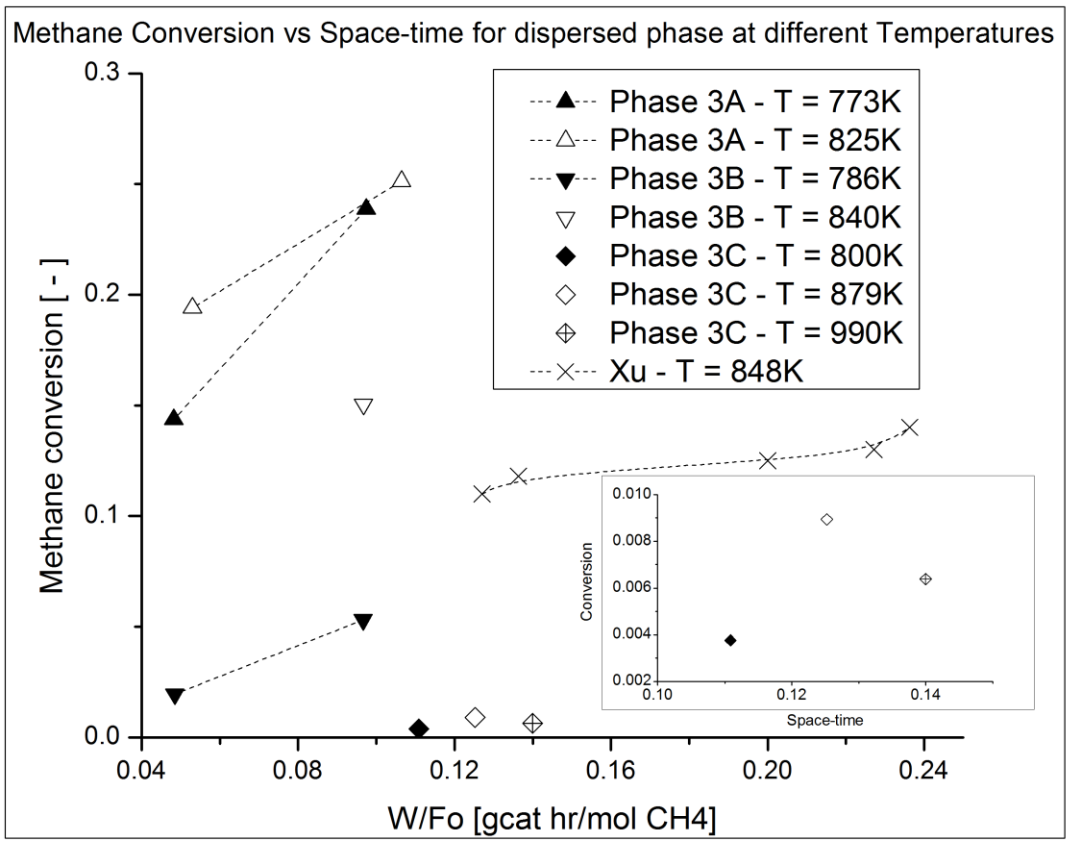

W/Fo [gcat hr/mol CH4]	Methane conversion [-]	Comment
0.048	0.144	Phase 3A - T = 773K
0.048	0.019	Phase 3B - T = 786K
0.053	0.194	Phase 3A - T = 825K
0.097	0.053	Phase 3B - T = 786K
0.097	0.150	Phase 3B - T = 840K
0.097	0.239	Phase 3A - T = 773K
0.106	0.251	Phase 3A - T = 825K
0.111	0.004	Phase 3C - T = 800K
0.125	0.009	Phase 3C - T = 879K
0.127	0.110	Xu - T = 848K
0.136	0.118	Xu - T = 848K
0.140	0.006	Phase 3C - T = 990K
0.200	0.125	Xu - T = 848K
0.227	0.130	Xu - T = 848K
0.236	0.140	Xu - T = 848K

Figure 15: methane conversion vs space-time for the dispersed phase (above) and ancillary Table (below). Figure shows a trend of increasing conversion with space-time (n=10). Full data Table provided on Appendix C.

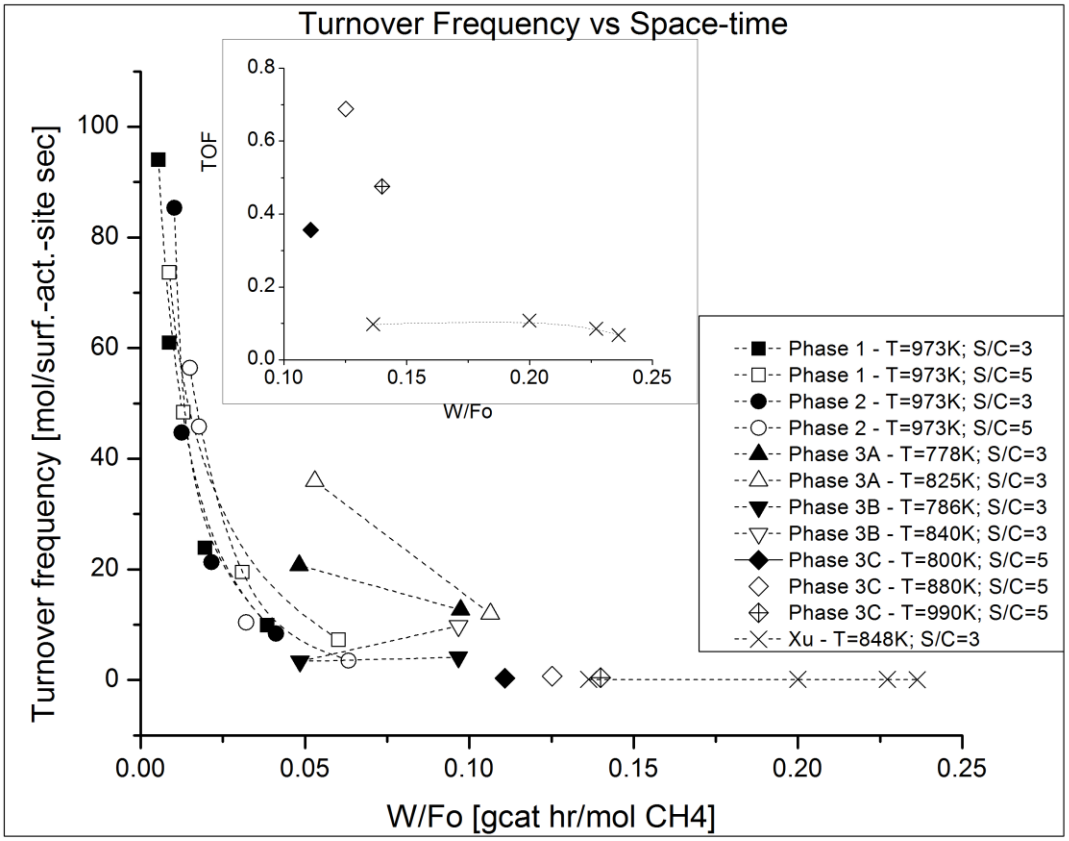

W/Fo [gcat hr/mol CH4]	TOF [mol/surf.-act.-site sec]	Comment	W/Fo [gcat hr/mol CH4]	TOF [mol/surf.-act.-site sec]	Comment
0.005	94.037	Phase 1 - T=973K; S/C=3	0.048	3.372	Phase 3B - T=786K; S/C=3
0.009	73.646	Phase 1 - T=973K; S/C=5	0.053	35.982	Phase 3A - T=825K; S/C=3
0.009	60.954	Phase 1 - T=973K; S/C=3	0.060	7.230	Phase 1 - T=973K; S/C=5
0.010	85.341	Phase 2 - T=973K; S/C=3	0.063	3.480	Phase 2 - T=973K; S/C=5
0.012	44.731	Phase 2 - T=973K; S/C=3	0.097	4.097	Phase 3B - T=786K; S/C=3
0.013	48.390	Phase 1 - T=973K; S/C=5	0.097	9.750	Phase 3B - T=840K; S/C=3
0.015	56.396	Phase 2 - T=973K; S/C=5	0.097	12.707	Phase 3A - T=778K; S/C=3
0.018	45.810	Phase 2 - T=973K; S/C=5	0.106	11.950	Phase 3A - T=825K; S/C=3
0.020	23.898	Phase 1 - T=973K; S/C=3	0.111	0.356	Phase 3C - T=800K; S/C=5
0.022	21.292	Phase 2 - T=973K; S/C=3	0.125	0.688	Phase 3C - T=880K; S/C=5
0.031	19.474	Phase 1 - T=973K; S/C=5	0.136	0.097	Xu - T=848K; S/C=3
0.032	10.413	Phase 2 - T=973K; S/C=5	0.140	0.476	Phase 3C - T=990K; S/C=5
0.039	9.892	Phase 1 - T=973K; S/C=3	0.200	0.108	Xu - T=848K; S/C=3
0.041	8.381	Phase 2 - T=973K; S/C=3	0.227	0.085	Xu - T=848K; S/C=3
0.048	20.731	Phase 3A - T=778K; S/C=3	0.236	0.068	Xu - T=848K; S/C=3

Figure 16: turnover frequency vs space-time for all phases (above) and ancillary Table (bellow). Figure shows the trends on the TOF with changing space-time, and the strong dependence of the TOF on the addition of an inhibitor (n=26). Full data Table provided on Appendix C.

A similar demarcation to Figure 16 appears on the hydrogen selectivity (Figure. 17). Even when the space-times of the different phases overlap, the hydrogen selectivity is about 11% greater on the dispersed phase than on the fixed phase. These changes in selectivity were very likely due to, not only the inhibiting action of hydrogen, but to reactor configuration as well.

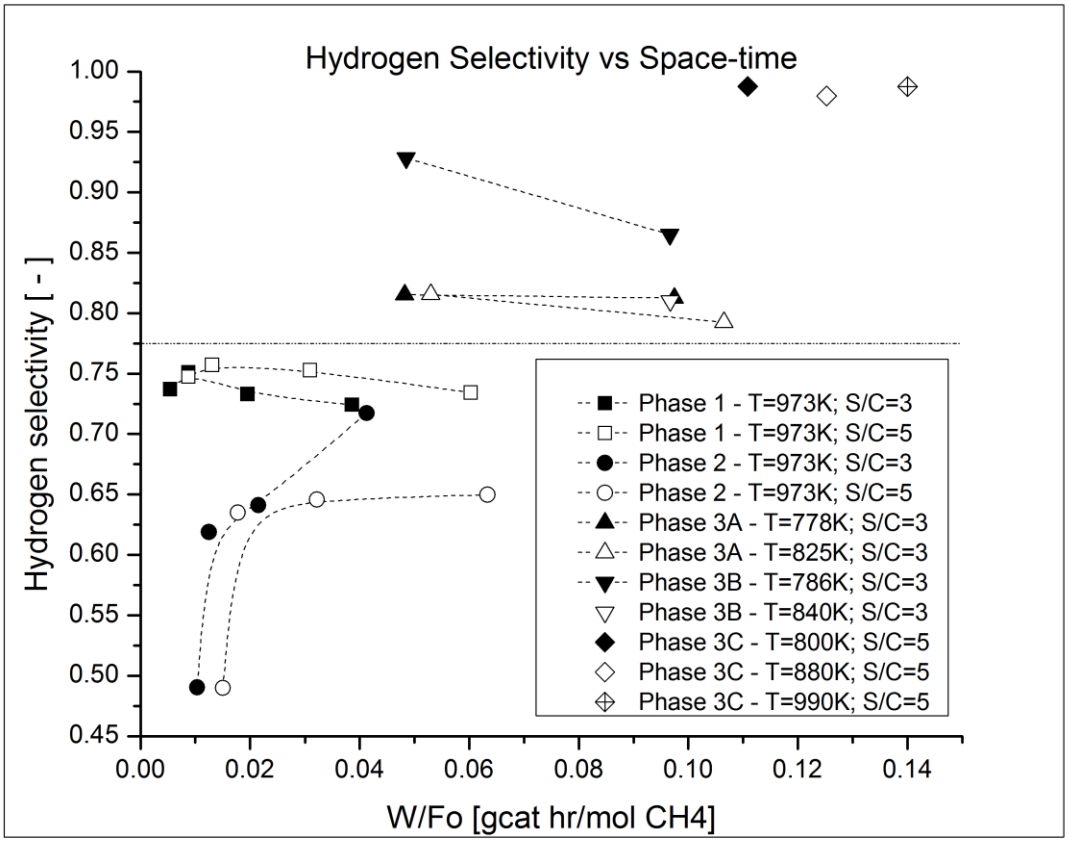

W/Fo [gcat hr/mol CH4]	Hydrogen Selectivity [-]	Comment	W/Fo [gcat hr/mol CH4]	Hydrogen Selectivity [-]	Comment
0.005	0.737	Phase 1 - T=973K; S/C=3	0.041	0.717	Phase 2 - T=973K; S/C=3
0.009	0.748	Phase 1 - T=973K; S/C=5	0.048	0.815	Phase 3A - T=778K; S/C=3
0.009	0.751	Phase 1 - T=973K; S/C=3	0.048	0.928	Phase 3B - T=786K; S/C=3
0.010	0.490	Phase 2 - T=973K; S/C=3	0.053	0.816	Phase 3A - T=825K; S/C=3
0.012	0.619	Phase 2 - T=973K; S/C=3	0.060	0.734	Phase 1 - T=973K; S/C=5
0.013	0.757	Phase 1 - T=973K; S/C=5	0.063	0.650	Phase 2 - T=973K; S/C=5
0.015	0.490	Phase 2 - T=973K; S/C=5	0.097	0.865	Phase 3B - T=786K; S/C=3
0.018	0.635	Phase 2 - T=973K; S/C=5	0.097	0.810	Phase 3B - T=840K; S/C=3
0.020	0.733	Phase 1 - T=973K; S/C=3	0.097	0.813	Phase 3A - T=778K; S/C=3
0.022	0.641	Phase 2 - T=973K; S/C=3	0.106	0.793	Phase 3A - T=825K; S/C=3
0.031	0.753	Phase 1 - T=973K; S/C=5	0.111	0.988	Phase 3C - T=800K; S/C=5
0.032	0.646	Phase 2 - T=973K; S/C=5	0.125	0.980	Phase 3C - T=880K; S/C=5
0.039	0.724	Phase 1 - T=973K; S/C=3	0.140	0.988	Phase 3C - T=990K; S/C=5

Figure 17: hydrogen selectivity vs space-time for all data (above) and ancillary Table (below). Figure shows clear distinction in selectivity between fixed and dispersed phases (n=26). Full data Table provided on Appendix C.

4.8: Activation energies and pre-factors

As mentioned during the introduction, the SMR process can be simplified to the chemical equations shown here,

$$CH_4 + H_2O = CO + 4H_2;\ \Delta H = +206\ kJ/mol \quad \text{(eq. 1)}$$

$$CH_4 + 2H_2O = CO_2 + 3H_2;\ \Delta H = +165\ kJ/mol \quad \text{(eq. 2)}$$

$$CO + H_2O = CO_2 + H_2;\ \Delta H = -41\ kJ/mol \quad \text{(eq. 3)}$$

To study the kinetics of the catalyst, the model of Xu and Froment [14] will be employed. For the reactions outlined above, the model proposes the following reaction rates

$$r_1 = \frac{\frac{k_1}{p_{H_2}^{2.5}}\left(p_{CH4}p_{H2O} - \frac{p_{H2}^3 p_{CO}}{K_1}\right)}{(DEN)^2} \quad \text{(eq. 19)}$$

$$r_2 = \frac{\frac{k_2}{p_{H2}}\left(p_{CO}p_{H2O} - \frac{p_{H2}p_{CO2}}{K_2}\right)}{(DEN)^2} \quad \text{(eq. 20)}$$

$$r_3 = \frac{\frac{k_3}{p_{H_2}^{3.5}}\left(p_{CH4}p_{H2O}^2 - \frac{p_{H2}^4 p_{CO2}}{K_3}\right)}{(DEN)^2} \quad \text{(eq. 21)}$$

$$DEN = 1 + K_{CO}p_{CO} + K_{H2}p_{H2} + K_{CH4}p_{CH4} + K_{H2O}\frac{p_{H2O}}{p_{H2}} \quad \text{(eq. 22)}$$

where r_i is the rate of reaction of equation i, k_i is the rate constant for reaction for reaction i, $p_j$is the partial pressure of species j, $K_\#$ is the equilibrium constant of reaction i, and K_j is the adsorption constant for species j.

The reaction rates are combined to obtain species rates as

$$r_{CO}^{fm} = r_1 - r_2 \quad \text{(eq. 23)}$$

$$r_{CO_2}^{fm} = r_2 + r_3 \quad \text{(eq. 24)}$$

$$-r_{CH_4}^{fm} = r_1 + r_3 \quad \text{(eq. 25)}$$

where fm represents the model. This model requires a constant GHSV with varying temperatures. Therefore, only the data from phases 1 and 2 will be used.

For this analysis the equilibrium constants were calculated from the reactions standard Gibbs free energies. The species adsorption constants were not provided by the ASC and their characterization was well beyond the scope of this thesis. However, because the catalyst used in this work was nickel based and the catalyst used by Xu was also nickel based, it will be assumed that their species adsorption constants would fall within a reasonable range from each other. Therefore, this work will use the adsorption constants reported by Xu. The adsorption constants can be found in Table 7.

Adsorption constant	Value
K_{CO}	$8.23x10^{-5}$ exp[70650/RT]
K_{H2}	$6.12x10^{-9}$ exp[82900/RT]
K_{CH4}	$6.65x10^{-4}$ exp[-88680/RT]
K_{H2O}	$1.77x10^{5}$ exp[-65053/RT]

Table 7: adsorption constants used where R=8.314472 J/mole K and T is the absolute temperature of the system

The rates of methane conversion, carbon dioxide formation, and carbon monoxide formation were calculated from the data by:

$$-r_{CH_4}^{fd} = \frac{n_{CH_4}^{in} - n_{CH_4}^{out}}{t_{res} W_{cat}}$$

(eq. 26)

$$r_{CO_2}^{fd} = \frac{n_{CO_2}^{out}}{t_{res} W_{cat}}$$

(eq. 27)

$$r_{CO}^{fd} = \frac{n_{CO}^{out}}{t_{res} W_{cat}}$$

(eq. 28)

where $-r_{CH_4}^{fd}$ is the rate of conversion of methane calculated from the data, $n_{CH_4}^{in}$ is the number of moles of methane delivered, $n_{CH_4}^{out}$ is the number of moles of methane measured at the dry effluent, $r_{CO_2}^{fd}$ is the rate of formation of CO_2 calculated from the data, $n_{CO_2}^{out}$ is the number of moles of CO_2 measured at the dry

effluent, r_{CO}^{fd} is the rate of formation of CO calculated from the data, n_{CO}^{out} is the number of moles of CO measured at the dry effluent, t_{res} is the residence time, and W_{cat} is the weight of the catalyst.

These rates from data were compared to the rates estimated from the model as,

$$-r_{CH_4}^{fm} = -r_{CH_4}^{fd}$$

(eq. 29)

$$r_{CO_2}^{fm} = r_{CO_2}^{fd}$$

(eq. 30)

$$r_{CO}^{fm} = r_{CO}^{fd}$$

(eq. 31)

where the model was adjusted to the data by minimizing the reaction constants. The reaction constants, in turn, underwent Arrhenius analysis. The reaction constant is defined as

$$k(T) = k_o e^{-\frac{Ea}{RT}}$$

(eq. 32)

where k(T) is the reaction constant at a given temperature, ko is the prefactor, Ea is the activation energy, R is the universal gas constant, and T is the absolute temperature of the system. By taking the natural logarithm of the reaction constant we obtain

$$\ln k = \ln k_o - \frac{Ea}{R}\frac{1}{T}$$

(eq. 33)

which resembles a linear equation y = a + bx, from which the Arrhenius parameters are extracted. This parameter minimization method was employed using the Microsoft Excel solver tool.

Unfortunately, this technique did not yield the set of values expected. It was impossible to constraint all the carbon species reaction rates. In order to see where would the Arrhenius parameters approximate, one of the species rates constraints was relaxed at a time. For phase 1, r_{CH4} and r_{CO} were constrained while r_{CO2} was relaxed, then r_{CH4} and r_{CO2} were constrained while r_{CO} was relaxed, and r_{CO2} and r_{CO} were constrained while r_{CH4} was relaxed.

Figures 18, 19 and 20 show the results obtained from the parameter estimation for phase 1 in terms of ln k vs 10^3/T. These Figures are shown in the following order: r_{CH4} and r_{CO} constrained with relaxed r_{CO2}; r_{CH4}

and r_{CO2} constrained with relaxed r_{CO}; and r_{CO2} and r_{CO} constrained with relaxed r_{CH4}. The analysis shown in Figure 18 was the only to not yield a complete set of 3 reaction constants. The Arrhenius parameters obtained from this analysis were condensed in Table 8. For the data collected on phase 2 it was not necessary to apply the same series of constrain relaxations to the system as in phase 1. Figure 21 shows the results of the analysis of data from phase 2 in terms of ln k vs 10^3/T. The Arrhenius parameters have been condensed in Table 8.

ko[1]	Ea[1]	ko[2]	Ea[2]	ko[3]	Ea[3]	Batch	Comment
1.04E+18	227870.1	-	-	9.10E+13	211167.3	Phase 1	rCO relaxed
2.81E+22	329774.8	1.49E+12	129673.5	1.90E+20	287265.3	Phase 1	rCO2 relaxed
1.19E+13	223023.1	0.017218	-365641	2.05E+11	186458.1	Phase 1	rCH4 relaxed
7.19E+53	997513.7	6.48E+10	131527.5	2.89E+28	482311.8	Phase 2	

Table 8: Arrhenius parameters for k1, k2, and k3; where the square brackets denote the reaction constant. ko[1], ko[3] are in [kmole bar$^{1/2}$/(kg-cat hr)]; ko[2] in [kmol/(kg-cat hr bar)]; and Ea[1], Ea[2] and Ea[3] in [J/mol]

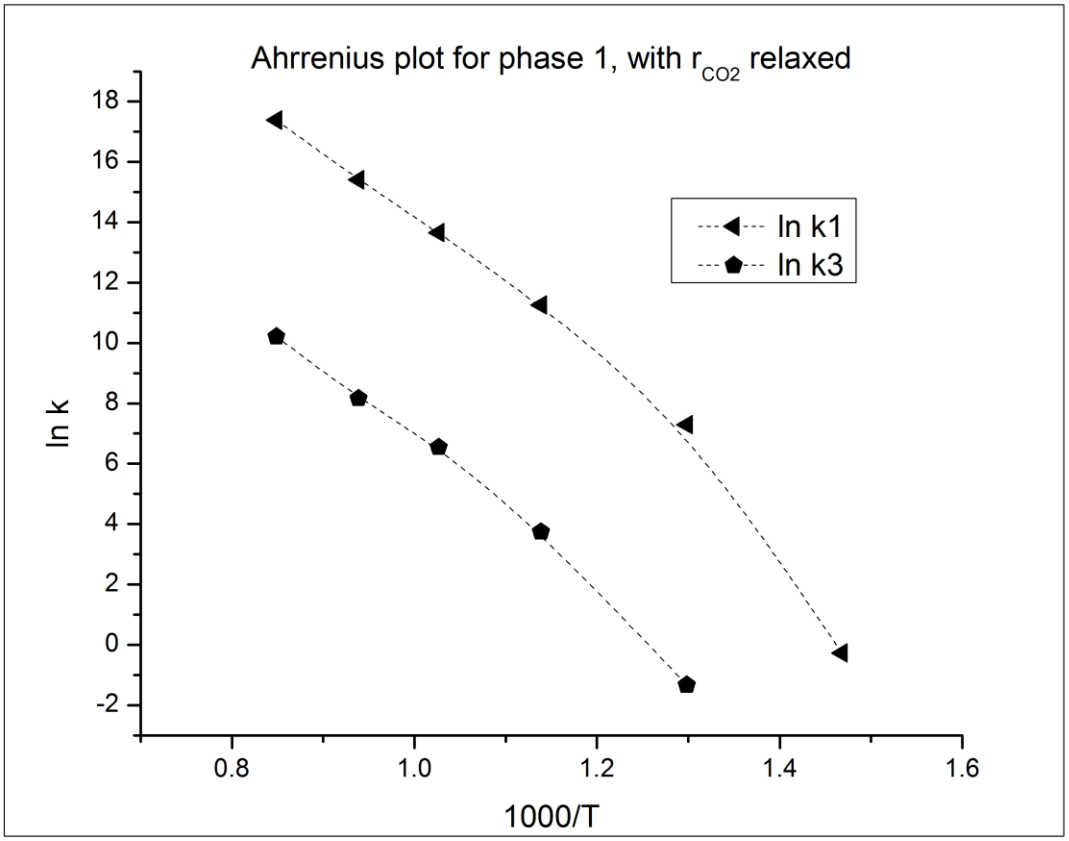

1000/T	ln k1	ln k3
0.849	17.387	
0.939	15.406	10.219
1.027	13.659	8.161
1.139	11.256	6.545
1.298	7.286	3.743
1.468	-0.267	-1.335

Figure 18: Arrhenius plot for phase 1 data (above) and ancillary Table (below). Figure shows Arrhenius plot for phase 1 data with r_{CO2} relaxed for temperature range between 681 – 1178 K at GHSV = 84,204 hr^{-1}.

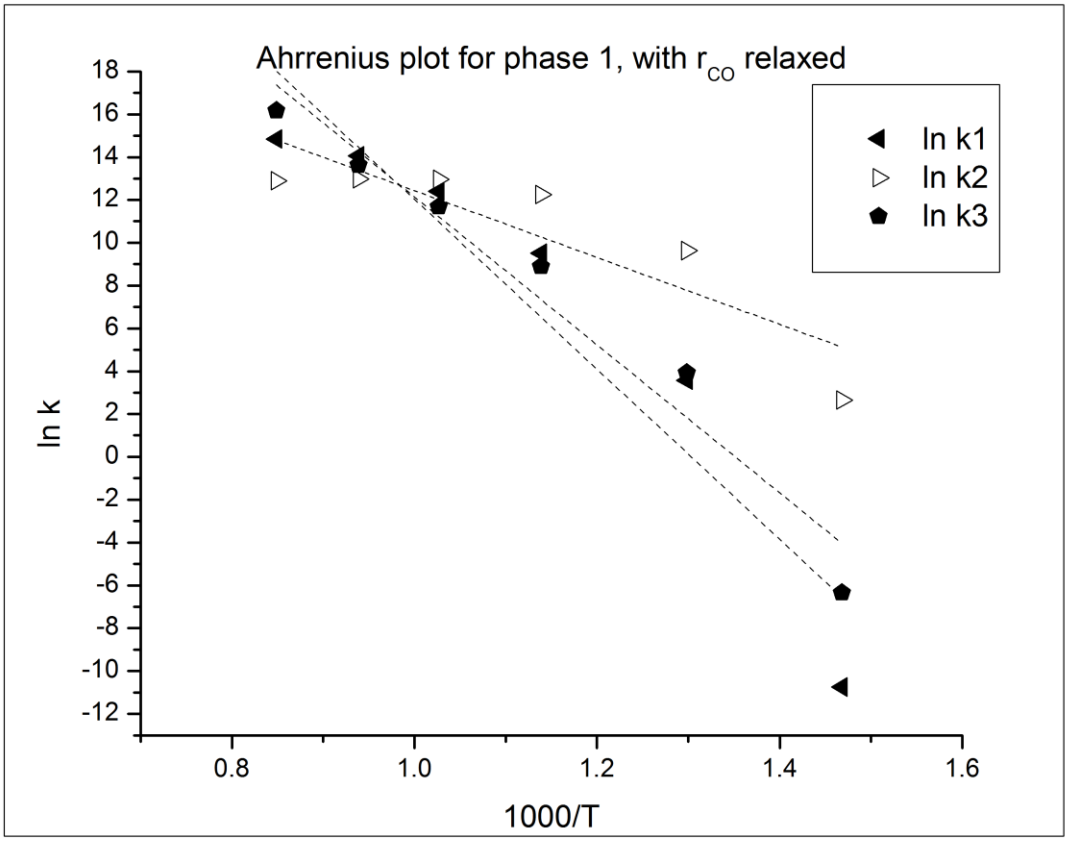

1000/T	ln k1	ln k2	ln k3
0.849	14.833	12.885	16.164
0.939	14.048	12.986	13.632
1.027	12.402	12.970	11.682
1.139	9.504	12.255	8.900
1.298	3.573	9.625	3.938
1.468	-10.751	2.639	-6.334

Figure 19: Arrhenius plot for phase 1 data (above) and ancillary Table (below). Figure shows Arrhenius plot for phase 1 with r_{CO} relaxed for temperature range between 681 – 1178 K at GHSV = 84,204 hr^{-1}.

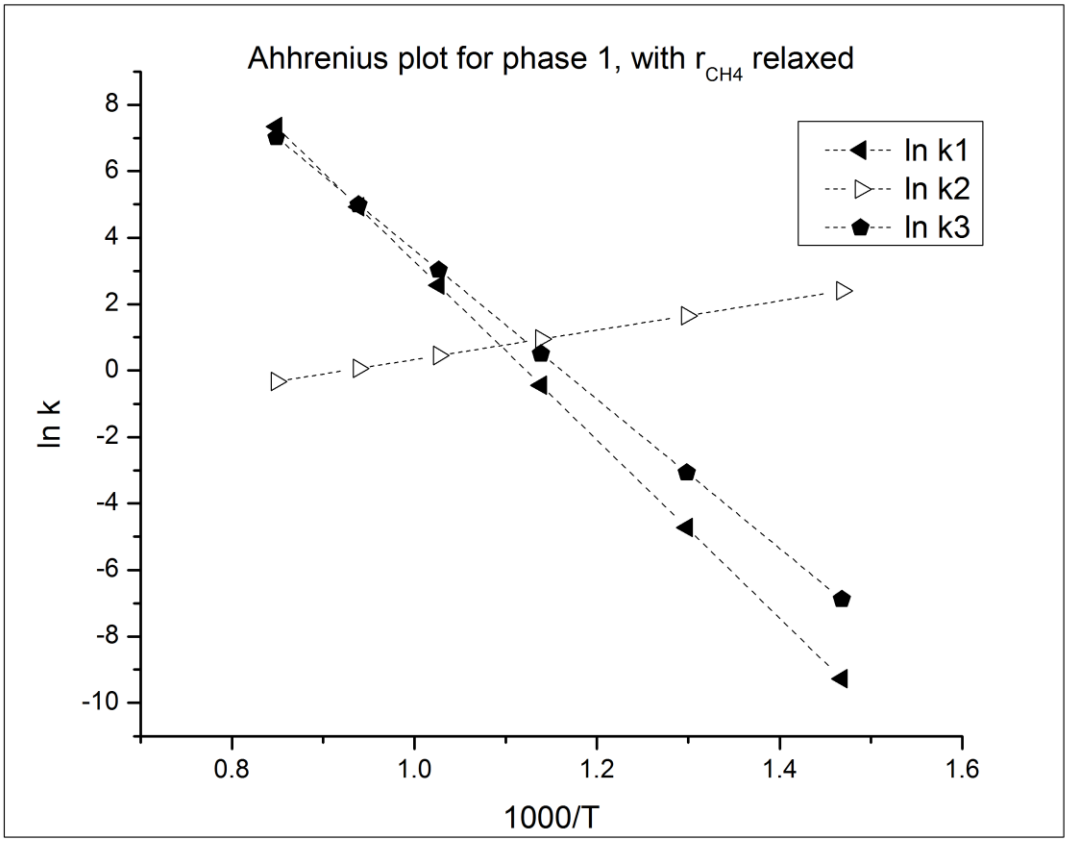

1000/T	ln k1	ln k2	ln k3
0.849	7.340	-0.329	7.011
0.939	4.924	0.067	4.991
1.027	2.572	0.453	3.025
1.139	-0.439	0.946	0.508
1.298	-4.722	1.649	-3.074
1.468	-9.274	2.395	-6.879

Figure 20: Arrhenius plot for phase 1 data (above) and ancillary Table (below). Figure shows Arrhenius plot for phase 1 data with r_{CH4} relaxed for temperature range between 681 – 1178 K at GHSV = 84,204 hr^{-1}.

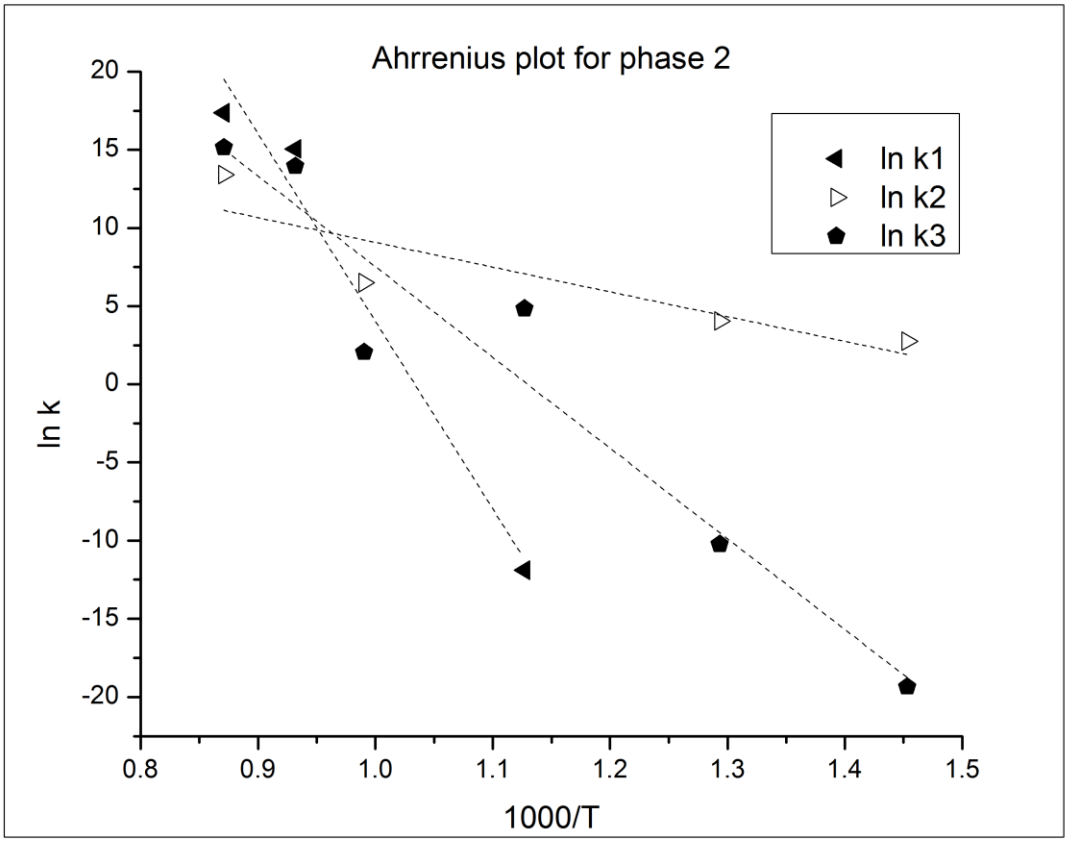

1000/T	ln k1	ln k2	ln k3
0.871	17.357	13.400	15.140
0.932	15.044	-	13.946
0.990	-	6.488	2.056
1.127	-11.899	-	4.846
1.293	-	4.042	-10.214
1.453	-	2.753	-19.342

Figure 21: Arrhenius plot for phase 2 data (above) and ancillary Table (below). Figure shows Arrhenius plot for phase 2 data for temperature range between 688 – 1148 K at GHSV = 84,204 hr^{-1}.

The results summarized on Table 8 were used to generate parity plots. Figures 22 through 25 show conversion parities where the x-axes are the measured conversion and the y-axes are the calculated conversions. Figures 22, 23 and 24 show the parity plot for the data collected in phase 1, where the analysis was carried with relaxed r_{CO2}, r_{CO} and r_{CH4}, respectively. Figure 25 shows the parity plot for the data collected in phase 2.

As it can be observed on these parity plots, the data points lie far from the parity line. Among the chief reasons for the disparity is the fact that our estimation tools were considerably rudimentary. Besides our analytic tools, after several discussions with the team, we converged on the hypothesis that the bulk of the reactions that were being measured at the outlet were occurring on the first few millimeters of the length of the reactor.

After discussions with our collaborators at UC Louvain we were able to develop an improved test matrix (see Table 4 for phase 3B). The improvement of the test matrix along with more sophisticated modeling tools allowed our collaborator to generate better parity plots for phase 3B.

Figure 26 shows the parity plots generated by our collaborator at UC Louvain. The x-axes represent the measured mole% on a dry basis of the specified species, and the y-axes represented the calculated mole% on a dry basis of the specified species. Figures 26 a, b, c and d show the parity plots for hydrogen, methane, carbon monoxide and carbon dioxide respectively.

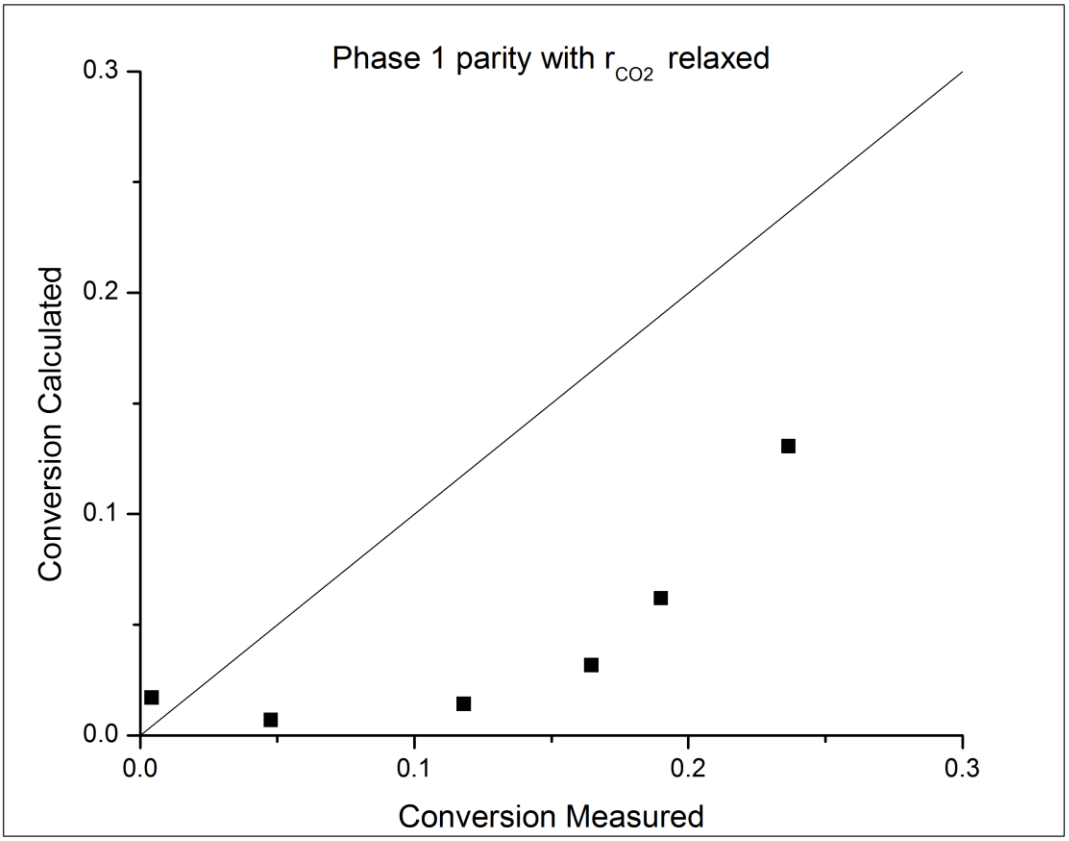

X meas	X calc
0.004	0.017
0.048	0.007
0.118	0.014
0.165	0.032
0.190	0.062
0.236	0.131

Figure 22: parity plot for phase 1 with r_{CO2} relaxed (above) and ancillary Table (below). Figure shows that the model is not able to predict conversion given the input data.

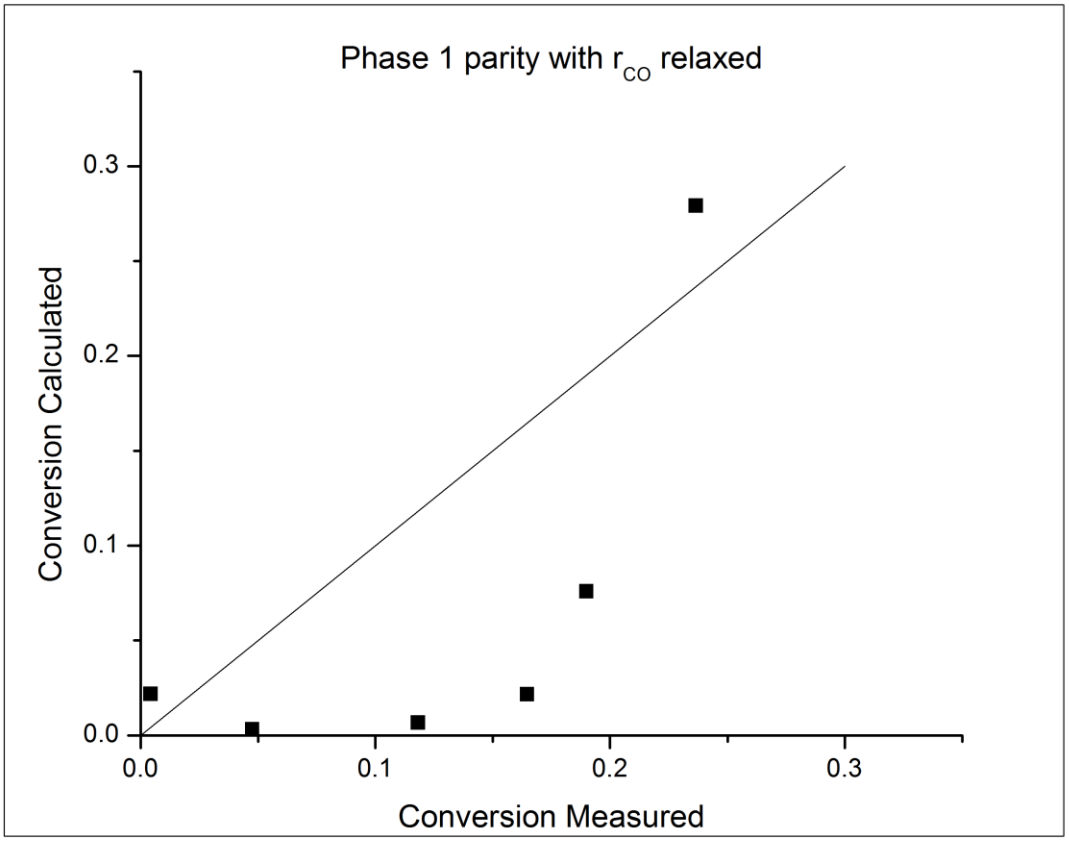

X meas	X calc
0.004	0.022
0.048	0.003
0.118	0.007
0.165	0.022
0.190	0.076
0.236	0.279

Figure 23: parity plot for phase 1 with r_{CO} relaxed (above) and ancillary Table (below). Figure shows that model is not able to predict conversion given the input data.

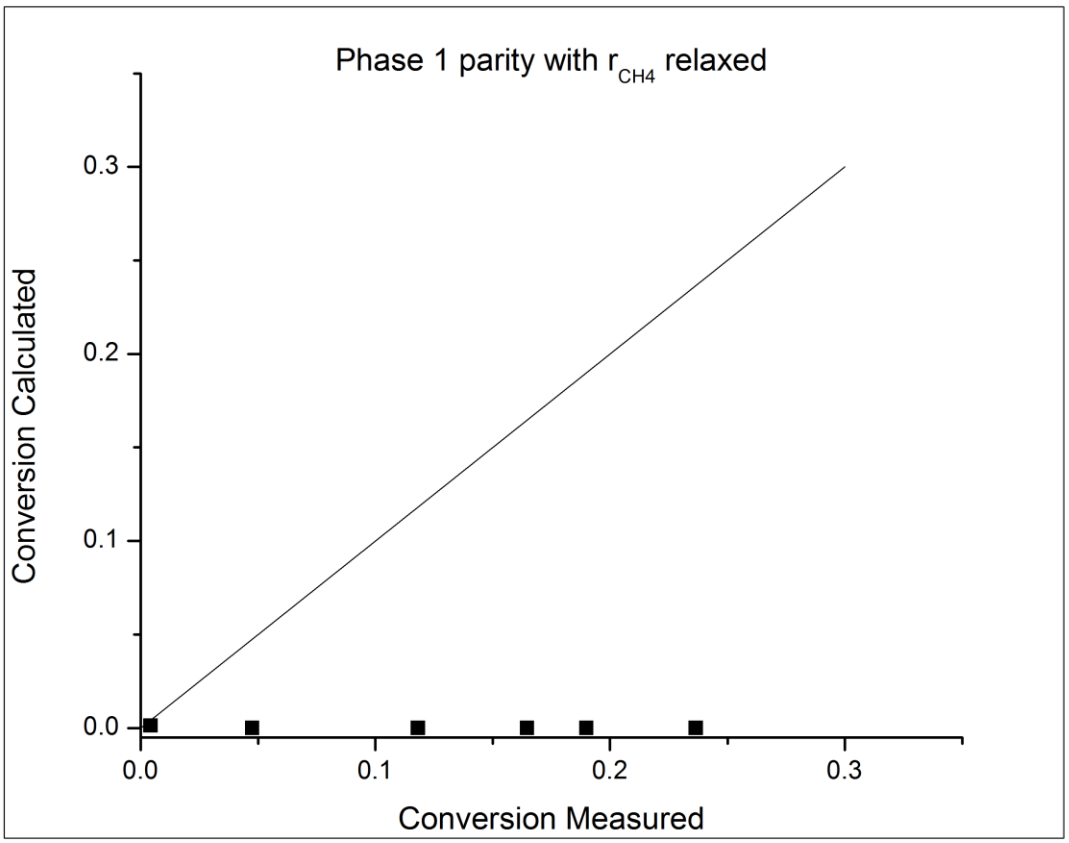

X meas	X calc
0.004	0.001
0.048	0.000
0.118	0.000
0.165	0.000
0.190	0.000
0.236	0.000

Figure 24: parity plot for phase 1 with r_{CH4} relaxed (above) and ancillary Table (below). Figure shows that the model is not able to predict conversion given the input data.

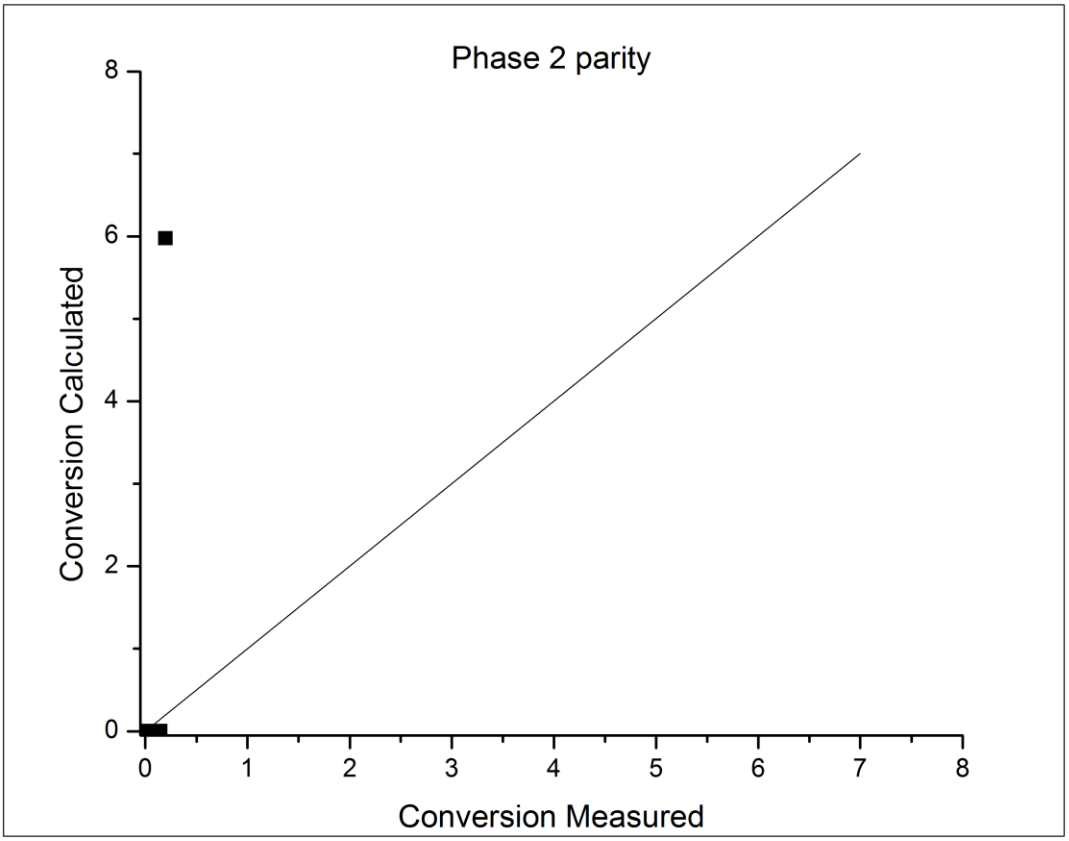

X meas	X calc
8.01E-05	0.000739
1.2E-05	4.67E-07
0.000211	9.62E-06
0.019742	4.1E-06
0.145003	0.004534
0.196358	5.974574

Figure 25: parity plot for phase 2 (above) and ancillary Table (below). Figure shows that model is not able to predict conversion given the input data.

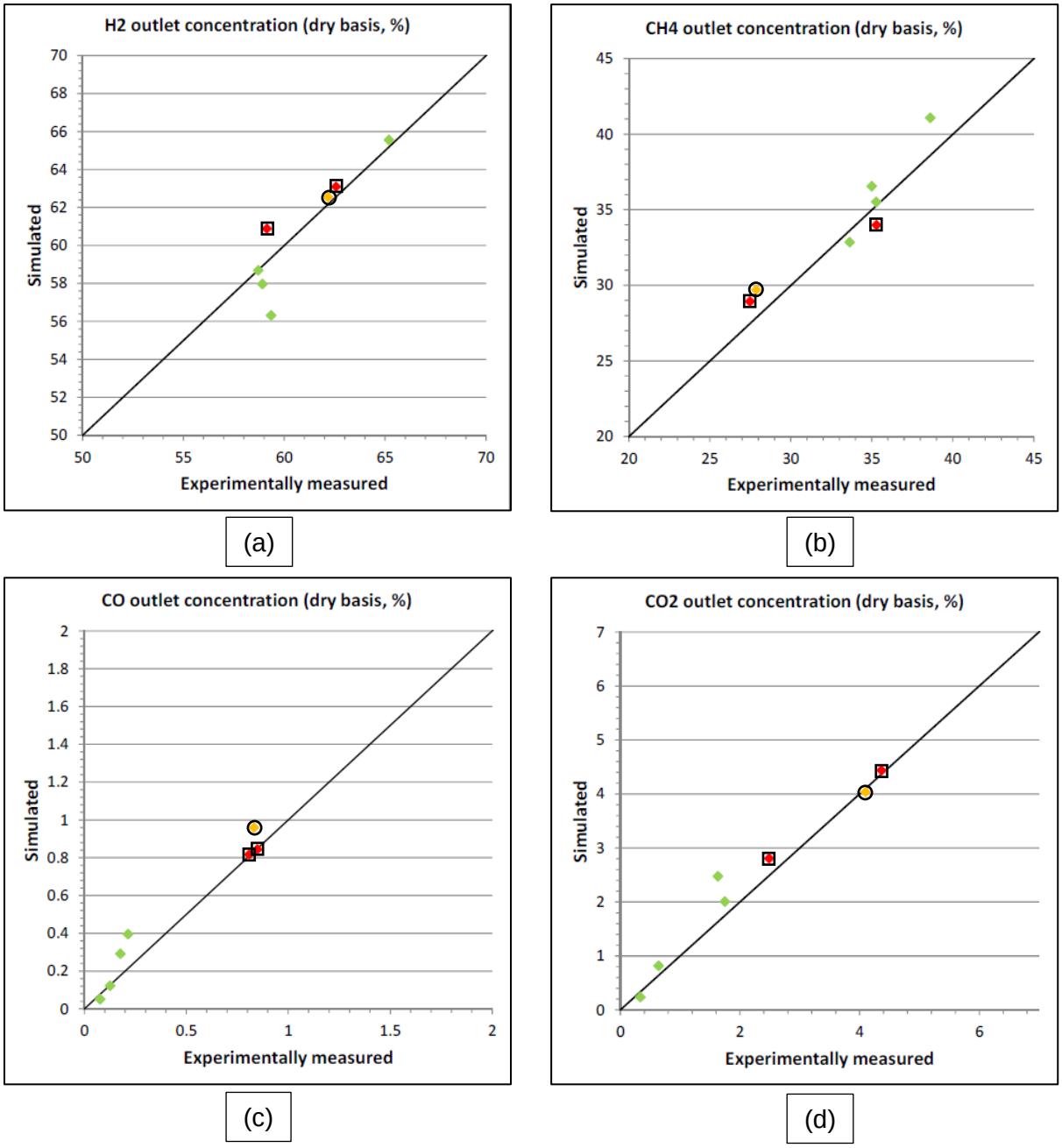

Figure 26: Parity plots generated by collaborator at UCLouvain. These plots present the parity of dry mol fraction of species (a) hydrogen, (b) methane, (c) carbon monoxide, (d) carbon dioxide, as measured by the μGC at the system effluent. Where the green unbounded symbols represent data taken at 784 K, the yellow circle bounded symbols represent data taken at 840 K, and the red square bounded symbols represent data taken at 848 K.

Chapter 5: Conclusion

A first step has been taken towards assessing the potential of ASC's catalytic technology. In the process of achieving this, a new testing facility was built capable of handling gases and liquids at relatively high pressures.

Many tests were performed and a range of conversions were observed. The activity of the catalyst seemed superior to typical catalysts on the market. In addition to these, selectivity observations were performed, which yielded satisfactory results.

Although the potential for the facility and the catalyst have been appreciated, more work needs to be done. Better characterization of the surface of the catalyst is needed. This includes, among others, better understanding of catalyst dispersion, and the determination of the adsorption constants for the different species involved.

Tests at vast temperature ranges are also needed. Although it is clear from the data that the catalyst used for this work is very active, a quantitative determination of the catalyst activity is in order. Many tests with different GHSVs and inlet distributions for some discrete and wide temperature range will be needed. In addition to these, a better reactor vessel, which allows for the sampling at different positions along the reactor should be used.

Finally, several destructive tests are in order as well. The behavior of the catalyst through aging, poisoning and/or fouling has not been studied yet. Along with these destructive tests, mitigation strategies should be developed and the catalyst regeneration cycles should be characterized.

References

1. World population projected to reach 9.7 billion by 2050 | UN DESA Department of Economic and Social Affairs. http://www.un.org/en/development/desa/news/population/2015-report.html
2. Water, food and energy nexus. http://www.unwater.org/topics/water-food-and-energy-nexus/en/
3. The unprecedented expansion of the global middle class | Brookings Institution. Homi Kharas. https://www.brookings.edu/research/the-unprecedented-expansion-of-the-global-middle-class-2/
4. Hydrogen Production: Natural gas reforming. (n.d.). Retrieved August 24, 2015, http://energy.gov/eere/fuelcells/hydrogen-production-natural-gas-reforming
5. https://www.eia.gov/dnav/ng/hist/rngwhhdd.htm
6. Holladay, J. D., Hu, J., King, D. L., & Wang, Y. (2009). An overview of hydrogen production technologies. *Catalysis Today*, *139*(4), 244-260.
7. Spath, P. L., & Mann, M. K. (2000). *Life cycle assessment of hydrogen production via natural gas steam reforming*. Golden, CO: National Renewable Energy Laboratory.
8. Smith, R. J., Loganathan, M., & Shantha, M. S. (2010). A review of the water gas shift reaction kinetics. International Journal of Chemical Reactor Engineering, 8(1).
9. Mendes, D., Mendes, A., Madeira, L. M., Iulianelli, A., Sousa, J. M., & Basile, A. (2010). The water-gas shift reaction: from conventional catalytic systems to Pd-based membrane reactors—a review. Asia-Pacific Journal of Chemical Engineering, 5(1), 111-137.
10. Hougen, O. A., & Watson, K. M. (1943). Solid catalysts and reaction rates. *Ind. Eng. Chem*, *35*(5), 529-541.
11. Yang, K. H., & Hougen, O. A. (1950). Determination of mechanism of catalyzed gaseous reactions. Chem. Eng. Prog, 46(3), 146-157.
12. Allen, D. W., Gerhard, E. R., & Likins Jr, M. R. (1975). Kinetics of the methane-steam reaction. *Industrial & Engineering Chemistry Process Design and Development*, *14*(3), 256-259.
13. Bodrov, I.M., Apel'baum, L.O., Timkin, M.I., Kinet. Katal., 9, 1965 (1968).
14. Xu, J., & Froment, G. F. (1989). Methane steam reforming, methanation and water-gas shift: I. Intrinsic kinetics. *AIChE Journal*, *35*(1), 88-96.
15. Adris, A. M., Lim, C. J., & Grace, J. R. (1997). The fluidized-bed membrane reactor for steam methane reforming: model verification and parametric study. *Chemical Engineering Science*, *52*(10), 1609-1622.
16. Ahmed, K., & Foger, K. (2000). Kinetics of internal steam reforming of methane on Ni/YSZ-based anodes for solid oxide fuel cells. *Catalysis Today*, *63*(2), 479-487.
17. Wang, Y., Yoshiba, F., Kawase, M., & Watanabe, T. (2009). Performance and effective kinetic models of methane steam reforming over Ni/YSZ anode of planar SOFC. *International Journal of Hydrogen Energy*, *34*(9), 3885-3893.
18. Oliveira, E. L., Grande, C. A., & Rodrigues, A. E. (2010). Methane steam reforming in large pore catalyst. *Chemical Engineering Science*, *65*(5), 1539-1550.
19. Maestri, M., Vlachos, D. G., Beretta, A., Groppi, G., & Tronconi, E. (2008). Steam and dry reforming of methane on Rh: Microkinetic analysis and hierarchy of kinetic models. *Journal of Catalysis*, *259*(2), 211-222.

20. Ramırez-Cabrera, E., Atkinson, A., & Chadwick, D. (2004). Catalytic steam reforming of methane over Ce 0.9 Gd 0.1 O 2− x. Applied Catalysis B: Environmental, 47(2), 127-131.
21. Häussinger, P., Lohmüller, R., Watson, A. M., (2003). Hydrogen, 6. Uses. Ullmann's Encyclopedia of Industrial Chemistry. Retrieved from http://onlinelibrary.wiley.com/book/10.1002/14356007
22. Fogler, H. S. (1999). Elements of chemical reaction engineering.
23. Levenspiel, O., & Levenspiel, C. (1972). *Chemical reaction engineering*. New York etc.: Wiley.
24. Levenspiel, O. (2014). *Engineerilng flow and heat exchange*. Springer.
25. Smith, J. M. (1981). *Chemical engineering kinetics*. McGraw-Hill.
26. Froment, G. F., De Wilde, J., & Bischoff, K. B. Chemical reactor analysis and design. Vol. 2011, Hoboken.
27. Bird, R. B., Stewart, W. E., & Lightfoot, E. N. (1960). Transport Phenomena John Wiley & Sons. *New York*, 413.

Appendix A: Calibration curves

Micro-GC calibration curves:

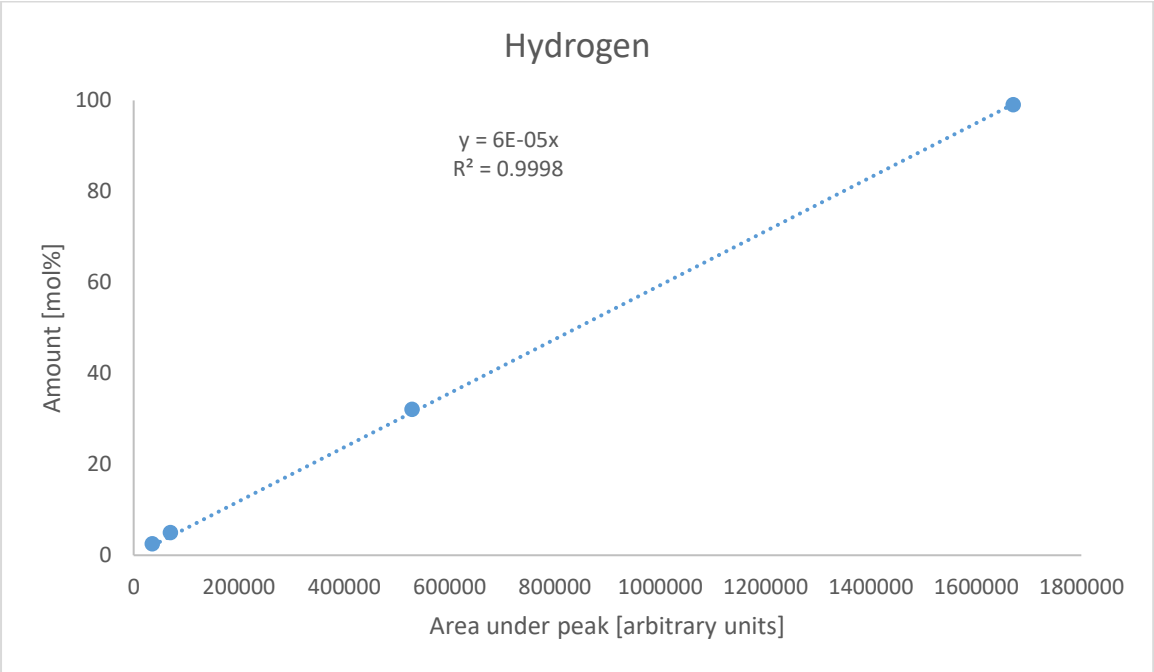

Figure 27: hydrogen calibration curve for Inficon micro-GC 3000.

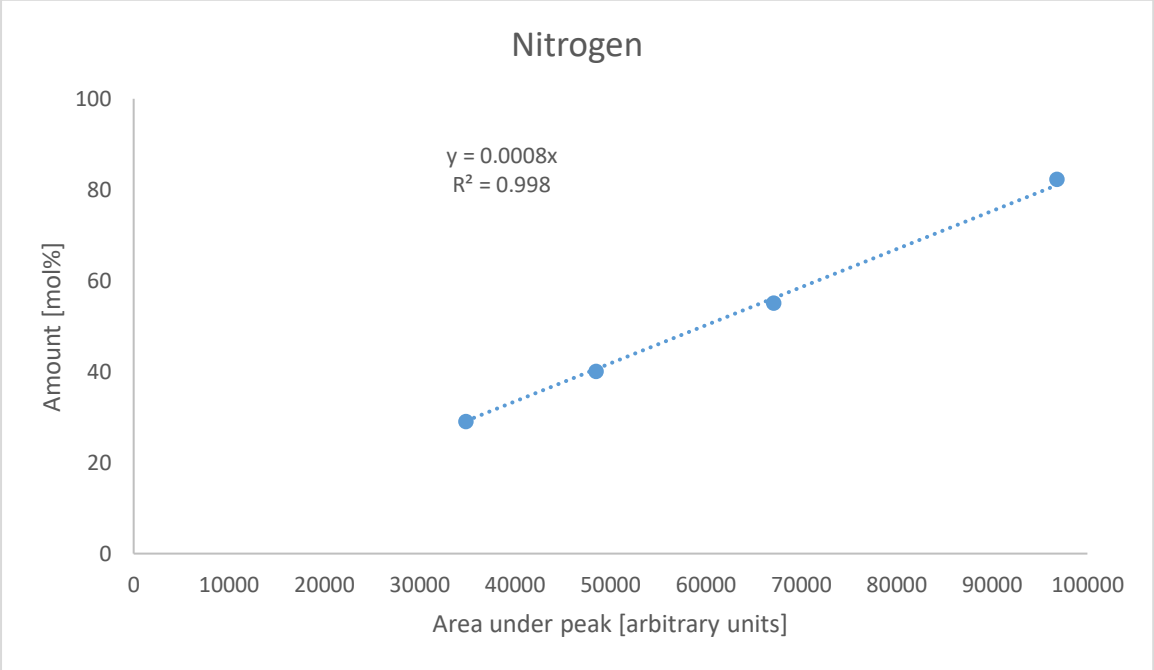

Figure 28: nitrogen calibration curve for Inficon micro-GC 3000.

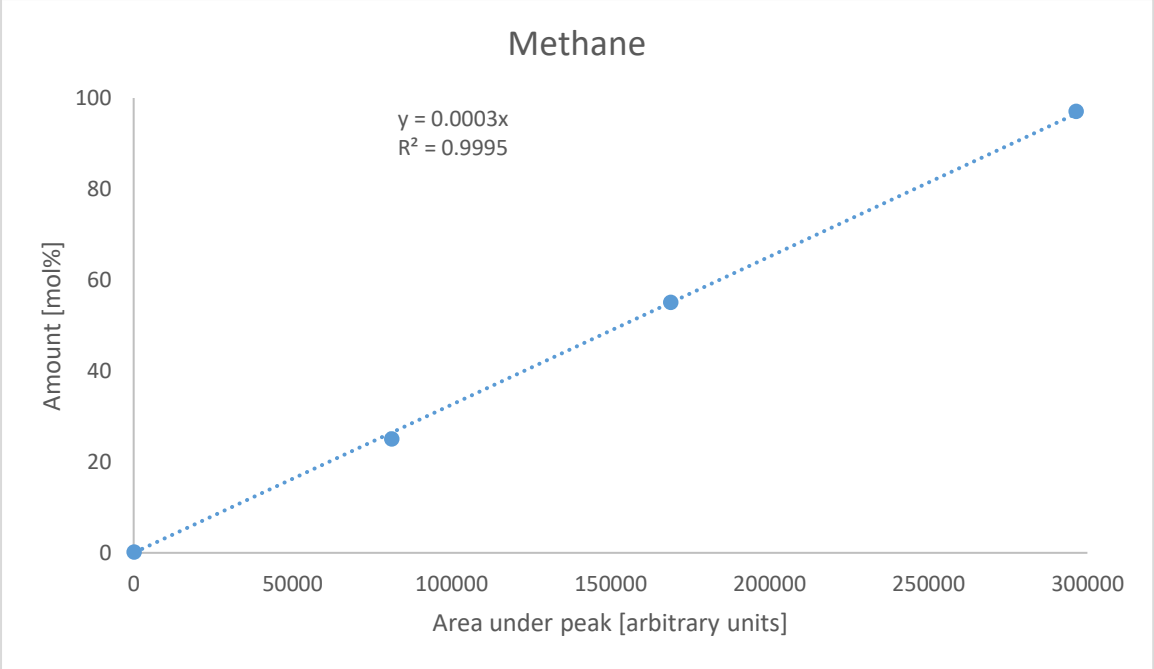

Figure 29: methane calibration curve for Inficon micro-GC 3000.

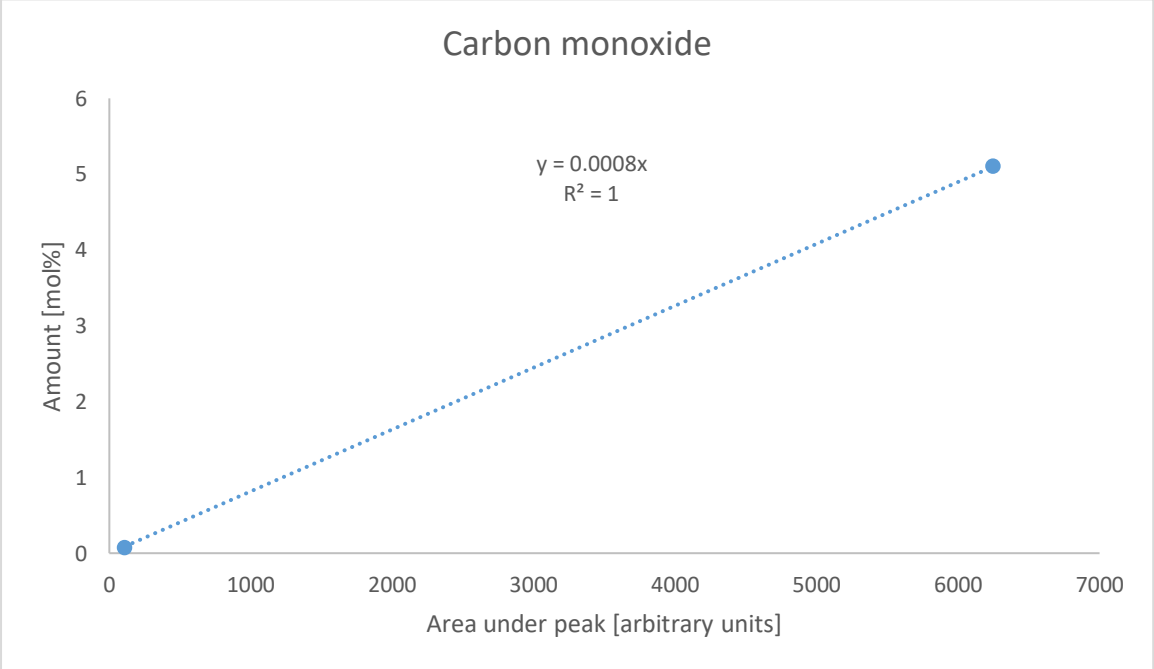

Figure 30: carbon monoxide calibration curve for Inficon micro-GC 3000.

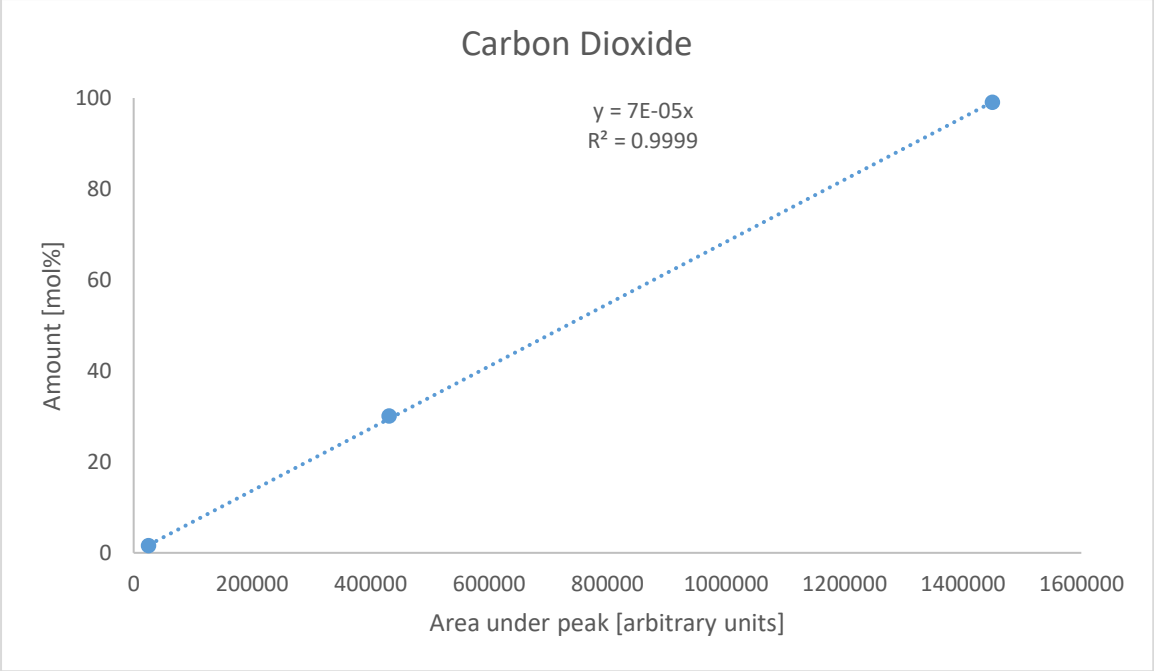

Figure 31: carbon dioxide calibration curve for Inficon micro-GC 3000.

Orifices calibration curves

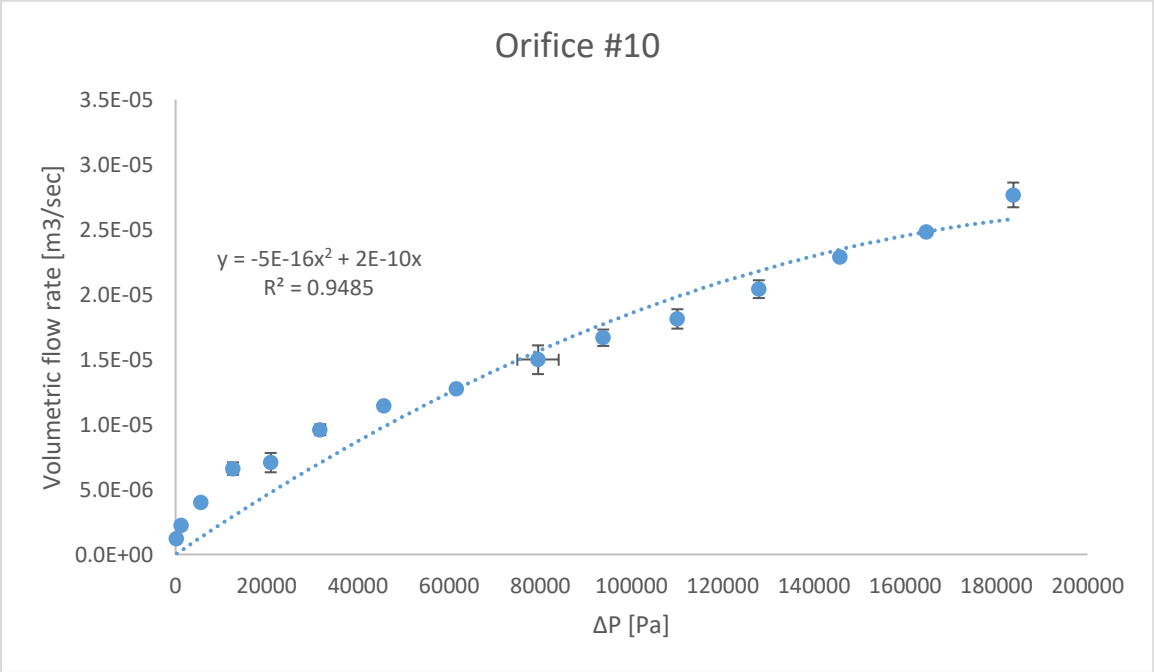

Figure 32: orifice calibration curve for d = 0.254 mm (0.01 in).

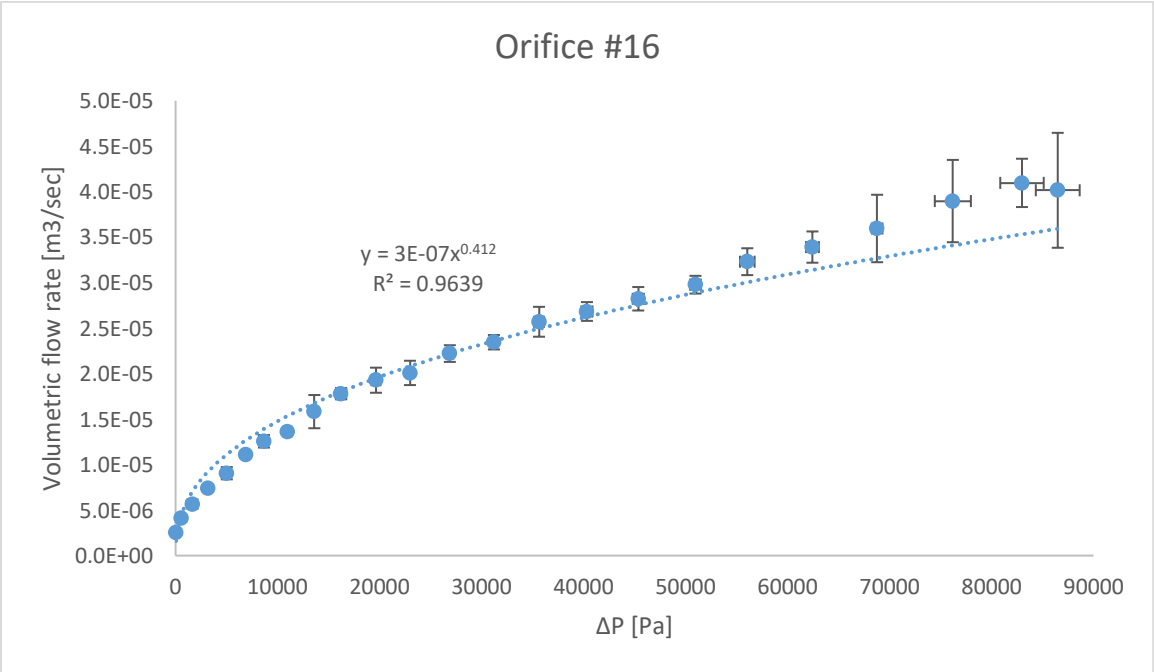

Figure 33: orifice calibration curve for d = 0.4064 mm (0.016 in).

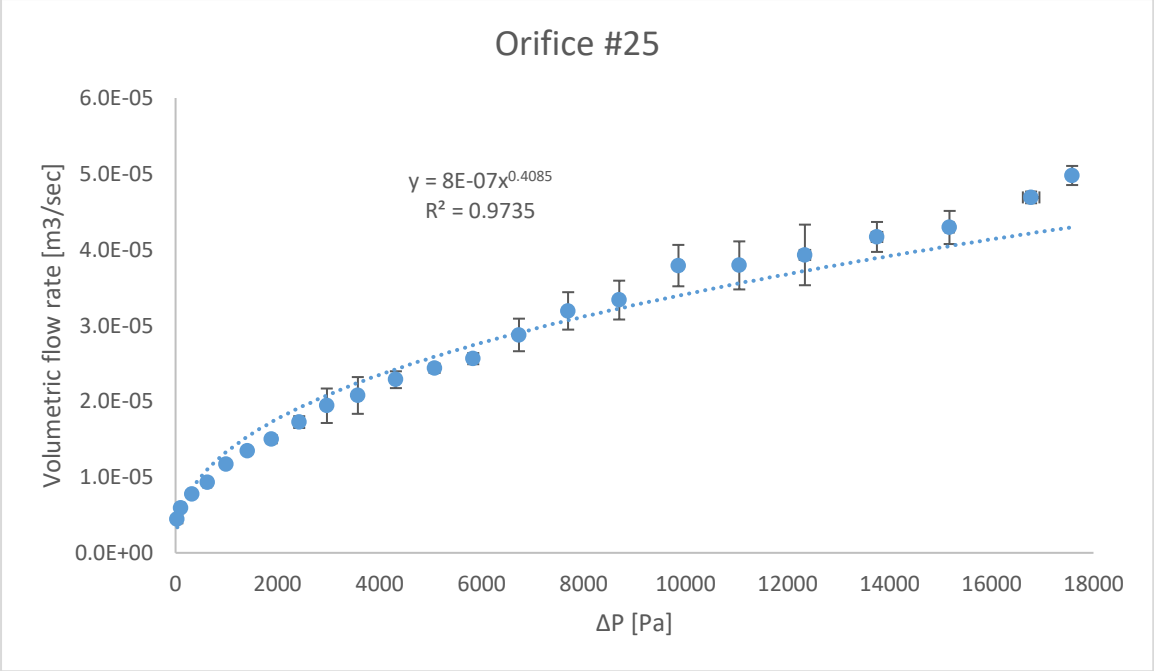

Figure 34: orifice calibration curve for d = 0.635 mm (0.025 in).

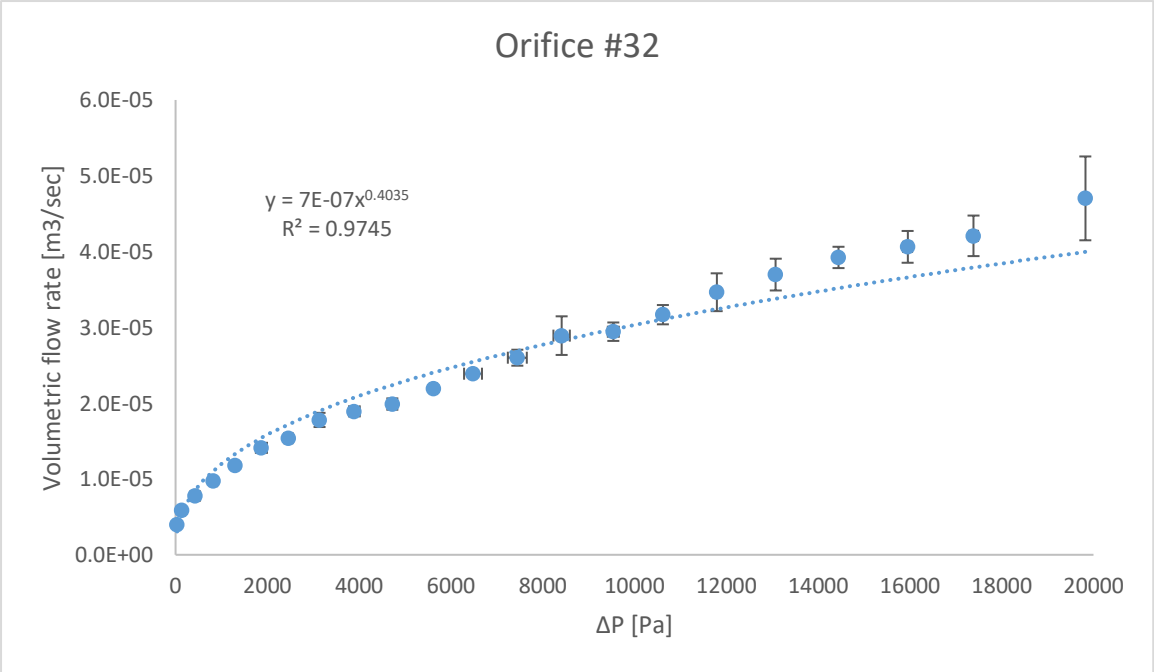

Figure 35: orifice calibration curve for d = 0.8128 mm (0.032 in).

Mass flow controller calibration curves:

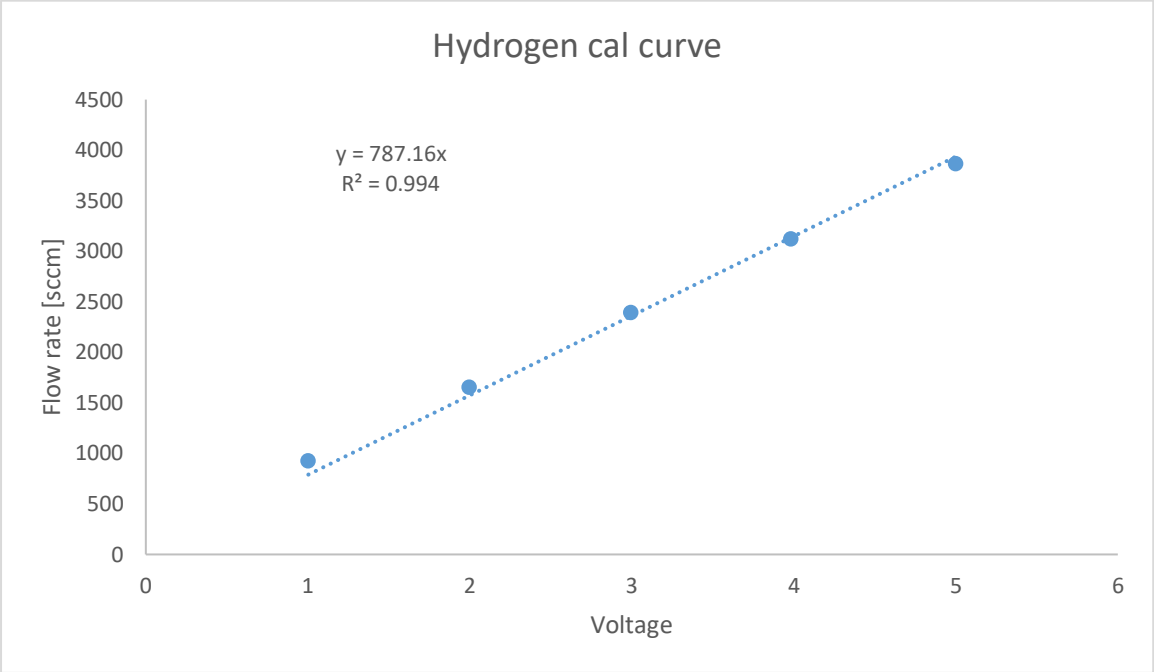

Figure 36: hydrogen calibration curve for Tylan FC-280S.

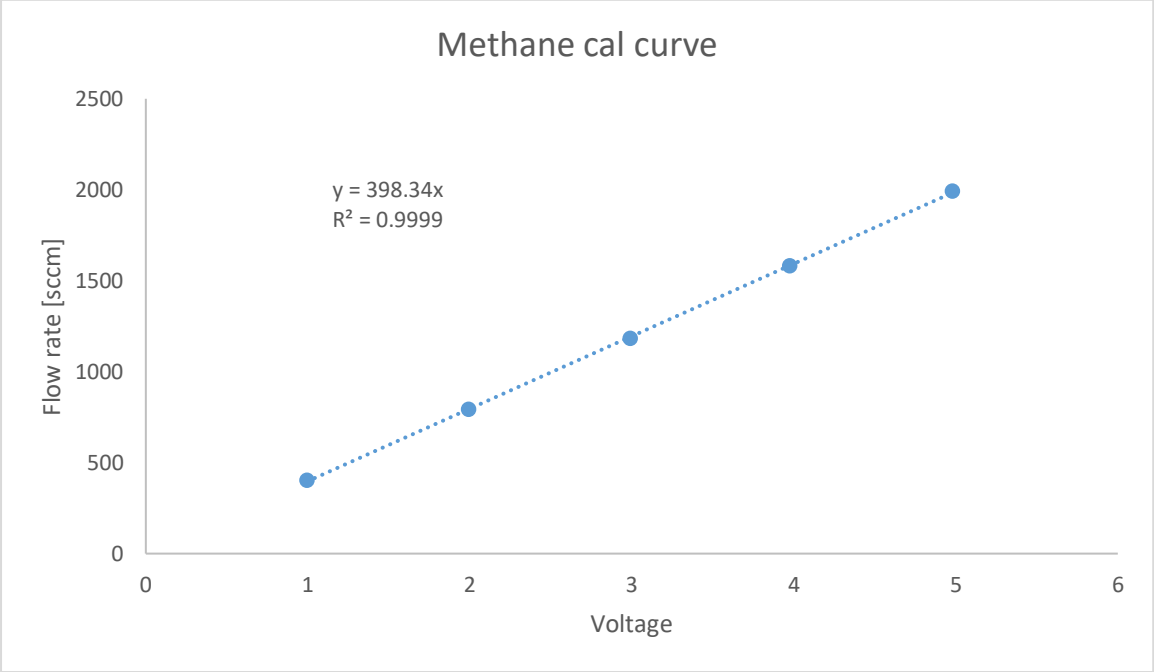

Figure 37: methane calibration curve for Tylan FC-280S.

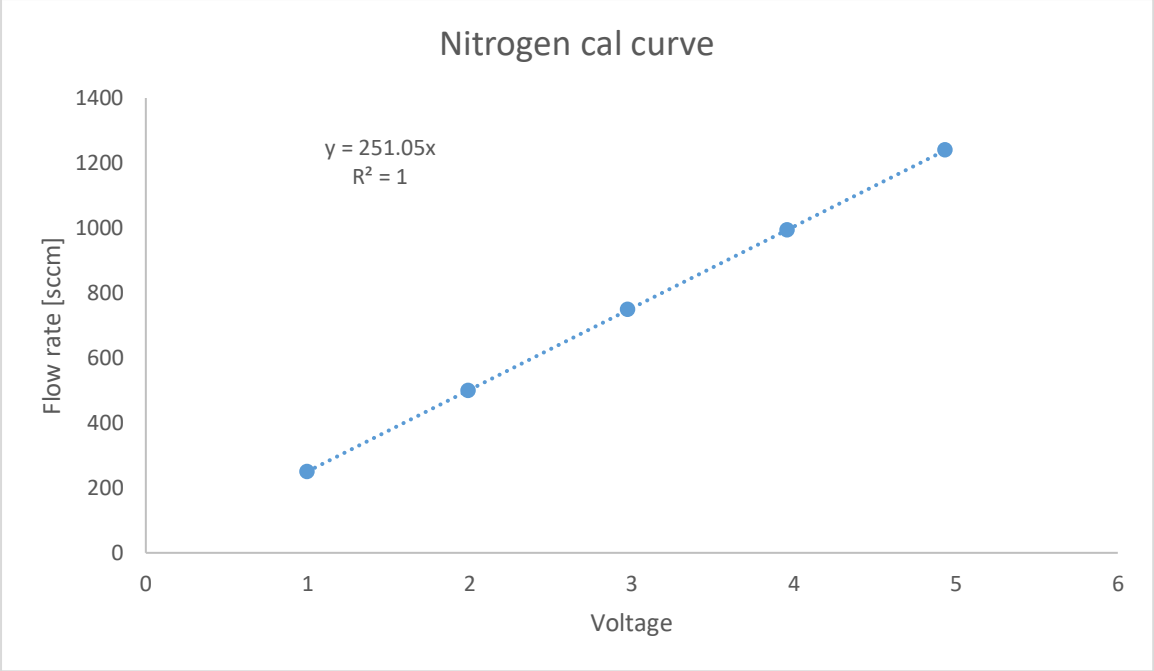

Figure 38: nitrogen calibration curve for Tylan FC-280S.

Appendix B: System schematics and photographs

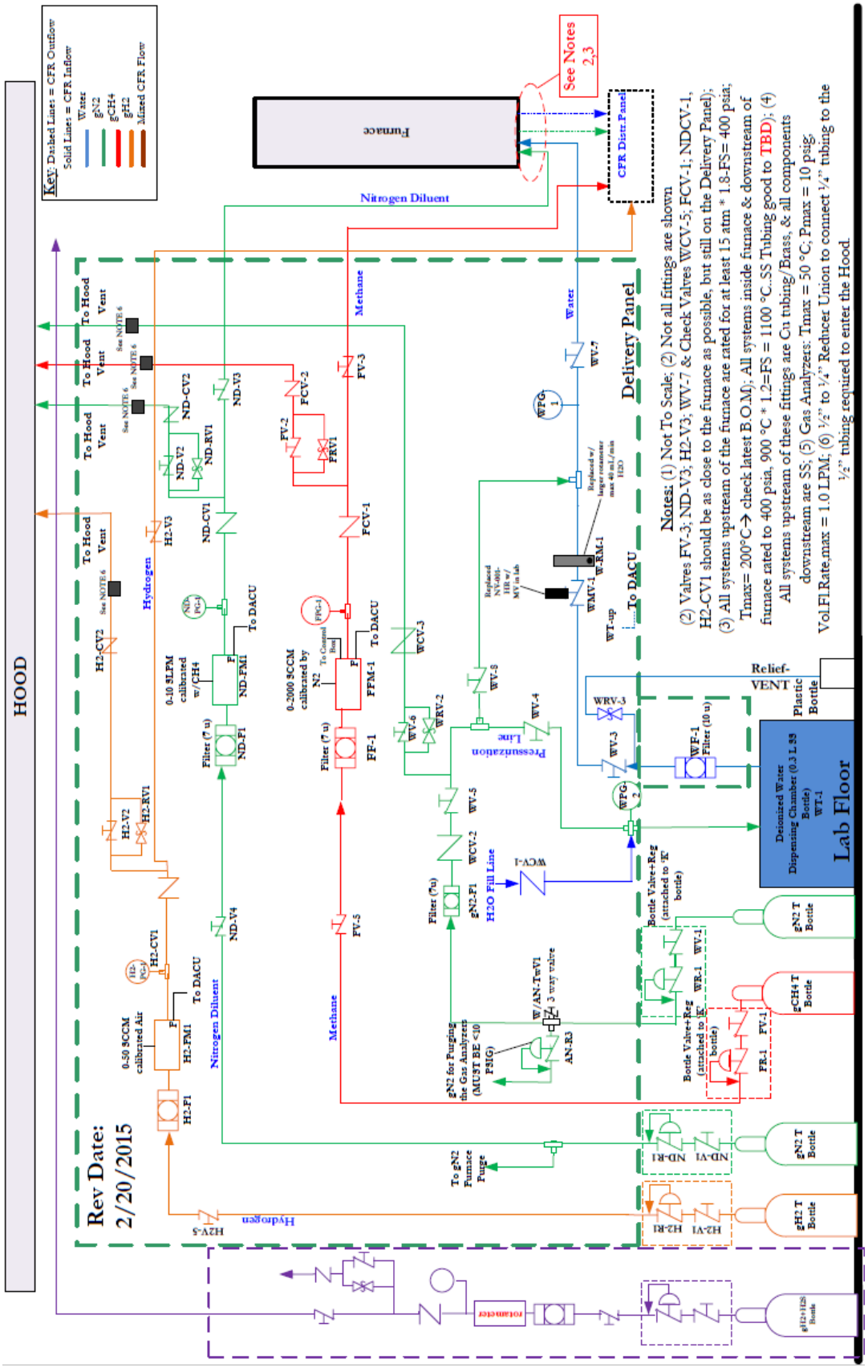

Figure 39: Schematics for delivery panel.

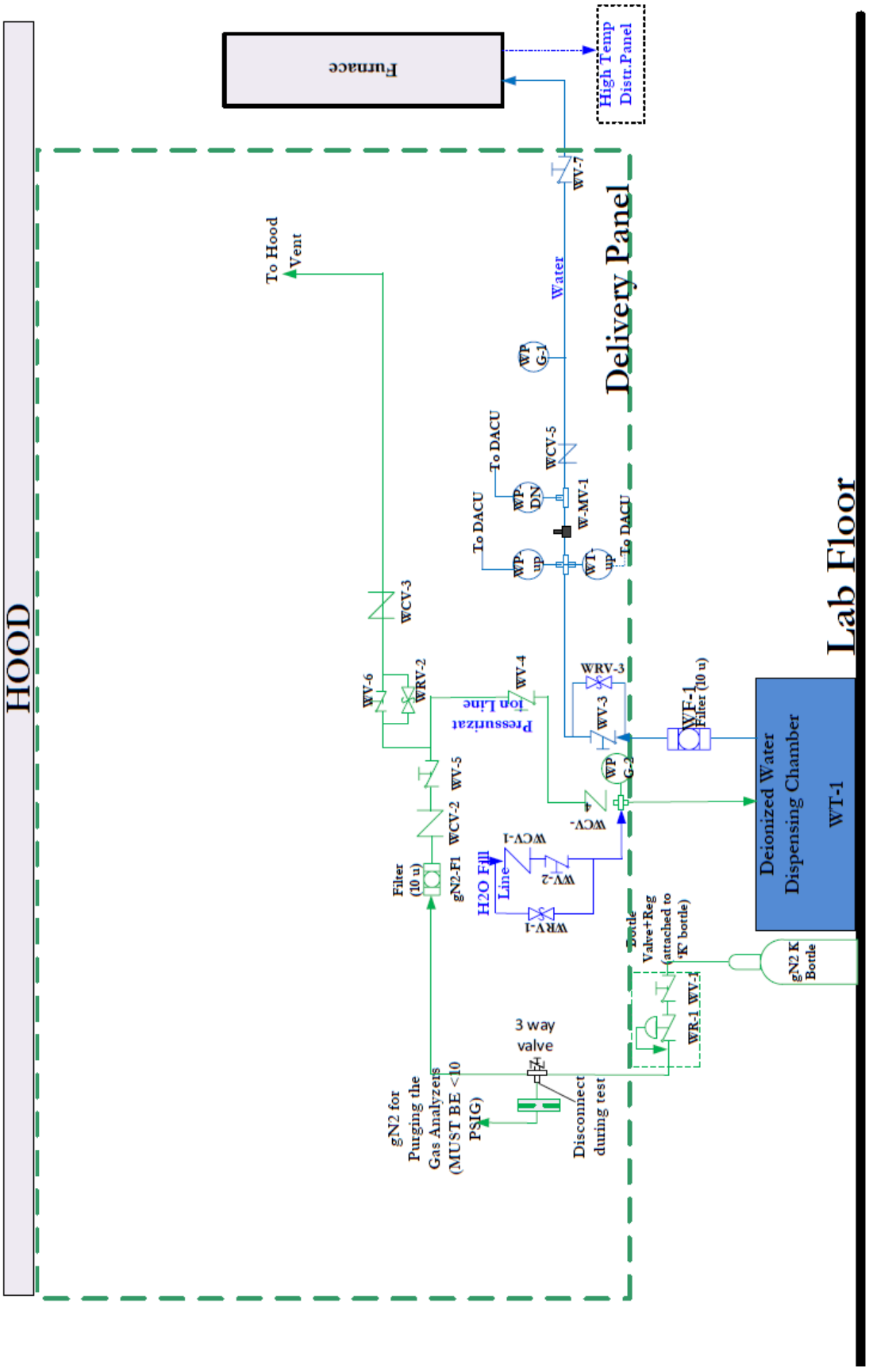

Figure 40: schematics liquid water delivery system.

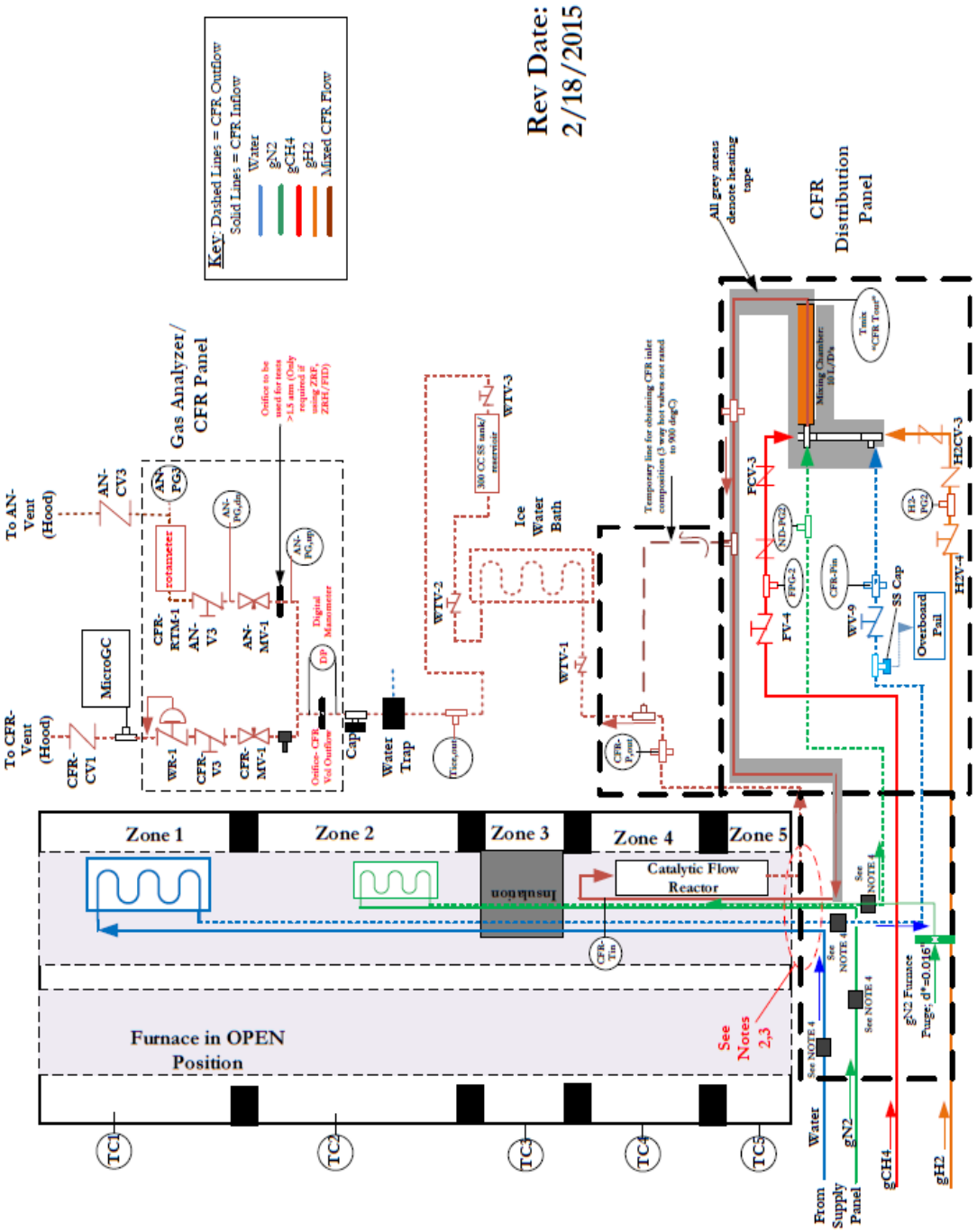

Figure 41: schematics for the hot zone and the hot panel.

Figure 41: photo of furnace used (hot zone).

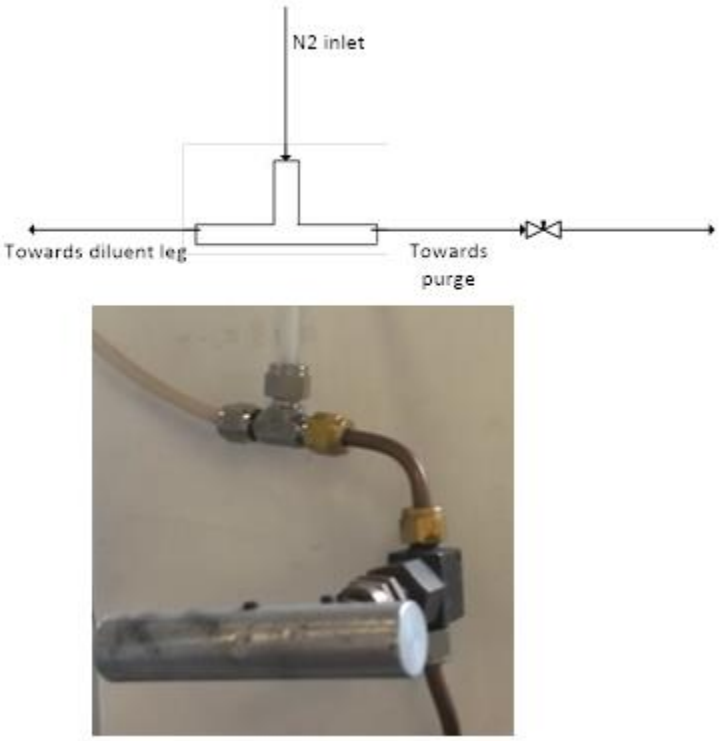

Figure 42: metering valve towards furnace purge.

Figure 43: Samples of substrates. Left: uncoated, corrugated disk; Center: coated, corrugated disk; Right: coated punch-out.

Figure 44: Calibration bomb used for microGC calibration equipped with a high pressure gauge and isolated low pressure gauge.

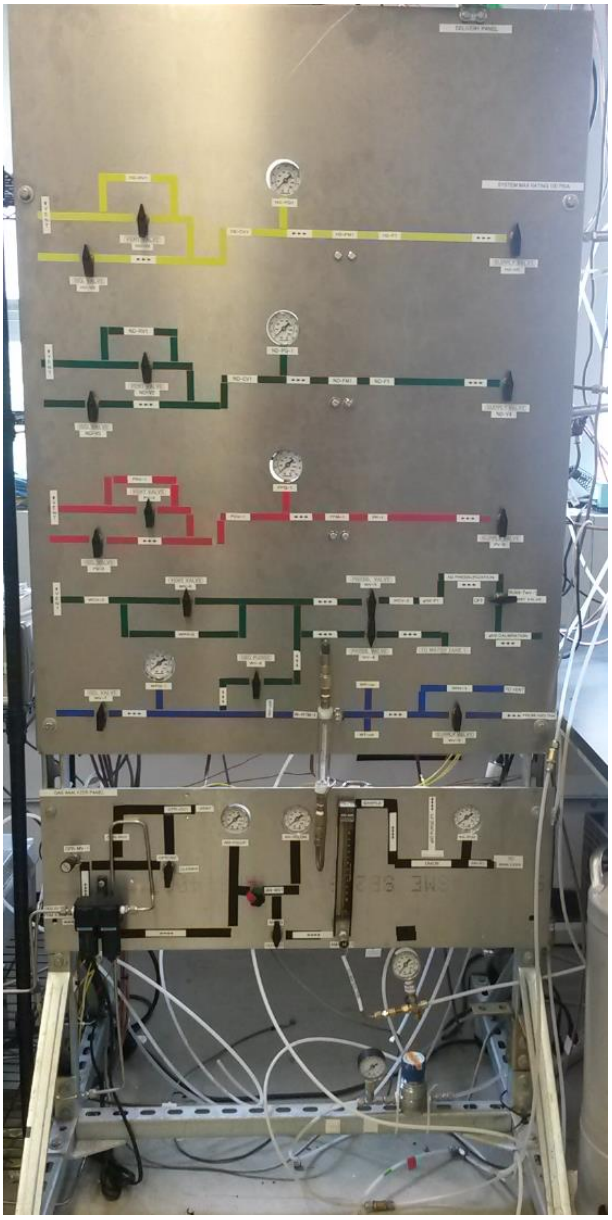

Figure 45: photo of delivery panel and analyzer panel.

Figure 46: Inficon filter, rotameter and overpressure protection.

Appendix C: data collected

Data collected during phase 1. The data Table was sliced for easy printing and reading. The first three columns were kept the same on all the Tables for continuity. These columns contain the test number, which is the test day on which the data were collected; test condition number, which is the test condition outlined on Table 1; and time slice, which is the time interval on test number in which the data were collected.

Test			CFR Target Test Conditions												
Test #	TC #	Time Slice (Mins)	Target-T_CFR (deg C)	TargetP-CFR (atm)	P_CH4 (atm)	P_H2O (atm)	P_H2 (atm)	P_gN2 Dil (atm)	S/C	Target-Vdot-N2Dil (LPM)	Target-Vdot-H2O (SCCM)	Target-Vdot-CH4 (SCCM)	Target-Vdot-H2 (SCCM)	(Vdot_CFR)min:@ CFR Test Conds (LPM)	CFR Total VdotMULTIPLIER
CFR-T7	1	615-630	700	1.56	0.383	1.13	0	0	3.0	0	1.6	487	0	4.2	1
CFR-T6	1	388-418	700	1.56	0.383	1.13	0	0	3.0	0	1.6	487	0	4.2	1
CFR-T6	1	505-519	700	1.56	0.383	1.13	0	0	3.0	0	1.6	487	0	4.2	1
CFR-T6	2	539-578	700	1.5	0.383	1.13	0	0	3.0	0	3.21	973	0	8.4	2
CFR-T11	3	111-126	700	1.5	0.383	1.13	0	0	3.0	0	4.8	1460	0	12.6	3
CFR-T11	4	247-271	700	1.5	0.383	1.13	0	0	3.0	0	6.4	1946	0	16.8	4
CFR-T9	5	185-204	700	1.5	0.25	1.245	0	0	5.0	0	1.8	318	0	4.2	1
CFR-T9	6	233-262	700	1.5	0.25	1.245	0	0	5.0	0	3.5	635	0	8.4	2
CFR-T11	7	155-169	700	1.5	0.25	1.245	0	0	5.0	0	5.2	953	0	12.6	3
CFR-T11	8	183-213	700	1.5	0.25	1.245	0	0	5.0	0	7	1271	0	16.8	4
CFR-T11	9		700	6.4	1.6	4.8	0	0	3.0	0	29	2033	0	4.2	1
CFR-T7	10	383-422	400	1.56	0.383	1.13	0	0	3.0	0	2.3	704	0	4.2	1
CFR-T7	11	475-509	500	1.56	0.383	1.13	0	0	3.0	0	2	613	0	4.2	1
CFR-T7	12	552-581	600	1.56	0.383	1.13	0	0	3.0	0	1.8	542	0	4.2	1
CFR-T9	13	122-141	800	1.56	0.383	1.13	0	0	3.0	0	1.5	441	0	4.2	1
CFR-T6	14	452-481	900	1.5	0.383	1.13	0	0	3.0	0	1.33	404	0	4.2	1

Test			CFR Actual Average& SS Test Conditions								
Test #	TC #	Time Slice (Mins)	Actual-T_CFR_Inlet (deg C)	Actual P-CFR_Inlet (atm)	Actual-Vdot-N2Dil (LPM)	Actual-Vdot-H2O (SCCM)	Actual-Vdot-CH4 (SCCM)	Actual-Vdot-H2 (SCCM)	Actual-CFR TOTAL Vdot (LPM)	Carbon Balnce [avg % diff]	Water Balnce [avg % diff]
CFR-T7	1	615-630	701	1.55	0	1.6	486.8	0	0.734	1.4	55%
CFR-T6	1	388-418	700	1.53	0	1.6	487	0	0.892	6%	31%
CFR-T6	1	505-519	763	1.53	0	1.6	487.8	0	0.750	0%	31%
CFR-T6	2	539-578	708	1.53	0	3.2	974.3	0	1.344	1%	31%
CFR-T11	3	111-126	699	2.28	0	4.8	1460	0	1.994	0.34	49%
CFR-T11	4	247-271	696	2.78	0	6.4	1946	0	2.478	0.46	49%
CFR-T9	5	185-204	701	1.53	0	1.8	315.7	0	0.526	26%	48%
CFR-T9	6	233-262	700	1.48	0	3.5	635.9	0	0.961	26%	48%
CFR-T11	7	155-169	698	2.34	0	5.2	953	0	1.415	0.27	49%
CFR-T11	8	183-213	698	2.63	0	7	1271	0	1.752	0.8	49%
CFR-T11	9		N/A	N/A	N/A	N/A	N/A	N/A	N/A	N/A	N/A
CFR-T7	10	383-422	408	1.52	0	2.3	705	0	0.729	0.5300	55%
CFR-T7	11	475-509	497	1.49	0	2	612.8	0	0.682	0.1800	55%
CFR-T7	12	552-581	605	1.52	0	1.8	541	0	0.704	0.3100	55%
CFR-T9	13	122-141	792	1.51	0	1.5	442.3	0	0.763	0.0	48%
CFR-T6	14	452-481	905	1.53	0	1.33	404	0	0.820	2%	31%

Test			Actual Average Catalyst Performance at SS												
Test #	TC #	Time Slice (Mins)	CH4 Conv. (%)	[H2] (%)	[CH4] (%)	[CO] (%)	[CO2] (%)	[N2] (%)	GHSV [hr^{-1}]	rate [mol/g-cat sec]	TOF [molecule/surf atm of cat * sec]	S-H2	W/Fo (g cat-hr/mol CH4)	res time [sec]
CFR-T7	1	615-630	15.6	40.9	50.8	2.7	12.9	0.0	84,204	0.007	9.892	0.724	0.039	15.037
CFR-T6	1	388-418	18.8	49.27	35.83	4.24	14.54	0.0	84,204	0.010	14.431	0.724	0.039	14.906
CFR-T6	1	505-519	14.9	40.37	51.30	3.69	11.23	0.0	84,204	0.007	10.091	0.730	0.039	13.994
CFR-T6	2	539-578	10.4	28.61	63.42	2.71	7.71	0.0	168,407	0.016	23.898	0.733	0.020	7.392
CFR-T11	3	111-126	10.5	31.8	62.7	0.002	10.5	0.0	252,611	0.042	60.954	0.751	0.009	6.589
CFR-T11	4	247-271	9.2	25.7	69.4	0.004	9.1	0.0	336,815	0.064	94.037	0.737	0.005	5.628
CFR-T9	5	185-204	15.9	43.9	44.1	3.2	12.7	0.0	84,204	0.005	7.230	0.734	0.060	14.842
CFR-T9	6	233-262	12.0	36.7	54.1	1.6	10.5	0.0	168,407	0.013	19.474	0.753	0.031	7.388
CFR-T11	7	155-169	12.5	38.9	54.9	0.0	12.5	0.0	252,611	0.033	48.390	0.757	0.013	7.174
CFR-T11	8	183-213	11.1	32.9	61.5	0.004	11.1	0.0	336,815	0.050	73.646	0.748	0.009	5.831
CFR-T11	9		N/A	N/A	N/A	N/A	N/A	N/A	N/A	N/A				
CFR-T7	10	383-422	0.4	0.654	96.1	0.001	0.419	0.0	84,204	0.000	0.266	0.609	0.027	14.716
CFR-T7	11	475-509	4.7	9.9	85.2	0.09	4.6	0.0	84,204	0.002	2.714	0.678	0.032	14.748
CFR-T7	12	552-581	11.5	28.1	65.5	0.754	10.7	0.0	84,204	0.005	7.012	0.711	0.035	14.658
CFR-T9	13	122-141	17.3	45.4	40.7	6.3	11.0	0.0	84,204	0.008	11.563	0.724	0.044	14.499
CFR-T6	14	452-481	20.5	53.5	28.8	10.8	9.7	0.0	84,204	0.010	14.589	0.723	0.047	14.820

Test			
Test #	TC #	Time Slice (Mins)	Comments
CFR-T7	1	615-630	
CFR-T6	1	388-418	
CFR-T6	1	505-519	This condeition was conducted AFTER TC#14 which exposed the catalyst to 900 deg C (from
CFR-T6	2	539-578	
CFR-T11	3	111-126	methane conversion #'s are not available since we did not have CFR outflow orifice installed &
CFR-T11	4	247-271	methane conversion #'s are not available since we did not have CFR outflow orifice installed &
CFR-T9	5	185-204	
CFR-T9	6	233-262	
CFR-T11	7	155-169	methane conversion #'s are not available since we did not have CFR outflow orifice installed &
CFR-T11	8	183-213	methane conversion #'s are not available since we did not have CFR outflow orifice installed &
CFR-T11	9		methane conversion #'s are not available since we did not have CFR outflow orifice installed &
CFR-T7	10	383-422	
CFR-T7	11	475-509	
CFR-T7	12	552-581	
CFR-T9	13	122-141	
CFR-T6	14	452-481	

Data collected during phase 2. The data Table was sliced for easy printing and reading. The first two columns were kept the same on all the Tables for continuity. These columns contain the test number, which is the test day on which the data were collected; and test condition number, which is the test condition outlined on Table 2.

Test		CFR Target SS Test Conditions												
Test #	TC #	Target-T_CFR (deg C)	TargetP-CFR (atm)	P_CH4 (atm)	P_H2O (atm)	P_H2 (atm)	P_gN2 Dil (atm)	S/C	Target-Vdot-N2Dil (LPM)	Target-Vdot-H2O (SCCM)	Target-Vdot-CH4 (SCCM)	Target-Vdot-H2 (SCCM)	(Vdot_CFR) (LPM)	CFR Total VdotMULTIPLIER
CFR-PH2-T2	1	700	1.56	0.383	1.13	0	0	3.0	0	1.6	487	0	4.2	1
CFR-PH2-T8	2	700	1.5	0.383	1.13	0	0	3.0	0	3.21	973	0	8.4	2
CFR-P2-T9	3	700	1.5	0.383	1.13	0	0	3.0	0	4.8	1460	0	12.6	3
CFR-P2-T12	4	700	1.5	0.383	1.13	0	0	3.0	0	6.4	1946	0	16.8	4
CFR-PH2-T8	5	700	1.5	0.25	1.245	0	0	5.0	0	1.8	318	0	4.2	1
CFR-PH2-T8	6	700	1.5	0.25	1.245	0	0	5.0	0	3.5	635	0	8.4	2
CFR-P2-T9	7	700	1.5	0.25	1.245	0	0	5.0	0	5.2	953	0	12.6	3
CFR-P2-T12	8	700	1.5	0.25	1.245	0	0	5.0	0	7	1271	0	16.8	4
CFR-P2-T10	9	700	6.4	1.6	4.8	0	0	3.0	0	29	2033	0	4.2	1
CFR-P2-T11	9													1
CFR-PH2-T7	10	400	1.56	0.383	1.13	0	0	3.0	0	2.3	704	0	4.2	1
CFR-PH2-T8	11	500	1.56	0.383	1.13	0	0	3.0	0	2	613	0	4.2	1
CFR-PH2-T8	12	600	1.56	0.383	1.13	0	0	3.0	0	1.8	542	0	4.2	1
CFR-PH2-T6	13	800	1.56	0.383	1.13	0	0	3.0	0	1.5	441	0	4.2	1
CFR-PH2-T2	14	900	1.5	0.383	1.13	0	0	3.0	0	1.33	404	0	4.2	1

Test		CFR Actual Average & SS Test Conditions										
Test #	TC #	Actual-T_CFR_Inlet (deg C)	Actual P-CFR_ Inlet (atm)	Actual-Vdot-N2Dil (LPM)	Actual-Vdot-H2O (SCCM)	Actual-Vdot-CH4 (SCCM)	Actual-Vdot-gN2 TRACER (SCCM)	Actual-CFR TOTAL Vdot (LPM)	Actual-Vdot-gH2 (SCCM)	Tice-out (deg C)	Carbon balance [avg %diff]	Water balance [avg %diff]
CFR-PH2-T2	1	706	1.5	0	1.6	487	50	0.873		16.2	23.2%	7.9%
CFR-PH2-T8	2	708	1.4	0	3.2	970	49.5	1.137	0.000	17.9	5.9%	8.1%
CFR-P2-T9	3	835	1.6	0	4.81	1467.2	49.5	1.702	0.000	19.5	0.1%	7.5%
CFR-P2-T12	4	719	1.5	0	6.4	1924.3	48.5	2.112	0.000	23.3	1.1%	11.5%
CFR-PH2-T8	5	700	1.5	0	1.8	313	49.5	0.530	0.000	18.7	23.3%	4.8%
CFR-PH2-T8	6	710	1.4	0	3.5	633.1	49.3	0.776	0.000	17.9	0.4%	3.7%
CFR-P2-T9	7	859	1.7	0	5.2	953	49.5	1.380	0.000	19.2	11.8%	7.5%
CFR-P2-T12	8	726	1.5	0	7	1273	48.7	1.137	0.000	22.8	17.9%	7.4%
CFR-P2-T10	9	734	6.0	0	28	1986.6	49.0	2.036	0.000	18.8	5.1%	0.2%
CFR-P2-T11	9	736	6.2	0	28	1994.5	49.1	2.096	0.000	21.3	3.9%	0.0%
CFR-PH2-T7	10	415	1.4	0	2.3	705	49.5	0.715	0.000	11.5	4.4%	0.0%
CFR-PH2-T8	11	500	1.5	0	2	614	49.3	0.672	0.000	18.5	1.5%	0.0%
CFR-PH2-T8	12	614	1.5	0	2	541	49.5	0.654	0.000	18.8	6.9%	1.7%
CFR-PH2-T6	13	800	1.4	0	1.5	443	49.5	0.849	0.000	16.7	4.1%	11.6%
CFR-PH2-T2	14	875	1.5	0	1.3	406	42.3	1.008	0	16.3	0.8%	16.4%

Test		Actual Average Catalyst Performance at SS											
Test #	TC #	CH4 Conv. (%)	[H2] (%)	[CH4] (%)	[CO] (%)	[CO2] (%)	[N2] (%)	GHSV [hr^{-1}]	rate [mol/g-cat sec]	TOF [molecule/surf atm of cat * sec]	S-H2	W/Fo (g cat-hr/mol CH4)	res time [sec]
CFR-PH2-T2	1	13.6	34.46000	53.98	3.94	9.65	7.84	84204	0.005712	8.381123655	0.71717	0.04124134	14.23012
CFR-PH2-T8	2	10.2	18.23074	68.73	1.97	8.24	5.7	168408	0.014511	21.29210306	0.641004	0.02152888	6.900425
CFR-P2-T9	3	8.7	14.06252	76.0	2.455707	6.2	4.3	252612	0.030484	44.73096575	0.61898	0.01246929	4.481534
CFR-P2-T12	4	11.6	11.14200	79.0	1.792	9.8	3.1	336816	0.05816	85.34070072	0.490462	0.01030391	3.554135
CFR-PH2-T8	5	9.3	17.21845	62.4	1.5	7.7	12.9	84204	0.002371	3.47962846	0.64969	0.06332118	14.38174
CFR-PH2-T8	6	7.8	14.17686	72.1	1.2	6.6	8.5	168408	0.007096	10.41276878	0.645668	0.03219997	7.104977
CFR-P2-T9	7	12.2	21.20652	63.7	2.8	9.4	5.8	252612	0.03122	45.80958107	0.634823	0.01775553	4.832791
CFR-P2-T12	8	11.6	11.09300	78.9	1.466	10.1	6.0	336816	0.038434	56.39587459	0.48988	0.01506408	3.676074
CFR-P2-T10	9	0.4	0.89700	90.6	0.19	0.234667	13.5	84204	0.00964	14.1446347	0.678689	0.0024473	3.296014
CFR-P2-T11	9	0.0	0.16386	89.90629	0	0.009714	13.5	84204	0.000227	0.332883928	0.944033	0.00235131	3.375589
CFR-PH2-T7	10	0.001	0.00607	92.7	0.000	0.001	9.5	84204	6.54E-07	0.000960274	0.805843	0.02877899	13.95387
CFR-PH2-T8	11	0.026	0.04294	91.1	0	0.0	10.2	84204	1.01E-05	0.014771863	0.625073	0.03198322	14.63209
CFR-PH2-T8	12	2.4	4.38393	84.5	0	2.4	10.7	84204	0.000954	1.399282861	0.649882	0.03564485	13.32945
CFR-PH2-T6	13	15.7	36.35416	37.66841	6.170144	9.526606	7.508674	84204	0.007645	11.21756631	0.698435	0.0480781	13.3378
CFR-PH2-T2	14	19.4	49.30000	19.9	11.2	8.2	5.9	84204	0.011283	16.55582727	0.717613	0.04814785	15.14466

Data collected during phase 3A. The data Table was sliced for easy printing and reading. The first three columns were kept the same on all the Tables for continuity. These columns contain the test number, which is the test day on which the data were collected; test condition number, which is the test condition outlined on Table 3; and time slice, which is the time interval on test number in which the data were collected.

Test			CFR Target SS Test Conditions												
Test #	TC #	SS Time Slice (Mins)	Target-T_CFR (deg C)	TargetP-CFR (atm)	P_CH4 (atm)	P_H2O (atm)	P_H2 (atm)	P_gN2 Dil (atm)	S/C	Target-Vdot-N2Dil (SCCM)	Target-Vdot-H2O (SCCM)	Target-Vdot-CH4 (SCCM)	Target-Vdot-H2 (SCCM)	(Vdot_CFR)min: @ CFR Test Conds (LPM)	CFR Total VdotMULTIPLIER
CFR-P3-T1A		374 - 401	550	1.500	0.451	1.010	0.000	0.039	3.0	40	1.05	469	0	1.5	1
CFR-P3-T1A		414 - 422	550	1.500	0.451	1.010	0.000	0.039	3.0	40	2.1	938	0	3.0	2
CFR-P3-T1A		447 - 451	550	1.500	0.451	1.010	0.000	0.039	3.0	40	4.2	1876	0	6.1	4
CFR-P3-T1A		464	550	1.500	0.451	1.010	0.000	0.039	3.0	40	4.2	1876	0	6.1	4
CFR-P3-T2	1	350 - 370	500	1.500	0.454	1.016	0.012	0.018	3.0	20.58	1.15	514	13.72	3.6	1
CFR-P3-T2	1	375 - 383	500	1.500	0.428	1.073	0.011	0.017	3.0	20.58	1.15	514	13.72	3.6	1
CFR-P3-T2	2	425 - 446	500	3.000	0.585	2.376	0.016	0.024	6.0	20.58	2.3	514	13.72	3.6	2
CFR-P3-T2	3	462 - 479	500	3.000	0.903	2.067	0.012	0.018	3.0	20.58	2.3	1028	13.72	3.6	2
CFR-P3-T2	4	500 - 512	500	3.000	0.895	2.060	0.018	0.027	3.0	30.18	2.3	1028	20.12	3.6	2

Test			CFR Actual Average & SS Test Conditions							
Test #	TC #	SS Time Slice (Mins)	Actual-T_CFR_Inlet (deg C)	Actual P-CFR_Inlet (atm)	Actual-Vdot-H2 (SCCM)	Actual-Vdot-H2O (SCCM)	Actual-Vdot-CH4 (SCCM)	Actual-Vdot-gN2 TRACER (SCCM)	Actual-CFR TOTAL Vdot (LPM)	Tice-out (deg C)
CFR-P3-T1A		374 - 401	553	1.94	0	1.05	468	44.0	0.510	22.81
CFR-P3-T1A		414 - 422	551	1.99	0	2.1	941	44.2	0.886	23.04
CFR-P3-T1A		447 - 451	477	2.48	0	4.2	1834	43.9	1.185	22.76
CFR-P3-T1A		464	394	2.34	0	4.2	1835	43.8	0.872	22.70
CFR-P3-T2	1	350 - 370	505	1.96	14	1.15	511	21	0.529	25.35
CFR-P3-T2	1	375 - 383	495	1.94	14	1.15	512	21	0.490	25.11
CFR-P3-T2	2	425 - 446	503	2.69	14	2.3	513	20	0.375	25.72
CFR-P3-T2	3	462 - 479	500	2.91	14	2.3	1033	20	0.572	25.06
CFR-P3-T2	4	500 - 512	502	3.00	20	2.3	1033	29	0.590	25.38

Test			Actual Average Catalyst Performance at SS									
Test #	TC #	SS Time Slice (Mins)	CH4 Conv. (%)	[H2] (%)	[CH4] (%)	[CO] (%)	[CO2] (%)	[N2] (%)	Sum	water	carbon	GHSV [hr^{-1}]
CFR-P3-T1A		374 - 401	11.9	45.60	35.58	0.00	11.94	8.62	101.74	1.74%	1.92	13448
CFR-P3-T1A		414 - 422	10.2	45.2	42.5	0.0	10.2	5.0	102.91	3.19%	0.66	25571
CFR-P3-T1A		447 - 451	8.4	36.95	54.53	0.00	8.43	3.7	103.61	1.84%	2.37	45426
CFR-P3-T1A		464	0.5	2.15	93.06	0.00	0.54	5.0	100.77	0.01%	5.40	39099
CFR-P3-T2	1	350 - 370	11.6	50.38	37.05	0.00	11.62	3.9	102.93	2.11%	0.38	14058
CFR-P3-T2	1	375 - 383	11.1	47.6	41.9	0	11.1	4.2	104.77	1.36%	0.12	13803
CFR-P3-T2	2	425 - 446	10.5	46.7	40.2	0.000	10.5	5.5	102.89	1.21%	1.42	24081
CFR-P3-T2	3	462 - 479	8.8	38.8	52.4	0.0	8.8	3.6	103.68	1.72%	0.20	26313
CFR-P3-T2	4	500 - 512	9.3	37.8	50.2	0.0	9.3	5.0	102.20	0.25%	3.43	25095

Test			res time [sec]	rate [mol/g-cat sec]	TOF [molecule/surf atm of cat * sec]	W/Fo (g cat-hr/mol CH4)	S-H2
Test #	TC #	SS Time Slice (Mins)					
CFR-P3-T1A		374 - 401	4.829081	0.008144	11.94978002	0.106454434	0.792552
CFR-P3-T1A		414 - 422	2.488495	0.024522	35.98228325	0.052993994	0.815572
CFR-P3-T1A		447 - 451	1.708913	0.048029	70.47489352	0.027181321	0.814271
CFR-P3-T1A		464	1.812962	0.001954	2.867141944	0.027156764	0.798838
CFR-P3-T2	1	350 - 370	4.71494	0.00866	12.70709404	0.097465469	0.812564
CFR-P3-T2	1	375 - 383	4.720708	0.007565	11.10033194	0.097440638	0.811239
CFR-P3-T2	2	425 - 446	3.703615	0.009564	14.03317062	0.097168452	0.816803
CFR-P3-T2	3	462 - 479	3.514977	0.014128	20.73057703	0.048232508	0.815288
CFR-P3-T2	4	500 - 512	3.61258	0.014917	21.88799611	0.048234292	0.803067

Test			Comments
Test #	TC #	SS Time Slice (Mins)	
CFR-P3-T1A		374 - 401	
CFR-P3-T1A		414 - 422	
CFR-P3-T1A		447 - 451	
CFR-P3-T1A		464	
CFR-P3-T2	1	350 - 370	Set point of zone 3 = 600
CFR-P3-T2	1	375 - 383	Set point of zone 3 = 700
CFR-P3-T2	2	425 - 446	
CFR-P3-T2	3	462 - 479	
CFR-P3-T2	4	500 - 512	H2 MFC set to maximum. MFC was oscilating erratically. Could explain lack of C balance closure

Data collected during phase 3B. The data Table was sliced for easy printing and reading. The first three columns were kept the same on all the Tables for continuity. These columns contain the test number, which is the test day on which the data were collected; test condition number, which is the test condition outlined on Table 4; and time slice, which is the time interval on test number in which the data were collected. In addition to the SMR tests outlined on Table 4, water gas shift tests were performed as well and are outlined under phase 3B data.

Test			CFR Target SS Test Conditions														
Test #	TC #	SS Time Slice (Mins)	Target-T_CFR (deg C)	TargetP-CFR (atm)	P_CH4 (atm)	P_H2O (atm)	P_H2 (atm)	P_gN2 Dil (atm)	P_CO2 (atm)	S/C	Target-Vdot-N2Dil (SCCM)	Target-Vdot-H2O (SCCM)	Target-Vdot-CH4 (SCCM)	Target-Vdot-CO2 (SCCM)	Target-Vdot-H2 (SCCM)	(Vdot_CFR)min: @ CFR Test Conds (LPM)	CFR Total VdotMULTIPLIER
	1		500	1.38	0.238875	0.716625	0.402686	0.025012	0	3.0	40	1.15	514	0	644	3.6	
	2		500	1.72	0.184991	1.109946	0.402686	0.025012	0	6.0	40	2.31	514	0	644	3.6	
	3		500	2.21	0.344762	1.034286	0.805998	0.025012	0	3.0	40	2.31	1028	0	1289	3.6	
	4		500	2.56	0.320197	0.96059	1.250578	0.025012	0	3.0	40	2.31	1028	0	2000	4.4	
	5		550	1.39	0.241111	0.723334	0.402769	0.026629	0	3.0	40	1.1	483	0	605	3.6	
	6		550	1.72	0.184908	1.109446	0.402769	0.026629	0	6.0	40	2.17	483	0	605	3.6	
	7		550	2.21	0.344753	1.03426	0.805539	0.026629	0	3.0	40	2.17	966	0	1210	3.6	
			THESE DATA REFER TO THE WGS TEST														
CFR-P3-T5	1	596 - 617	545	2.23	0	0.465483	1.664336	0.046601	0.04993		70	1.15	0	75	2500		
CFR-P3-T5	2	625 - 641	545	2.25	0	0.460463	1.664336	0.04993	0.075894		75	1.15	0	114	2500		
CFR-P3-T5	3	653 - 669	545	2.28	0	0.454756	1.664336	0.056587	0.103189		85	1.15	0	155	2500		
CFR-P3-T5	4	678 - 694	545	2.31	0	0.449274	1.664336	0.059916	0.133147		90	1.15	0	200	2500		
CFR-P3-T4	1	332 - 352	550	1.38	0	0.754	0.429	0.03	0.166		44	1.15	0	250	644		
CFR-P3-T4	2	374 - 394	550	1.51	0	0.687407	0.428733	0.06	0.333		88	1.15	0	500	644		
CFR-P3-T4	3	420 - 441	550	1.65	0	0.629738	0.428733	0.09	0.499		132	1.15	0	750	644		

Test			CFR Actual Average & SS Test Conditions								
Test #	TC #	SS Time Slice (Mins)	Actual-T_CFR_Inlet (deg C)	Actual P-CFR_Inlet (atm)	Actual-Vdot-H2 (SCCM)	Actual-Vdot-H2O (SCCM)	Actual-Vdot-CH4 (SCCM)	Actual-Vdot-gN2 TRACER (SCCM)	Actual-Vdot-CO2 (SCCM)	Actual-CFR TOTAL Vdot (LPM)	Tice-out (deg C)
	1		513	1.80	646	1.15	516	40.9	0	0.728	23.40
	2		512	2.24	646	1.7	516	41.0	0	0.600	23.40
	3		513	3.20	1289	2.3	1028	40.9	0	0.735	23.44
	4		514	3.57	1999	2.3	1028	40.9	0	0.854	23.50
	5		567	2.23	646	1.1	515	41	0	0.668	23.50
	6		574	2.28	646	2.1	515	41	0	0.660	23.50
	7		576	3.18	1288	2.17	1028	41	0	0.843	23.30
										#DIV/0!	
			THESE DATA REFER TO THE WGS TEST								
CFR-P3-T5	1	596 - 617	545.15	1.89	2501	1.15	0	70.58	83.35	0.817	25.26
CFR-P3-T5	2	625 - 641	547.54	1.94	2501	1.15	0	76.06	114.38	0.880	25.36
CFR-P3-T5	3	653 - 669	545.94	2.02	2500	1.15	0	83.19	154.84	0.920	25.40
CFR-P3-T5	4	678 - 694	546.94	2.04	2500	1.15	0	90.99	199.12	0.972	25.25
CFR-P3-T4	1	332 - 352	552	2.08	643	1.15	0	48	270	0.493	23.40
CFR-P3-T4	2	374 - 394	551	2.08	643	1.15	0	95	541	0.668	23.41
CFR-P3-T4	3	420 - 441	552	2.02	640	1.15	0	142	806	0.850	23.89
			No water conditon								
			544	1.72	644	0	0	44	250	0.398	25.45286

Test			Actual Average Catalyst Performance at SS									res time	rate	TOF	W/Fo (g cat-hr/mol CH4)	S-H2
Test #	TC #	SS Time Slice (Mins)	CH4 Conv. (%)	[H2] (%)	[CH4] (%)	[CO] (%)	[CO2] (%)	[N2] (%)	C2H6 [%]	Sum	GHSV [hr^{-1}]	[sec]	[mol/g-cat sec]	[molecule/surf atm of cat * sec]		
	1		2.0	58.92	35.01	0.21	1.75	3.12	0.00	99.01	13758	3.279031	0.002792	4.096858623	0.096676945	0.865105
	2		1.8	58.71	35.28	0.18	1.63	3.05	0.00	98.85	13758	3.207105	0.002621	3.845435286	0.096676885	0.871263
	3		0.8	59.36	38.61	0.13	0.64	1.74	0.00	100.48	13758	2.915275	0.002298	3.372037047	0.048488483	0.928453
	4		0.4	65.19	33.64	0.08	0.33	1.34	0.00	100.58	16815	2.872076	0.001444	2.1188452	0.048485181	0.71306
	5		4.9	62.16	27.87	0.83	4.10	2.74	0.00	97.70	13758	3.899465	0.006645	9.750383343	0.096724129	0.810123
	6		5.2	62.57	27.48	0.81	4.36	2.72	0.00	97.94	13758	2.612402	0.01045	15.33325628	0.096727806	0.806972
	7		3.3	59.14	35.30	0.85	2.49	1.52	0.00	99.30	13758	2.781085	0.010671	15.65789637	0.048493157	0.762536
			THESE DATA REFER TO THE WGS TEST													
CFR-P3-T5	1	596 - 617	1.4	93.21	0.10	0.41	3.89	4.57	0.43	102.61						
CFR-P3-T5	2	625 - 641	1.3	89.76	0.17	0.63	5.28	4.47	0.24	100.55						
CFR-P3-T5	3	653 - 669	1.4	87.70	0.21	0.77	6.72	4.47	0.23	100.10						
CFR-P3-T5	4	678 - 694	1.7	84.73	0.25	0.96	8.24	4.59	0.22	98.99						
CFR-P3-T4	1	332 - 352	27.2	61.87	0.17	1.96	25.24	4.64	0.00	93.88						
CFR-P3-T4	2	374 - 394	40.2	46.19	0.10	2.33	37.88	6.88	0.00	93.37						
CFR-P3-T4	3	420 - 441	48.2	36.98	0.06	2.53	45.70	8.28	0.00	93.56						
			No water conditon													
			29.3	50.55	7.32	9.79	19.47	6.42	0	93.55						

Data collected during phase 3C. The data Table was sliced for easy printing and reading. The first three columns were kept the same on all the Tables for continuity. These columns contain the test number, which is the test day on which the data were collected; test condition number, which is the test condition outlined on Table 5; and time slice, which is the time interval on test number in which the data were collected.

Test			CFR Target SS Test Conditions												
Test #	TC #	SS Time Slice (Mins)	Target-T_CFR (deg C)	TargetP-CFR (atm)	P_CH4 (atm)	P_H2O (atm)	P_H2 (atm)	P_gN2 Dil (atm)	S/C	Target-Vdot-N2Dil (SCCM)	Target-Vdot-H2O (SCCM)	Target-Vdot-CH4 (SCCM)	Target-Vdot-H2 (SCCM)	(Vdot_CFR)min:@ CFR Test Conds (LPM)	CFR Total VdotMULTIPLIER
CFR-P3C-T3	1	42-60	500	1.50	0.281	0.843	0.351	0.025	3.0	40	1.5	449	561	4.2	1
CFR-P3C-T3	3	189-201	600	1.50	0.281	0.843	0.351	0.025	3.0	35	1.3	398	497	4.2	1
CFR-P3C-T3	4	267-279	700	1.50	0.281	0.843	0.351	0.025	3.0	32	1.2	357	446	4.2	1
CFR-P3C-T3	1	42-60	500	1.50	0.281	0.843	0.351	0.025	3.0	40	1.5	449	561	4.2	1
CFR-P3C-T3	2	105-120	500	1.50	0.283	0.850	0.354	0.012	3.0	38	3.0	905	1132	8.4	2
CFR-P3C-T3			500	1.50	0.284	0.853	0.355	0.008	3.0	38	4.5	1363	1703	12.6	3

Test			CFR Actual Average & SS Test Conditions							
Test #	TC #	SS Time Slice (Mins)	Actual-T_CFR_Inlet (deg C)	Actual P-CFR_Inlet (atm)	Actual-Vdot-H2 (SCCM)	Actual-Vdot-H2O (SCCM)	Actual-Vdot-CH4 (SCCM)	Actual-Vdot-gN2 TRACER (SCCM)	Actual-CFR TOTAL Vdot (LPM)	Tice-out (deg C)
CFR-P3C-T3	1	42-60	528	1.65	561	1.8	450	37.4	0.763	19.16
CFR-P3C-T3	3	189-201	606	1.60	498	1.4	398	28	0.695	20.90
CFR-P3C-T3	4	267-279	717	1.61	445	1.4	356	32	0.681	21.06
CFR-P3C-T3	1	42-60	528	1.65	561	1.8	450	37.4	0.763	19.16
CFR-P3C-T3	2	105-120	516	1.89	1134	3.5	906	37	1.169	20.39

Test			Actual Average Catalyst Performance at SS								res time	rate	TOF	W/Fo (g cat-hr/mol CH4)	S-H2
Test #	TC #	SS Time Slice (Mins)	CH4 Conv. (%)	[H2] (%)	[CH4] (%)	[CO] (%)	[CO2] (%)	[N2] (%)		GHSV [hr^{-1}]	[sec]	[mol/g-cat sec]	[molecule/surf atm of cat * sec]		
CFR-P3C-T3	1	42-60	0.1	57.70	37.10	0.00	0.14	4.9	99.8	16974	2.328464	0.000243	0.356231369	0.11083953	0.987719
CFR-P3C-T3	3	189-201	0.3	60.20	35.50	0.00	0.32	4.00	100.0	16984	2.535711	0.000469	0.687982709	0.12523483	0.979638
CFR-P3C-T3	4	267-279	0.2	60.80	34.30	0.00	0.22	4.69	100.0	17286	2.341102	0.000324	0.475567556	0.139990141	0.987661
CFR-P3C-T3	1	42-60	0.1	57.70	37.10	0.00	0.14	4.9	99.8	16974	2.328464	0.000243	0.356231369	0.11083953	0.987719
CFR-P3C-T3	2	105-120	0.1	58.20	41.00	0.00	0.06	3.2	102.5	33932	1.374588	0.000322	0.47263208	0.055006556	0.991296